Order Number 9500970

Mechanical characteristics of implant/tissue interphases

Ko, Ching-Chang, Ph.D.

The University of Michigan, 1994

U·M·I

300 N. Zeeb Rd.
Ann Arbor, MI 48106

MECHANICAL CHARACTERISTICS OF IMPLANT/TISSUE INTERPHASES

by

Ching-Chang Ko

A dissertation submitted in partial fulfillment
of the requirements for the degree of
Doctor of Philosophy
(Biomaterials and Bioengineering)
in The University of Michigan
1994

Doctoral Committee:

Assistant Professor David H. Kohn, Co-chairman
Assistant Professor Scott J. Hollister, Co-chairman
Professor Emeritus Robert G. Craig
Professor Steven A. Goldstein
Professor Martha J. Somerman

To my parents, wife, and friends

ACKNOWLEDGMENTS

I wish to express my sincerest gratitude to my advisors, Professor D. H. Kohn, and Professor S. J. Hollister for their guidance and encouragement throughout the course of this research and my graduate work. Special thanks are due to Professor S. A. Goldstein for his valuable assistance and constant inspiration during the entire period of this study.

I owe the National Institute of Health, Professor D. H. Kohn, Professor R. G. Craig, Dean J. B. Machen of the School of Dentistry, and Rackham Graduate School my sincere appreciation for their financial support through this investigation.

I am grateful to professors M. J. Somerman and N. Kikuchi for their help in various aspects of this research work. Also, I would like to thank professor M-C Lee for his invaluable guidance to initiate my interest in biomechanics during my graduate study in Taiwan. I also wish to thank Mr. M. W. Stock, Mr. D. C. Kayner, and Bio-Vac Inc. for their assistance in machining the titanium specimens and sintering specimens.

Thanks are also due to the staff of the Biomaterials Program and the Orthopaedic Research Laboratory staff for providing the facilities as well as cooperation. Special thanks are due to Mr. E. R. Dootz, Mr. K. M. Boenke, Mr. J-N Wang, and Dr. W. C. Wagner for their help in preparing experimental set-up's. Deepest thanks go to Ms. V. A. Hristova for her proof reading.

I sincerely appreciate my parents, parents-in-law, brother and sister for their sacrifices as a result of my being away from them and for their financial support. Last but not least, I am indebted to my wife, Wen-Chi, for her endless love, long patience and continuous encouragement in pursuance of my graduate work.

TABLE OF CONTENTS

LIST OF FIGURES

Figure

LIST OF TABLES

Table

GLOSSARY OF VARIABLES

ε: A ratio between the dimension of one unit cell and that of the entire composite.

u^{ε}: The total displacement on the internal point of the composite.

u^{0}: The macroscopic or global displacement on the composite.

u^{1} and u^{2}: Perturbations in the displacements of the composite due to that composite microstructure.

t_i: Global tractions applied on a subject.

ε^{0}: Virtual strains on the composite material at the macroscopic level.

ε^{1}: Virtual strains on the composite material at the microscopic level.

$\overline{\varepsilon}$: The macroscopic strain tensor.

ε^{*}: The fluctuating strain due to the material microstructure.

C_{ij}: Effective elastic constants of the composite.

M_{ijkl}: A relation tensor between global strains and local strains for the composite.

Ω^{ε}: The total macroscopic domain plus the microscopic domain of the composite media.

E_L: The longitudinal elastic modulus of a composite material.

E_T: The transverse elastic modulus of a composite material.

G_{LT}: The shear modulus of a composite material.

K_i: The bulk modulus of an isotropic material.

V: Material volume fraction.

VMS^H: Von Mises stresses obtained from the homogenization analysis.

VMS^D: Von Mises stresses obtained from the standard finite element analysis.

CHAPTER I

INTRODUCTION

1.0 Background

Dental implants and total joint replacements have been used to restore anatomical integrity of hard tissues, and have improved the quality of life for thousands of people (Fig1.1). Aged people who suffer from edentulism and disabled patients need prostheses to help perform normal daily functions such as mastication, standing, and walking. One significant goal of bioengineering is to improve the longevity of these implants.

The design and development of osseointegrated implants, which allow osseous tissue to closely appose the implant surfaces, have focused on obtaining strong interfacial bonding as well as efficient stress transfer through implant/tissue interphases (Huiskes 1984, Pilliar et al. 1975, Pilliar and Bratina 1980). One example is the development of surface roughened implants which provide mechanical interdigitation between the protrusions on the material surfaces and the healing bone. Two types of surface roughened metallic implants are the screw threaded dental implant and porous coated implants, which are used as total hip, total knee, and dental implants. Porous metal coatings are made from powder cobalt-chromium alloy or titanium microspheres, which are bonded onto a dense metallic substrate.

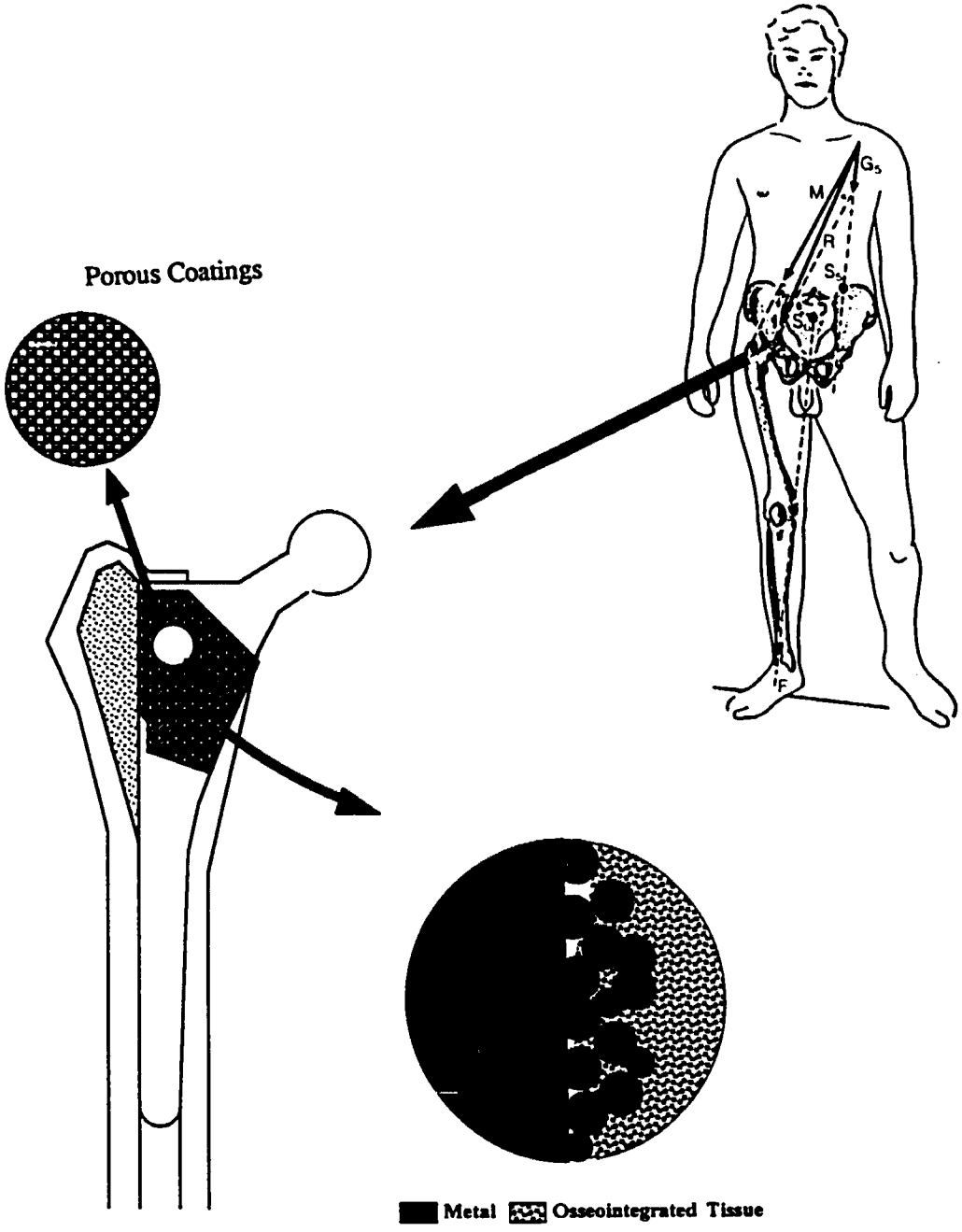

Figure 1.1 Biomaterials used to restore anatomical integrity due to missing normal bone have a complicated surface architecture and interphase complexity.

Clinically, the use of surface roughened titanium implants, which encourage osseointegration on or into implant surfaces to minimize implant mobility, has recently received widespread attention and become common in both orthopaedic and dental therapy (Morscher 1984, NIH 1988). While short term success has been reported to be greater than 84% for a three year period in dentistry and greater than 80% for a two to five year period in orthopaedics, the long-term (> 10years) success of these load bearing implants remains unknown (Cox and Zarb 1987, Albrektsson et al. 1988, Gustilo 1988).

During service, mobility due to material degradation, tissue damage, and bone resorption at the interphase can lead to implant loosening, cause pain, and ultimately result in implant failure. Material degradation is clearly dependent upon the mechanics of the implant/tissue interphase, while bone resorption may possibly be attributed to a coupling effect between the local stress state at the interphase and the demineralization induced by ions released from material surfaces.

The primary function of the implant/tissue interphase is to transfer load from prostheses to the surrounding bone tissues. Surface roughened implants provide a better mechanical interlock with the surrounding bone than smooth implants and may more effectively transmit stresses at the interphase. It is presumed that these stresses stimulate bone cells to maintain mineralized bone within the interphase (Bobyn et al. 1980b, Galante et al. 1971, Pilliar et al. 1975, Skalak 1983). The retention of bone, of a certain quantity or quality, within the interphase provides a biological fixation with the implant.

The amount of bone mass within the spaces or pores on the implant surfaces is usually referred to as the amount of *bone ingrowth*. This biological fixation concept, known as osseointegration, has been widely used in dental implantation. With dental implants, bone ingrowth occupies about 60% of the threaded surface area (Hale et al. 1991). Recent studies report clinical failure rate of less than 10% (Arvidson et al. 1994, Lemons 1988). Biological factors such as bacterial infection and tissue inflammation

(Meffert 1992) appear to play an equally important role as mechanical factors in the failure of osseointegrated dental implants. Although this dissertation uses a dental implant case to validate the analytical model (see section 1.1 and chapter 3), it is designed to study a porous coated THR. The main reason is that orthopaedic implants are completely encapsulated within the host tissues, and the infection is more easily controlled than dental implants. Mechanics could be the dominant factor to determine the clinical success rate of orthopaedic implants.

The osseointegrated implants have been applied to extend the service of total hip replacements for younger patients, where some cemented prostheses have failure rates greater than 57% after only five years (Chandler et al. 1981). It is hoped that ingrown bone tissue can fill the pore space and provide strong interfacial bonding through the mechanical interlock. It is also believed that if there is great amount of bone ingrowth and fully osseointegrated tissue can remain in place as much as possible, the implant could achieve a long-term success.

Histological data from porous coated orthopaedic implant studies have not shown fully ingrown bone within the interphase, even after prostheses have been implanted over one year. The amounts of bone ingrowth quantified from animal studies and human retrieval vary with location and are sporadic, ranging anywhere from 0% to 50% of the total available pore space (Hofmann et al. 1993; Galante 1988; Cook et al. 1988, 1993; Bobyn et al. 1987). The causes for the resulting quantity, quality and distribution of bone ingrowth and their effects on the mechanical properties of the interphase are unknown. It has been speculated that the mechanical environment may be a dominant factor influencing bone ingrowth at the interphase (Cameron et al. 1973, Ducheyne et al. 1977, Brunski et al. 1979a,b, Carter and Giori 1991). Local tissue properties may also determine the stress patterns transferred through the interphase. Nevertheless, quantification of the local tissue stress near the interphase has not been performed due to the extremely small scale of the tissue relative to the size of the entire implant and the

intimate contact of bone with rigid biomaterials which hinder the preparation of test specimens.

Moreover, the fatigue strength of porous implants is approximately one-third that of uncoated implants (Kohn and Ducheyne 1990; Yue et al. 1984). Clinical reports have demonstrated that coatings can detach from their substrate (Wevers and Cooke 1987, Cheng and Gross 1988). Debris denuded from implant coatings can decrease the performance of THR, cause adverse tissue reactions, and ultimately, reduce the longevity of the prostheses (Galante et al. 1991). The potential for coating debonding may also be determined by the local non-uniform stress fields resulting from material irregularities and osseointegrated tissue variables such as the depth of bone ingrowth and the tissue heterogeneity (Wolfarth et al. 1991, Pedersen et al. 1991). However, the potential for coating debonding *in vivo* has never been studied. The influence of the osseointegrated tissue on material failure at the interphase remains unknown. The mechanical information available for evaluating the failure risk of currently used porous coated prostheses is insufficient.

This study will focus on the mechanical influences on the bone ingrowth, the material failure, and the tissue damage of the interphase. Once the mechanical nature of the interphase is quantified, expanded applications for porous coated THR can be better explored. Therefore, determining how interphase components affect the mechanical properties of interphases and what the interphase local stress state is will yield valuable information regarding interphase mechanics.

1.1 Objectives

The general hypothesis that will be tested is that the local material and tissue microstructure within the implant/tissue interphase is the major factor determining the local stresses and therefore regulates osseointegration and adaptation, and ultimately the

success of implants. To investigate this hypothesis, the development of micromechanical stress analysis of implant/tissue interphases will be one focus of this dissertation.

The term micromechanics implies that mechanical entities such as stresses and strains can be quantified at a microscopic (1 to 100 μm) level, which is the size range for porous coating particles and osseointegrated tissue microstructure. During the development of the analytical model, I will validate the model experimentally and will use a dental implant to validate the model. Because the dental implant is small, in our case 11 mm long and 3.8 mm in diameter, it can be modeled with standard finite element methods using a sufficiently refined mesh. The stresses obtained from such a fine meshed model can converge to the exact solution, and will be used to verify the analytical model. Once the effectiveness of the model is determined, it can used to study the interfacial micromechanics for a porous coated THR.

Coatings on the surface of THR vary along the stem length of current prosthesis designs (Fig1.2). The most commonly used THR's today are proximally coated (40% coatings) and fully coated THR (80% coatings). One objective of this dissertation is to evaluate whether proximally coated THR can engender more bony fixation at the interphase than fully coated THR. Clinical experience suggests that proximal femoral loosening might occur more readily for the fully coated THR because there is less bone ingrowth at the proximal end than the distal end (Engh and Bobyn 1985). It has been stipulated that the bending stress on the proximal region for a fully coated THR is reduced due to the distal fixation. This reduction may result in less bone at the proximal interphase. Stress analysis, however, has not provided detailed information on interfacial stress fields to support this stipulation.

Before evaluating the quality of the design, I develop a rule which predicts the amount of bone ingrowth within the interphase according to the local strain environment created by the prosthetic implantation. The rule relates mechanics to bone ingrowth

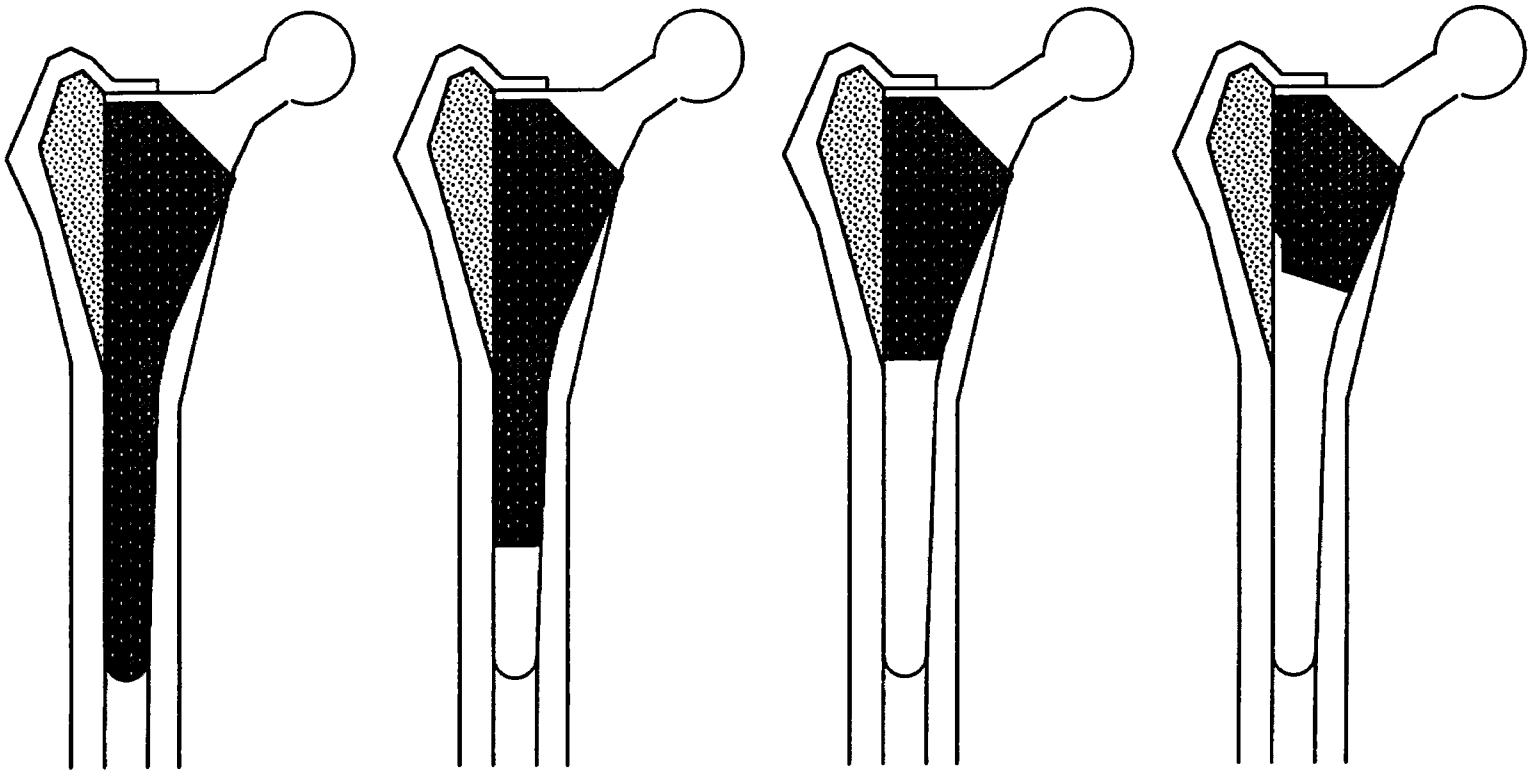

Figure 1.2 Coatings on the surface of total hip replacement have been reduced. Fear of bone resorption and coating debonding leads to a diminished coating only at the proximal region of the stem.

quantitatively rather than qualitatively as is the case with Wolff's law (1892). Therefore, my next objective is to investigate whether tissue strains show statistical correlation with osseointegration. The relationship (ingrowth rule) between the amount of bone ingrowth within the interphase and the local tissue strain will be studied by using a canine tibial model. The canine animal model designed by the Orthopaedic Laboratories, University of Michigan, provides sufficient ingrowth data for statistical analysis. The analogy of long bone remodeling derived from a tibial implant study is applicable to the study of osseointegration of a hip replacement prosthesis. The ingrowth rule will then be applied to the study of coating designs of hip replacements.

Finally, it is hoped that this study will demonstrate the effects of the porous structures of prostheses and ingrown tissues on the stress fields of THR. The results can be used for THR design information in order to prevent material failures or to induce an optimium amount of bone ingrowth at the interphase.

1.2 Literature Review

The literature is full of studies offering solutions to the mechanical problems of implant/tissue interphases. Work in this area can be classified into two major categories: histological evaluation through animal models and mechanical studies of implant systems. Histological evaluations have focused on quantifying bone ingrowth around implants. The causes for the resulting bone ingrowth and their effects on the mechanical properties of the interphase are largely not studied. The subject of this study will focus on the quantification of the mechanical environment which might influence bone ingrowth or is affected by the resulting bone ingrowth at the interphase. Mechanical studies have largely focused on the finite element analysis in order to gain more insight into the mechanisms of biological fixation and postoperative failure.

The finite element analysis is a numerical procedure for obtaining solution to the mechanical analysis of irregular-shaped objects composed of several different materials. Finite element models used in biomechanics are divided into global and local models. Global models contain the entire implant, the anatomy of surrounding bone, and global boundary conditions. Local models, on the other hand, represent a selected region extracted from the global model in order to model the detailed microstructures at that particular region. The literature review in the following section focuses on global and local models used in biomechanics and their advantages and disadvantages.

1.2.1 Global Models

For the last two decades, finite element models (FEM) have been widely used in the mechanical analysis of the implant/tissue interphase. They have also been instrumental in understanding macroscopic mechanical behavior of orthopaedic and dental implants. Andriacchi et al. (1976) and Svensson et al (1977, 1980) analyzed stress distributions on a human femur with a hip prosthesis by using the two-dimensional FEM. Similarly, Weinstein et al. (1976), Cook et al. (1982), Siegele and Soltesz (1989), and Rieger et al. (1990) studied the changes of jaw bone stresses due to dental implantation. These models assumed that all materials were rigidly bonded together. The models generated general stress patterns in the entire prostheses and the surrounding tissue. These analyses located areas of high stress concentration and studied parametrically the length and diameter of the stem necessary to minimize the maximum stress value. However, all of these models failed to characterize the effect of the tissue heterogeneity and the surface architecture of implanted materials on the interfacial stress distributions.

Lately, Huiskes (1986), Rohlmann et al. (1988), Brown et al. (1988), Chen (1991), Weinans et al. (1990), and Harrigan and Harris (1991), Vaillancourt and Johnson (1990) developed models containing non-linear material behavior in the interface to study

the effects on the stresses due to a loosened interface. The interface between the smooth surface of the prostheses and the bone was modeled to undergo sliding or separation when a shear or tensile stress occurred on that interface. Most of these studies were for cemented hip prostheses. For instance, Brown (1988) incorporates a fibrous tissue layer in the interface between the cement and the surroundng bone, and calculates approximately a 30% increase of the stress values in the proximal bone tissue. Only one study was designed to study the mechanical differences between a fully and a partially coated THR (Rohlmann et al., 1988). By using a simplified tube model, Rohlmann found that there was no difference between the proximal bone stress for proximally coated prostheses and fully coated prostheses. Although these non-linear models added loosening into the general elastic models, they were unable still to characterize interphase microstructure effects, such as porous coatings.

Many finite element models have provided mechanical remodeling objectives to predict bone density around an implant (Hollister et al., 1993; Orr et al., 1990; Weinans et al., 1992, 1993). The predicted bone structure of their models is closely correlated to that of human retrieval or results from animal study at the global level. However, in the local regions, these predictions proved to be inaccurate (Hollister et al., 1993).

Overall, the limited information which exists concerning the micromechanics of implant/tissue interphases can be attributed to two factors:

1. Size and Geometric Constraints - Both the complex geometry of roughened surfaces of implants and the small scale of ingrown tissues relative to the whole prosthesis inhibit mechanical simulations. Traditional numerical techniques, i.e. conventional finite element methods, are insufficient for understanding how external loads can be locally transferred to the interfacial tissues and how this interphase may fail under that mechanical usage.

2. Tissue Variables - The ingrown tissues are heterogeneous and vary with depth, distribution, and percentage of available interphase spaces during the service life of an

osseointegrated implant. The involvement of numerous unknown variables may decrease the reliability of global modeling.

These two factors make it difficult to include the heterogeneous microstructures of the interphases into the global models. Knowledge about the mechanical predictions for local bone ingrowth and microdamage within the interphases is therefore limited. However, in many animal studies the number of coating layers and the size of coating particles of implants have been shown to effect the amount of bone ingrowth and shear strength of the interphase (Clemow et al., 1981; Cook et al., 1985). In such instances, analyses of microstructural scale variations for stress and strain are necessary in order to correlate mechanical factors to bone ingrowth on the microscopic level at which histological data is obtained.

1.2.2 Local Models

Recently, finite element analyses assessing coating designs for orthopaedic implants were developed by using isolated, simplified local models which contained one to ten microspheres and a small region of bulk metal, and were resolved under assumed unit tractions (Wolfarth et al. 1990, Pedersen et al. 1991, Messersmith et al. 1990). By using such localized models, Wolfarth (1990) has demonstrated that the variation of stress concentration factors (K_t) is a function of the contact area between porous coating and substrate, and sinterneck radius. Increased contact areas, decreased sinterneck radii, and decreased interparticle distances result in increased K_t.

In addition, Pedersen (1991) showed that the interfacial bone stresses at simulated ingrowth initiation were ten-fold higher than the applied stress on the bone. It is possible that the high local stresses may cause tissue deformation and lead to clinical subsidence of the implant during function.

These results however do not indicate whether the critical areas are located on the medial side, lateral side, proximal end, or distal end of the implants, since local models are not linked to global implant models. Also, these simplified models do not address design parameters such as the length of coating layers.

To further develop the understanding of the micromechanics of the interfacial zone, and the prevention of coating debonding and implant loosening from the point of view of design, local modeling of selected regions of interphases must be coupled with global models of whole implants.

1.3 Composite Theory

Theories of composite mechanics can improve microstructural modeling and overcome the deficiencies of previous finite element studies. In what follows, I will evaluate the Rule of Mixtures (ROM), standard Representative Volume Element (RVE), and Homogenization RVE composite theories. I will show that for the purpose of this study, the homogenization theory most adequately executes the global-local coupling model and accounts for interphase microstructure.

In general, composite theories are developed to describe macroscopic mechanics by accounting for the effect of constituent materials. Some composite theories could be used to estimate the macroscopic material properties of the heterogeneous interphase and to provide estimated interphase properties for a computational model. However, if the estimated properties cannot represent the geometric information about the composite, the results of that global model cannot provide accurate local stress and strain fields. For example, the most common method of investigating the mechanical behavior of a biomaterial interphase is the rule of mixtures (ROM) for calculation of the average elastic properties from the two adjacent bulk materials (Moyle et al. 1973, Ducheyne at al. 1978). The obtained elastic properties are then assigned to the interphase properties in a

finite element model of the whole implant. This estimation of interphase properties is done because of the difficulties in modeling the complex geometry of the biomaterial interphase. My previous studies have shown that the interfacial stress and strain predicted by the rule of mixtures is uniform through the entire interfacial zone (Ko et al. 1992a). However, in a sufficiently refined standard FEM, the interfacial stresses are nonuniform and are perturbed by each thread on the implant. The use of ROM composite theory is therefore insufficient to reveal local stress fields, and as a result, the stress perturbations revealed in the interphase disappeared. Therefore, correlation of stress and strain fields with histological observations can be done on a global scale with only limited detail.

Another composite theory applicable to modeling the interphase mechanics within a whole implant is the Representative Volume Element (RVE) method. The RVE based composite mechanics was introduced by Hill (1963) and also by Hashin (1983). Hill defined the RVE as 1) structurally entirely typical of the composite material on the average and 2) containing a sufficient number of inclusions such that the apparent moduli are independent of the RVE boundary displacements or tractions. In general, RVE approaches decouple the analysis of a composite material into analyses at the local and global levels.

The local level analysis models the microstructural details to determine effective elastic properties. This analysis can also be used to calculate the relation of the effective or average RVE strain to the local strain within the RVE. The composite structure is then replaced by an equivalent homogeneous material having the calculated effective properties.

The global level analysis calculates the effective or average stress and strain within the equivalent homogeneous structure. It is easy to see that such RVE methods coupling local and global models meet the need for studying interphase mechanics.

There exist two RVE composite theories, standard RVE and homogenization RVE. Hollister and Kikuchi (1992) have examined these two theories for conducting

composite analysis. They have compared both methods to a classic finite element model and concluded that homogenization theory predicts more accurate local stresses than the standard RVE approach. As the ratio (ε) of the RVE size to the globai structure dimension becomes smaller, both local and global estimates become more accurate. In bone mechanics, homogenization theory has been successfully used to predict tissue stresses and strains on the trabeculae level (Hollister et al. 1991). In the present dissertation, I have chosen to study implant/tissue interphase mechanics within the framework of the homogenization theory for the following reasons:

1) Homogenization theory was originally developed to analyze the mechanics of composite materials assumed to have a repeating microstructure. Since an idealized implant/tissue interphase composite is most likely periodic in the direction along the interphase (see chapter 2), homogenization theory is shown to be a reliable tool for the study of interphase mechanics.

2) Previous studies (Hollister and Kikuchi 1992) have shown that even though the composite material is only locally periodic and ε is large, the homogenization theory is still preferable to standard mechanics of material approaches for such composites. It will be demonstrated that the homogenization theory provides a feasible analysis for interphase micromechanics even when the nonperiodic nature across to the interphase compositeis considered (see chapter 3).

1.4 Outline of the Dissertation

The goals of this dissertation are twofold. One is the development of an analytical model for interphase mechanics. The proposed model is verified through a comparison of simple models with solutions from standard finite element approaches and is also experimentally validated. The analytical model allows full quantification of the interfacial stresses. The second goal is to evaluate the performances of currently used THR,

measuring bone ingrowth, material failure, and tissue damage in the interphase (Fig 1.3). These two goals are related by using the ingrowth rule, which relates tissue strains to the actual ingrowth data. The rule transforms the mechanical characteristics of the interphase strains to quantitative indicators of measuring the degrees of biological fixation onto an implant. Such indicators are then used for the evaluation of orthopaedic implants in order to predict the long-term bone remodeling effects around a particular implant design.

1.4.1 Mechanical Development

The analytical model provides a solution to the problem of how to quantify the interfacial stresses by accounting for interfacial microstructures. The assumptions used to develop the model are described in Chapter Two. Chapter Three is a discussion of the development of a universal model and reveals the application of such a model for a dental implant and a hip replacement. The experimental protocol designed to validate the efficiency of the analytical model is discussed in Chapter Four. The local results from this analytical model concerning the interfacial stress fields of implants are also verified by using some simplified models in Chapter 5.

1.4.2 Biomedical Applications

The predictions of local stress states from my models provide information necessary for addressing the following biomedical questions: 1) Do tissue strains influence the modulation of the osseointegrated tissues and what is the extent to which they affect the amount of bone ingrowth? 2) How does the amount of mineralized ingrown tissue affect the failure risk of both synthetic materials and ingrown tissue? 3) Do current proximal porous coated THR designs provide a strain field which induces larger amounts of biological fixation in the proximal region than fully coated THRs?

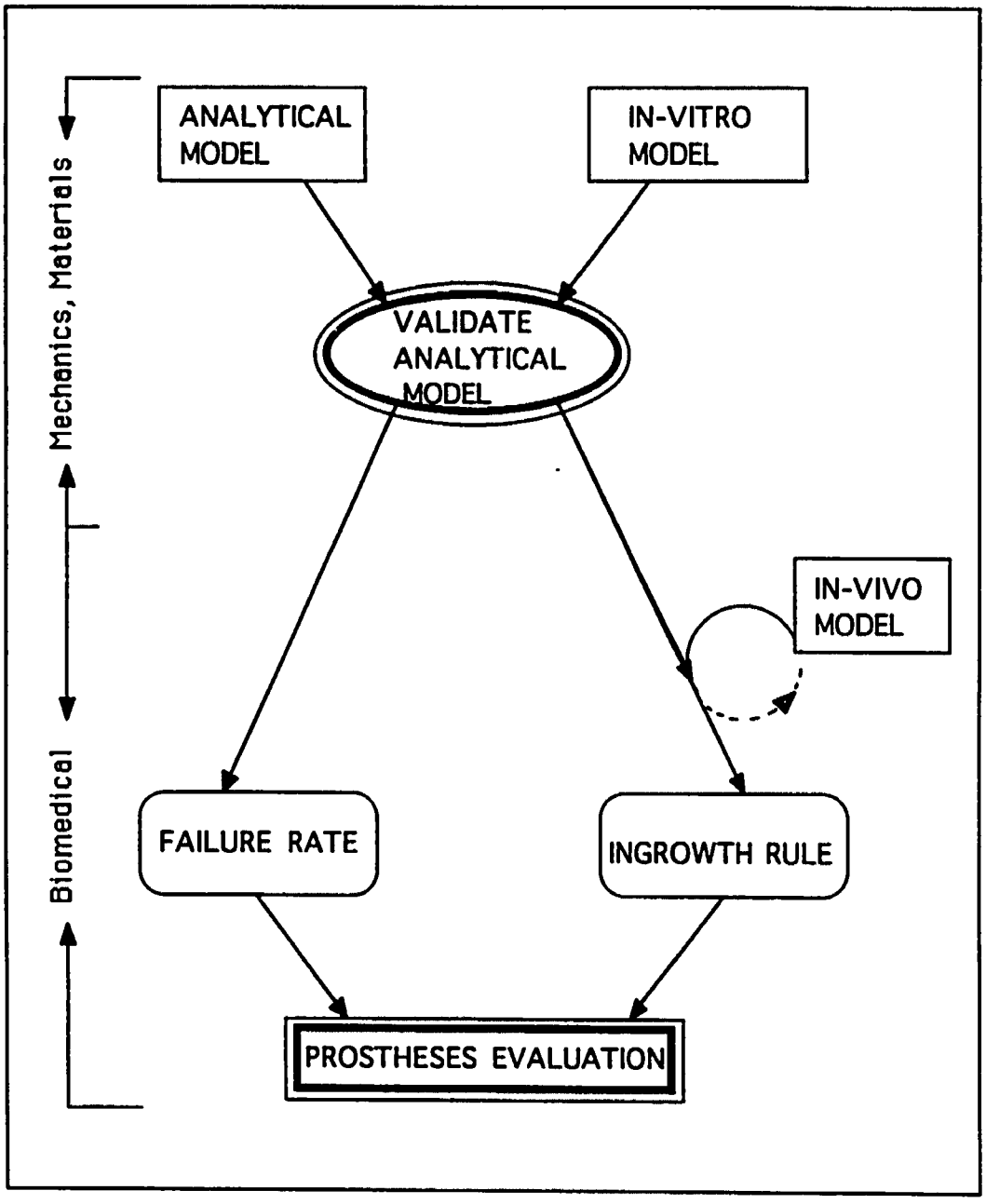

Figure 1.3 Diagram of the dissertation. Two major aspects devoted to the thesis are: the development of an analytical model for interphase mechanics and evaluation of biomedical efforts of currently used THR.

For a better understanding of osseointegration around the implant, I investigate the first question in Chapter Six . The relationship between the level of tissue strains and the amount of bone ingrowth in the interphase is tested statistically using the results of an animal study (Goldstein 1991). The resulting information may be used for the evaluation of commercial implant designs.

In Chapter Seven, the two most commonly used THR designs are evaluated with respect to the predicted amounts of bone ingrowth and the potential failure of each prosthesis. Failure is characterized by the percentage of interphase materials in which the local stress exceeds their yield strength. Both the bead debonding and the microdamage of osseointegrated tissue are estimated for different prosthesis designs.

Finally, Chapter 8 will summarize the clinical implications from this study and make recommendations for future studies.

1.4.3 Chapter Outline

Chapter I - Introduction: This chapter introduces the problems associated with implant interphases and reviews previous research relevant to the current study.

Chapter II - Assumptions: The two major assumptions used in this study are introduced. Evidence in support of these two assumptions is provided.

Chapter III - Analytical Models: The formulation of homogenization theory is briefly reviewed. The development of an interphase model and the modeling scheme are described in this chapter. The application of such an analytical model to a dental implant and hip replacement are demonstrated.

Chapter IV - Experimental Validation: The experimental protocol verifying the elastic constants is developed in this chapter.

Chapter V - Local Stress Validation: The accuracy of the interfacial stresses predicted by the homogenization interphase model is examined through simple models.

Chapter VI - Ingrowth Rule: The relationship between osseointegration and mechaincal stimuli is quantified through an animal model. A minimum strain threshold modulating the remodeling of ingrown tissue is determined.

Chapter VII - Hip Prosthesis Evaluation: The interphase micromechanics of fully coated and partially coated THR are compared.

Chapter VIII - Conclusions and Future Work: Conclusions and limitations of the model are discussed and future directions for research are also recommended.

CHAPTER II

ASSUMPTIONS

2.0 Introduction

The micromechanical analysis accounting for the interfacial microstructure performed in this study rests on two assumptions. The first one is that the initial healing of osseointegrated bone is assumed to be complete and homogeneous, referred to as the **Initial Full Ingrowth** assumption. This assumption is possible because a biocompatible material is selected for the current study. It also serves as a starting point for the construction of the analytical models.

The second assumption is that the interphase is geometrically **periodic**. This allows one to fulfill the boundary condition for mathematical operation in the homogenization theory discussed later in section 3.1.

In what follows, I will discuss the theoretical grounds leading to these assumptions.

Table 2.1 Classification of implant materials

Class	Definition	Examples
Compatible Materials	Release of ions or other constituents influencing the surrounding tissue in an unfavorable, but still tolerable manner	Stainless steel, PMMA-cement, UHMW-polyethylene,
Biocompatible Materials	Release of ions or other constituents not influencing the surrounding tissue appreciably; No unfavorable tissue response	Ti, Co, Cr, Mo
Bioinert Material	No detectable release of ions or any other constituents;	High purity Al_2O_3-ceramics
Bioactive Materials	Ability to bond to bony tissue in the sense of a gluing effect	Calcium phosphate ceramics, some calcium phosphates containing glasses

2.1 Evidence for Initial Full Ingrowth Assumption

For the last three decades, the medical field has seen a variety of implant materials used, including ceramics, metal, and polymers. They can roughly be classified according to tissue response into four categories: compatible materials, biocompatible materials, bioinert materials, and bioactive materials *(Table 2.1)*. Compatible materials may release ions influencing tissue activities, and bioactive materials can alter the healing process in a positive way, such as by providing favorable nucleation sites for mineralization. Both compatible and bioinert materials involve chemical reactions with the implanted tissues. The biocompatible materials cause minimum tissue reaction and can be retained within

the implanted sites without chemically interrupting a normal healing process of surrounding tissues after the surgery. Using such a biocompatible material system in this dissertation offers advantage in the investigation of mechanical adaptation of the surrounding bone for orthopaedic implants because no chemical factors need to be considered.

Biocompatible materials have been widely used in medical practice because they induce minimal tissue response. The best known ones are titanium and titanium alloy, hard tissue implant materials. The current work focuses on evaluation of the micromechanics of titanium implants. The following evidence provides the empirical grounds for the initial full ingrowth assumption.

In the 1960's it was demonstrated that titanium was a biocompatible metal, a quality which made it most suitable for hard tissue replacements (Laing et al., 1960; Brånemark et al., 1969). Compared to other metals, it causes minimum tissue reaction and directly contacts mineralized tissue as observed under light microscopic examination.

In the 1970s Brånemark (1977) conducted a series of studies in rabbits and humans, and showed that in both cases bone apposition on the titanium surface is in direct contact when the interfacial zone was viewed under light microscopy. He then introduced the term of "osseointegration" to indicate the phenomina of interdigitation between the mineralized tissues and the microirregularities of the titanium surface. Subsequent studies confirmed the occurrence of osseointegration (Albrektsson et al., 1983; Sisk et al., 1992; Steflik et al., 1992).

In addition, the influence of the size of the pores on porous coated implants to the bone ingrowth have undergone extensive studies (Clemow et al. 1981; Cook et al. 1985; Welsh et al. 1971; Pilliar 1983). Bobyn (1980a) has shown that pore size in the range from 50 to 400 μm is optimal for bone penetration. Nowadays, it is also widely accepted that if the pore size is greater than 150 μm and there is no relative motion between

implant and surrounding bone during the healing period, the mineralized tissue will fill the pore spaces of the titanium implant.

According to this evidence, the use of titanium material system in this study allows us to assume that there could exist a fully ingrown bone in the interphase if the implant is in an ideal situation, full immobilization, before it is in function .

2.2 Rationale for Periodic Assumption

Recalling the assumption of the initial full ingrowth, a two-dimensional schematic of implant/tissue interphases is shown in Fig 2.1A where all pore space is filled with homogeneous bone. Once I simplify the actual interphase into an ideal uniform composite shown in Fig 2.1B, the synthetic microspheres and osseointegrated tissue are periodically located parallel to the interphase. Each central point of the microsphere was connected using a rigid spring to simulate the interconnectivity of the porous coating in 3D and the high rigidity of the porous coating compared to bone. Such a composite geometrically satisfies the second assumption, periodicity. Two reasons for taking such an idealized periodic composite to characterize implant/tissue interphases are that (i) most of synthetic microspheres can be simplified into a regularly circular shape, (ii) an idealized model is the best assessment for understanding the mechanisms of interphase tissue adaptation and causes of material failure.

Studying an idealized model can provide typical mechanical fields for the typical structure and can allow me to incorporate general rules of failure mechanisms and implant osseointegration. Structural mechanics of osseointegrated tissues and porous materials existing on the implant surface have not been studied analytically yet. It is important for this dissertation to focus on the general mechanisms of material failure and tissue adaptation.

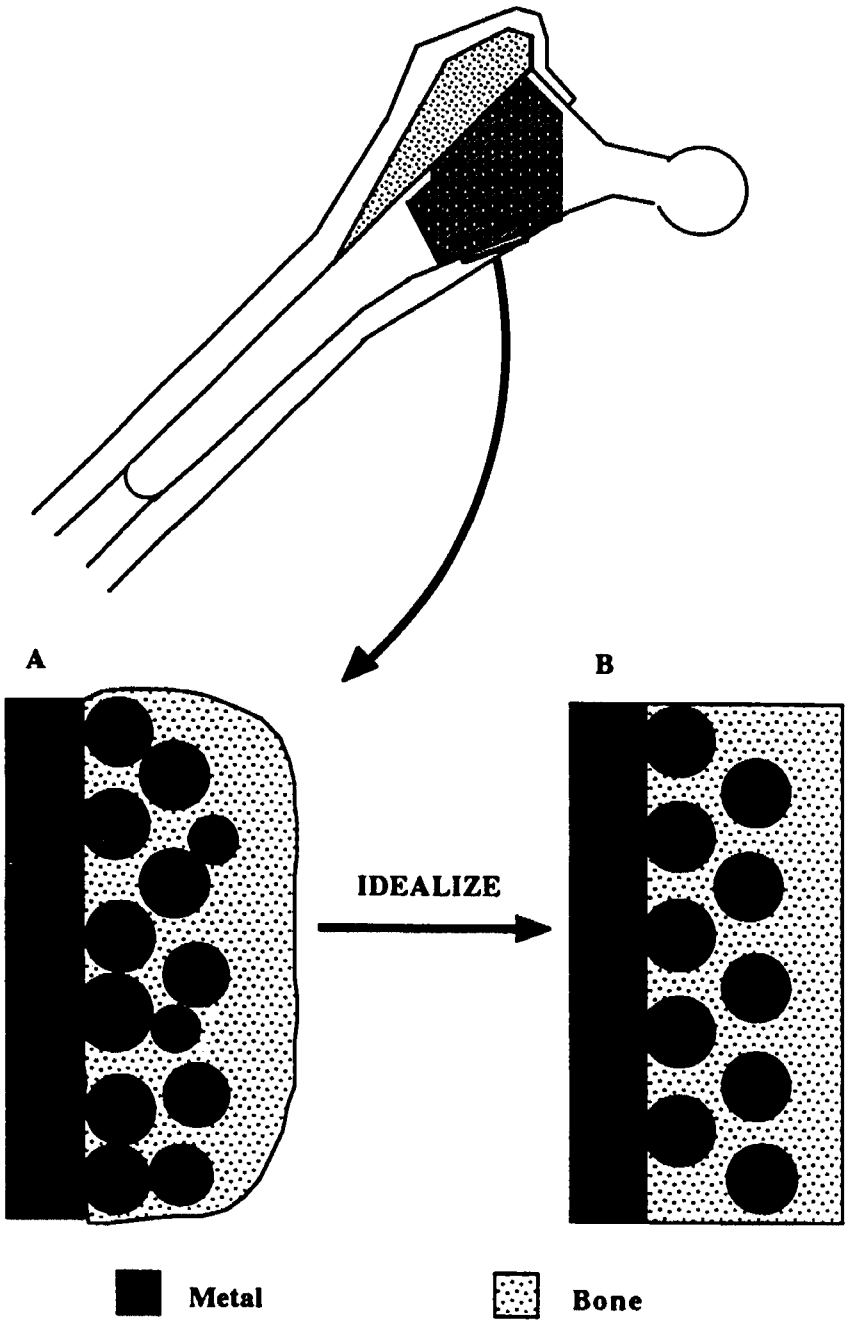

Figure 2.1 (A) Schematic of an actual full ingrown implant/tissue interphase. (B) Periodic interphase microstructure idealized from the actual interphase.

CHAPTER III

ANALYTICAL MODELS

3.0 Introduction

The most efficient method for understanding how interphase mechanics might govern the success or failure of osseointegrated implants is to develop an analytical model which demonstrates how stresses are transmitted through the implant/tissue interphase. The difficulties in developing such analytical models may be attributed to the extremely small size (1- 300 μm) of the osseointegrated entities and roughened surfaces of biomaterials compared to the size of the whole implant. If the interphase micromechanics is analyzed using the finite element method, then the modeling of such differences requires the elements to be of the same scale as the tissue and roughened surface architecture.

Huiskes (1983) and Fyhrie (1986) mention that the meshes of a finite element model must be sufficiently refined with regard to the size of the physiological structure of interest. One goal in this dissertation is to quantify the stresses on the level of coating particles and ingrown tissues. Under such circumstances, the smallest element used to calculate the stress values at the sinterneck of each titanium microsphere, i.e. the contact area between the coating particles and metallic substrate, must be less than 20 x 20 μm.

The same requirement will hold for modeling osseointegrated tissues in order to understand tissue adaptation around the implant. For a two-dimensional FE model of a THR having a dimension of 25 x 8 cm, billions of elements are necessary to model its complicated porous structure on the implant surface. This could be an extremely difficult task with the current computational capability and also be very time consuming .

One way to solve this computational problem is to decouple the analysis into a global and local level of FE modeling. The total number of elements of both the global and the local models can then be reduced to amounts feasible for computation. The framework for global-local modeling is adopted from the composite theory. Rigorous physical linkage of these two models is necessary in order to obtain an accurate result. The process is described in the current chapter, and homogenization theory is employed to perform such global-local study of the interphase mechanics.

In what follows I will first review the homogenization theory. Then, I will develop the homogenization interphase model (HIM) and apply it to quantify interfacial stresses of a threaded dental implant and a total hip replacement (THR). Finally, the conclusions drawn from these applications will be given.

3.1 Brief Review of Homogenization Theory

The homogenization theory was originally developed for analyzing the mechanics of composite media (Babuska, 1976). The microscopic constituents of the composite media are assumed to form a spatially repetitive pattern (Fig 3.1). The basic texture of such a composite can be represented by a unit cell which is very small in comparison to the entire structure. When the body is loaded, the resulting deformation and stresses rapidly vary from one point to another because of small scale of the microstructure relative to the global body size.

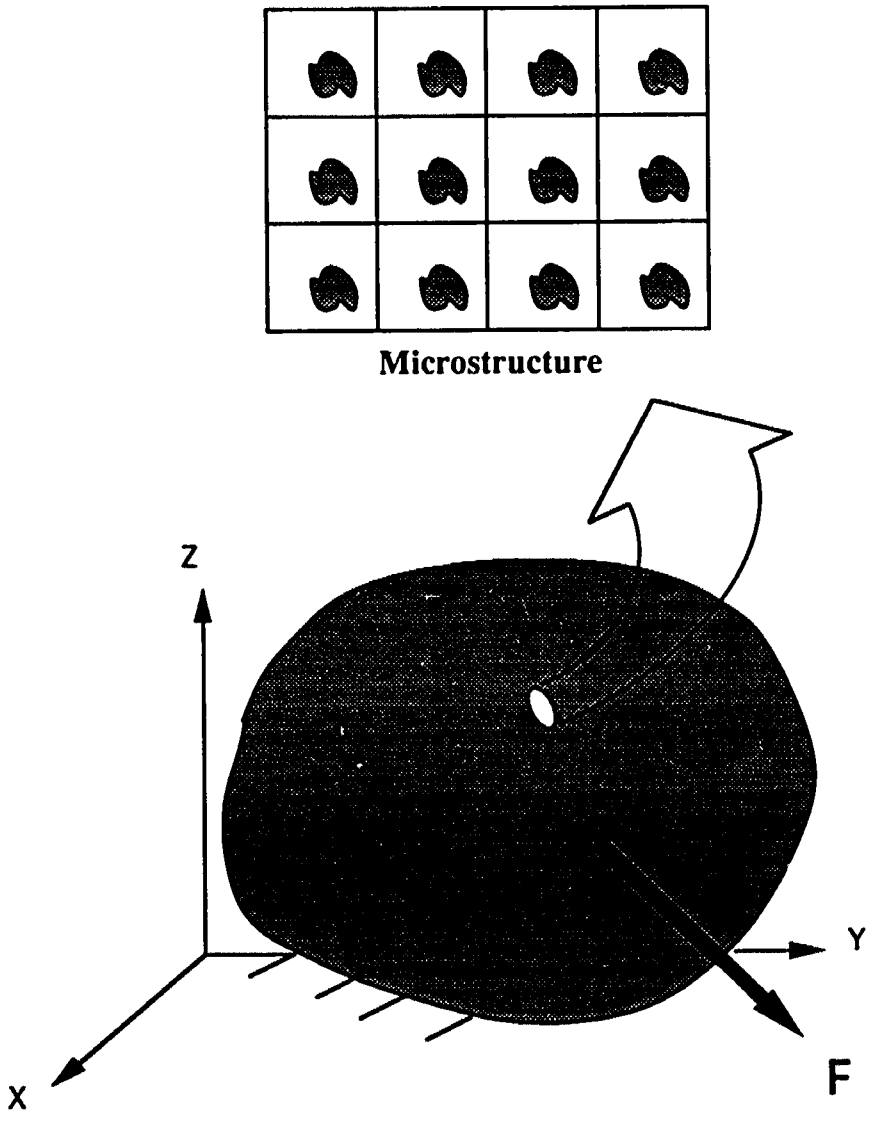

Figure 3.1 Composite having a repeatative microstructure subjects to an external load and a fixed boundary condition.

Two material coordinate systems are necessary to describe such rapidly varying field variables with respect to their locations. One is the macroscopic level x, and the other is microscopic level y. The relationship between these two coordinate systems is expressed in (3.1)

$$y = \frac{x}{\varepsilon} \tag{3.1}$$

where ε is the ratio between the dimension of one unit cell and that of the entire composite.

If the ε is very small, the total displacement, u^{ε}, on the internal point of the composite is a function of both x and y and can be expressed using the asymptotic expansion:

$$u^{\varepsilon} = u^{0}(x, y) + \varepsilon u^{1}(x, y) + \varepsilon^{2} u^{2}(x, y) + \ldots\ldots \tag{3.2}$$

where u^{0} is the macroscopic or global displacement, u^{1}, u^{2}, ... are perturbations in the displacements due to the microstructure. u^{ε} can be incorporated into the weak form of the equilibrium equation for classic mechanics given below:

$$\int_{\Omega^{\varepsilon}} C_{ijkl}\, \varepsilon_{ij}(v)\, \varepsilon_{kl}(u)\, d\Omega^{\varepsilon} = \int_{\Gamma} t_i v_i d\Gamma \tag{3.3}$$

where Ω^{ε} represents the total macroscopic domain plus the microscopic domain of the composite media, and t_i represents global tractions. ε is obtained by applying the small strain-displacement relationship

$$\varepsilon_{ij}(u) = \frac{1}{2}\left(\frac{\partial u_i}{\partial x_j} + \frac{\partial u_j}{\partial x_i}\right). \tag{3.4}$$

The detailed operations of substitution and expansion of the weak form equation are discussed in the literature (Guedes and Kikuchi, 1990; Hollister and Kikuchi, 1992). Important results derived from the weak form equation are the microscopic equilibrium equation

$$\int_{\Omega^e} C_{ijkl}\varepsilon^1_{ij}(v)\,(\overline{\varepsilon_{kl}} + \varepsilon^*_{kl})\,d\Omega^e = 0 \tag{3.5}$$

and the macroscopic equilibrium equation

$$\int_{\Omega} C^h_{ijkl}\varepsilon^0_{ij}(v)\,(\overline{\varepsilon_{kl}} + \varepsilon^*_{kl})\,d\Omega^e = \int_{\Gamma} t_i v_i\, d\Gamma \tag{3.6}$$

where ε^0 represents the virtual strain at the macroscopic level,

ε^1 represents the virtual strains at the microscopic level,

$\overline{\varepsilon}$ represents the macroscopic strain tensor, and

ε^* represents the fluctuating strain due to the microstructural repetition.

Guedes (1990) and Hollister (1992) have recently solved equation (3.5) using finite element implementation; from there they derive the effective elastic constants (C_{ij}), equivalent to C^h_{ijkl}, and a relation tensor (M_{ijkl}) between global strains and local strains for the composite. The M_{ijkl} which carries the information for material microstructures was named the *local structure matrix* (Hollister and Kikuchi 1992). However, it is important to notice that the solution of such an equation depends on the assumption for periodicity of the field variables. The periodic condition indicates that the deformation on the edge of each unit cell is equal to that on the opposite edge.

The macroscopic equilibrium equation (3.6) can be solved by using any standard finite element method. The resultant global (macroscopic) strains can then be converted into the local (microscopic) strains through the following equation:

$$\varepsilon_{ij} = M_{ijkl}\varepsilon_{kl} \tag{3.7}$$

Within the homogenization theory, the linkage between the global and local physical quantities, for e.g., stresses and strains, is mathematically rigorous because equation (3.5) and (3.6) are derived from the same equilibrium equation (3.3). With regard to the local strain energy density of a composite body, this theory makes more accurate predictions for periodic composites than other composite theories (Hollister and Kikuchi 1992).

3.2 Homogenization Modeling Scheme

The flow chart shown in Fig.3.2 reveals the practical sequence of FE modeling employed by the homogenization theory. Within the diagram, the localized unit cell model represents the finite element implementation of the microscopic equilibrium equation (3.5); the global model represents the finite element implementation of the macroscopic equilibrium equation (3.6). The selection of a correct representative microstructure of the composite is crucial for the construction of a local model. Analysis of the local model under characteristic unit normal and shear strains gives the effective interface stiffness and the local structure matrix M_{ij}, where the subscripts of the M_{ij} indicate the direction in Cartesian coordinates. M_{ij} represent the influence of the global strain $\overline{\varepsilon_j}$ on the local strain ε_i.

The global model is solved by inputing the C_{ij}, derived from the local model, into the corresponding composite regions. The resultant global strains are then mapped onto the local model and local strains are calculated by the assembly of the local structure matrix.

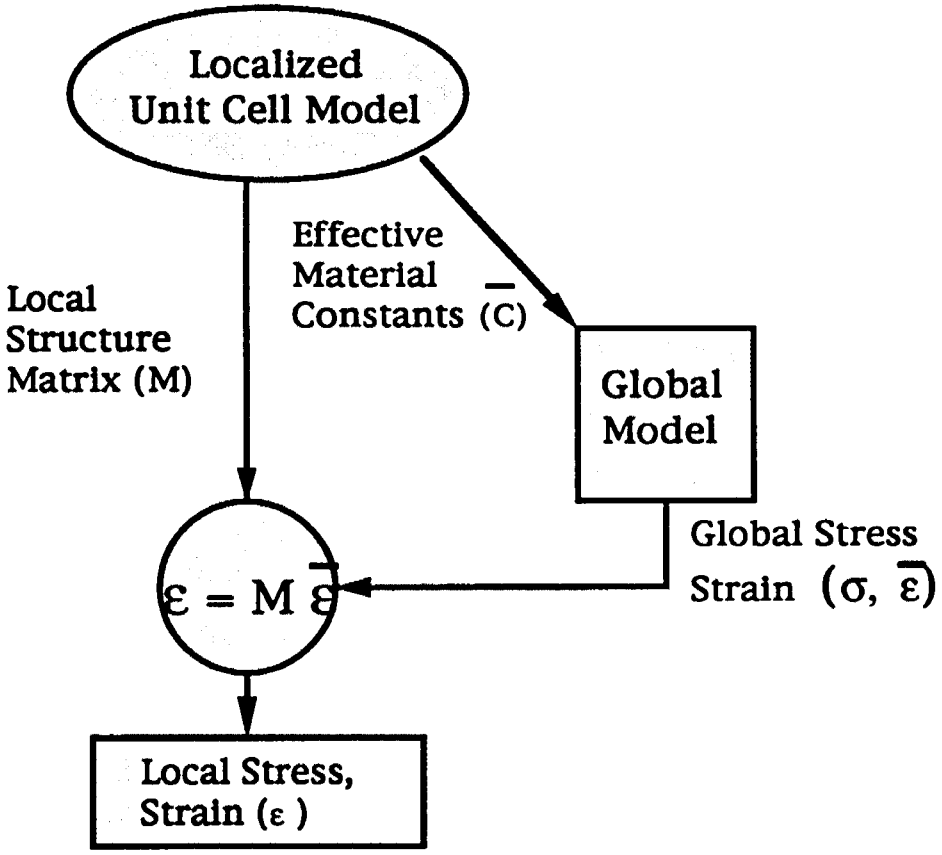

Figure 3.2 Flow chart of homogenization modeling scheme. The local model and the global model are coupled through the effective material constants and local structure matrix.

The global-local modeling scheme is used throughout the dissertation. In what follows, I will discuss two practical implant models of a dental implant and a hip implant. Both models follow the scheme described in this section.

3.3 Analysis of a Dental Implant

3.3.1 Local Model and Periodic Constraints

The schematic drawing of the interphase, Fig 3.3A, shows the repeating structure of an ideal synthetic material and an ideal osseointegrated tissue of the interphase. Based on the idealized structure, a representative microstructure was proposed and formulated into a unit cell model, UCM *(Fig 3.3B)*.

A two-dimensional 1200 x 600 μm UCM was developed. It included part of the implant substrate, one thread, and ingrown tissue. Each of these materials was assumed to have homogeneous, isotropic material properties (Table 3.1) and be rigidly bonded. The depth of each thread was 350 μm, similar to that dimension of Brånemark implants.

Quadrilateral elements were employed to discretize the whole unit cell and construct the FE local model. The smallest element size in the model was 10 x 10 μm, as this is the scaling of the tissues under investigation. Periodic constraints were used along the edges of the cells.

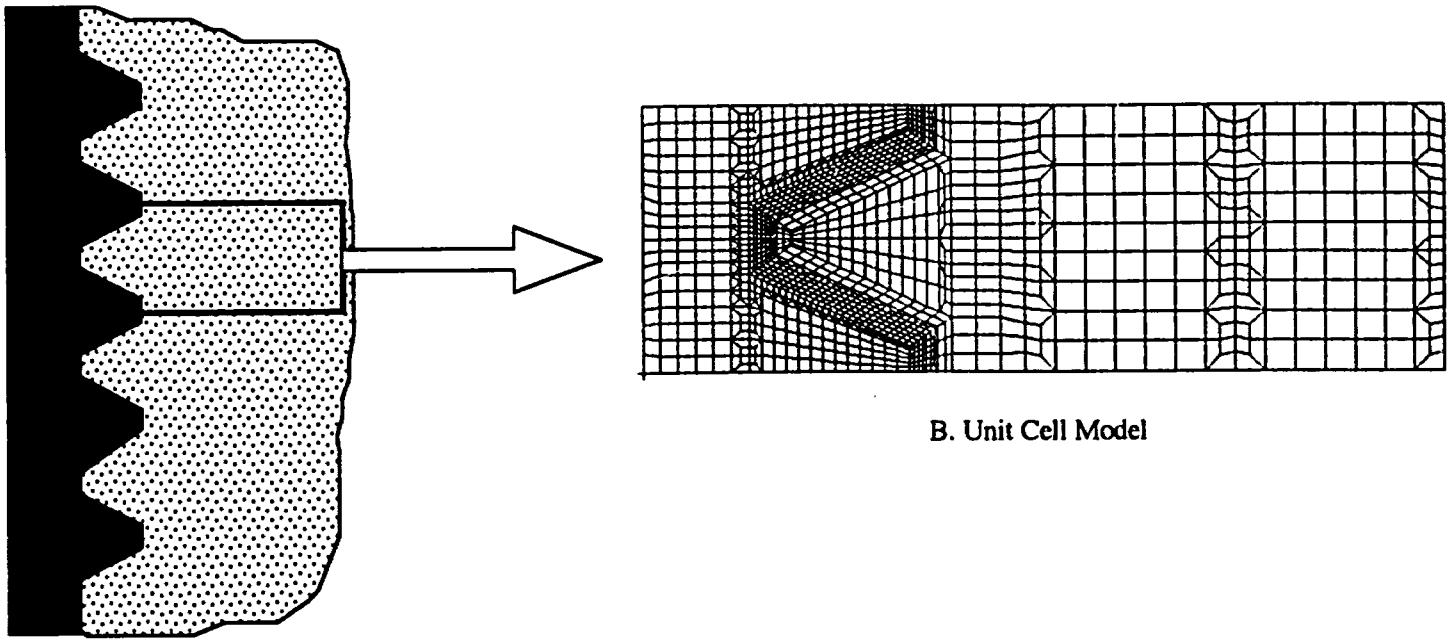

B. Unit Cell Model

A. Ideal Interphase

Figure 3.3 Schematic of the ideal interfacial zone of a screw thread dental implant (A), and the meshes of a unit cell model extracted from the ideal interphase (B).

Table 3.1 Material properties used in the dental implant finite element models

Material	E (GPa)	υ
Bone	5	0.33
Titanium	110	0.3

3.3.2 Effective Elastic Constants

The resultant elastic constants of the interphase calculated using homogenization theory are listed in *Table 3.2*. It is important to note that although both the tissue and metal were assumed to be isotropic, the resultant elastic constants for the composite interfacial zone indicate orthotropy.

E_{11} represents the computed interphase modulus in the horizontal direction which is the direction along the long axis of the dental implant. E_{22} represents the vertical interphase modulus which is in direction perpendicular to the long axis of the dental implant. The study shows that E_{22} is larger than E_{11} which implies that external

Table 3.2 The resultant elastic constants of dental implant

E_{11}	1.53 GPa
E_{22}	16.75 GPa
E_{12}	0.54 GPa
υ_{12}	0.03
υ_{21}	0.31

loads acting on the dental implant are transmitted more vertically than horizontally through the interphase .

3.3.3 Local Structure Matrices

The resultant local structure matrices represent the characteristic function of the local strains due to the microstructural influence. Plots of the local structure matrices for the UCM are shown in *Figure 3.4*. For the component of the normal load directed through the interphase perpendicular to the direction of the applied load, the strain is concentrated at the point where the tissue contacts the outer edge of the thread. For the component of the normal load directed along the interface, the strain is concentrated in the tissue at the interior points of the thread. The highest strains in the interphase are four times the global strain values and occur under the normal loads through the interface zone. In the case of shear loading, strains are again concentrated at the point where the tissue contacts the outer edge of the thread. The values of the local structure matrix relating the local to the global strains (i.e., the characteristic function of the local strains)

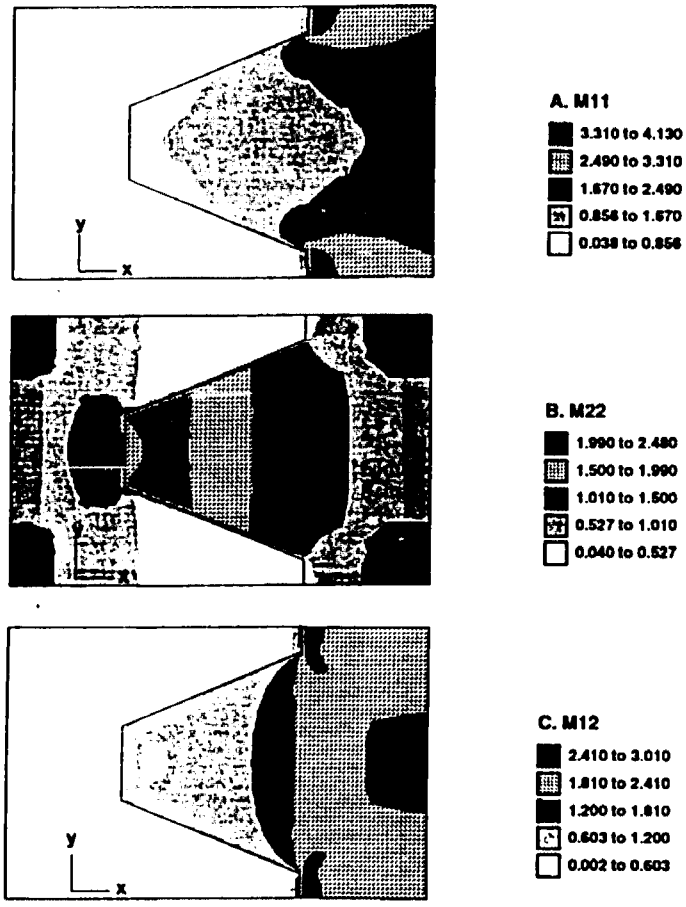

Figure 3.4 Plots of the local structure matrix for the dental implant unit cell model. (A) M_{11} revealed the local normal strain contour corresponding to the normal loads directed through the interface zone, (B) M_{22} corresponding to the normal loads directed along the interface, and (C) M_{12} corresponding to the shear loading.

of the tissue between two threads due to shear loading is less than 1.8. These values continuously decrease toward the interior surfaces of the thread. This result implies that local strains on the tissue in these areas should be minimal when a pure shear load exists. Albrektsson et al. (1983) noted a similar stress prediction based on the theoretical assumption for a pure shear load along the interface. This dissertation, however, provides an analytical visualization of the above strain patterns. A local stress and strain field of implant/tissue interfaces therefore can be obtained from the global strains through the characteristic functions.

3.3.4 Global Model

A titanium dental implant, 11 mm long and 3.8 mm in diameter, was constructed for the global model *(Fig 3.5)*. A homogeneous interphase with equivalent elastic constants obtained from the local model was employed . The global model was assumed to have direct bone/implant contact and a rigidly bonded interface. The bone core was 5 mm in radius from the implant surface. A plane stress model was built by means of quadrilateral elements. Titanium and bone were assigned Young's moduli of 110 GPa and 5 GPa, respectively, with Poisson's ratios of 0.30 and 0.35, (Ashman and Van Buskirk, 1987). All materials were treated as being homogeneous, isotropic, and linearly elastic. Distributed vertical displacements of 0.01 mm were applied to the top surface of the implants. The bone below the apex was taken to be fixed in all degrees of freedom. The model was solved by using standard finite element code Abaqus (Hibbitt, Karlsson and Sorensen, Inc.). The global interfacial strains obtained from this analysis were then used to calculate local interfacial strains and stresses through the equation (3.7).

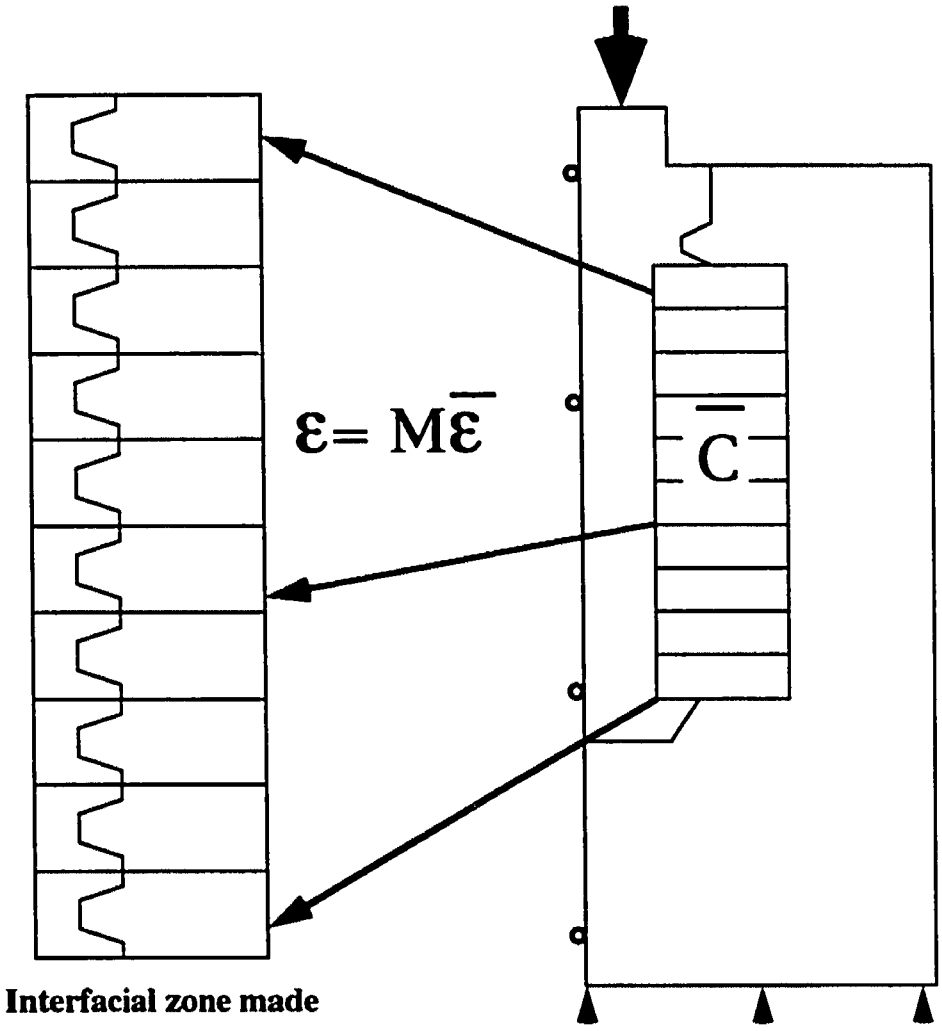

Figure 3.5 Homogenization interphase models of a dental implant included a global model with a homogeneous interfacial zone and localized unit cell models.

3.3.5 Resultant Interfacial Stresses

Shown in Fig 3.6 are the resultant local equivalent stresses of the interphase of a threaded dental implant computed from the homogenization global-local coupling scheme. The Mises stresses are concentrated at the bone near the tip and bottom surface of each thread. The bone near the upper surface of each thread sustains the smallest load transfer along the groove where it was located. The values of the stress gradually increase from the coronal region to the apical region of the prosthesis.

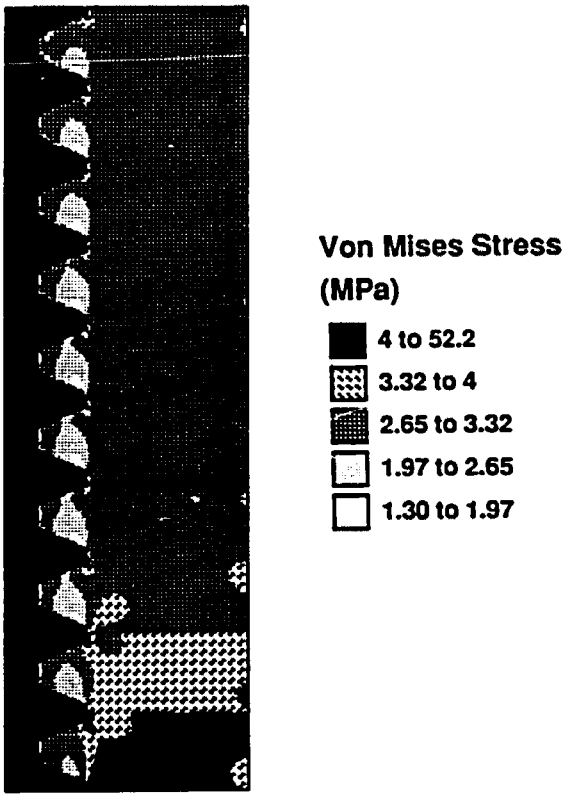

Figure 3.6 Interphase von Mises stress contour of the homogenization dental model. The non-uniform stress pattern was shown within each groove between the threads.

3.4 Analysis of a Hip Implant

3.4.1 Local Model and Periodic Constraints

For the porous coated THR, the two-dimensional UCM consisted of a part of the implant substrate, two microspheres, and surrounding tissue (Fig3.7). The diameter of each microsphere was 300 μm and a pore size of 200 μm was modeled. The full dimension of the unit cell was 910 x 910 μm. The microspheres of porous coatings on a hip prosthesis are sintered at high temperature, and contact each other to form a three-dimensional network. A rigid spring having a spring constant of 10^{11} was placed across each central point of the microsphere to simulate the interconnectivity of the porous coating in 3D and the high rigidity of the porous coating compared to bone.

The material properties and interface conditions among different materials were the same as those in the dental implant model. Periodic boundary conditions were also restrained along all edges of the UCM. The homogenization theory was employed to analyze the UCM.

3.4.2 Effective Elastic Constants

The effective elastic constants computed from the unit cell homogenization model were shown in *Table 3.3* E_{22} was larger than E_{11} and also demonstrated that load transfer was preferred vertically.

Table 3.3 The resultant interphase elastic constants of THR

E_{11}	2.26 GPa
E_{22}	25.69 GPa
E_{12}	0.81 GPa
υ_{12}	0.03
υ_{21}	0.29

3.4.3 Local Structure Matrices

Plots of the resultant local structure matrices, which determine the local strain distribution resulting from the global strain are shown in Figure 3.8. For normal loads directed through the interfacial zone, strain is concentrated at the point where the tissue contacts the outer surface of the microsphere. For normal loads directed along the interface, strain is concentrated in the tissue between the microspheres. In the case of shear loading, strains are concentrated at multiple points around the circumference of the microsphere. The highest strains in the interphase region are two times the global strain values. The values of this mapping tensor are coupled with global strains to calculate local interfacial stresses.

3.4.4 Global Model

A Ti-6Al-4V THR with a porous coating on the proximal-medial and lateral sides was also developed (Fig 3.9). A concentrated force of 3000 N was applied at the femoral

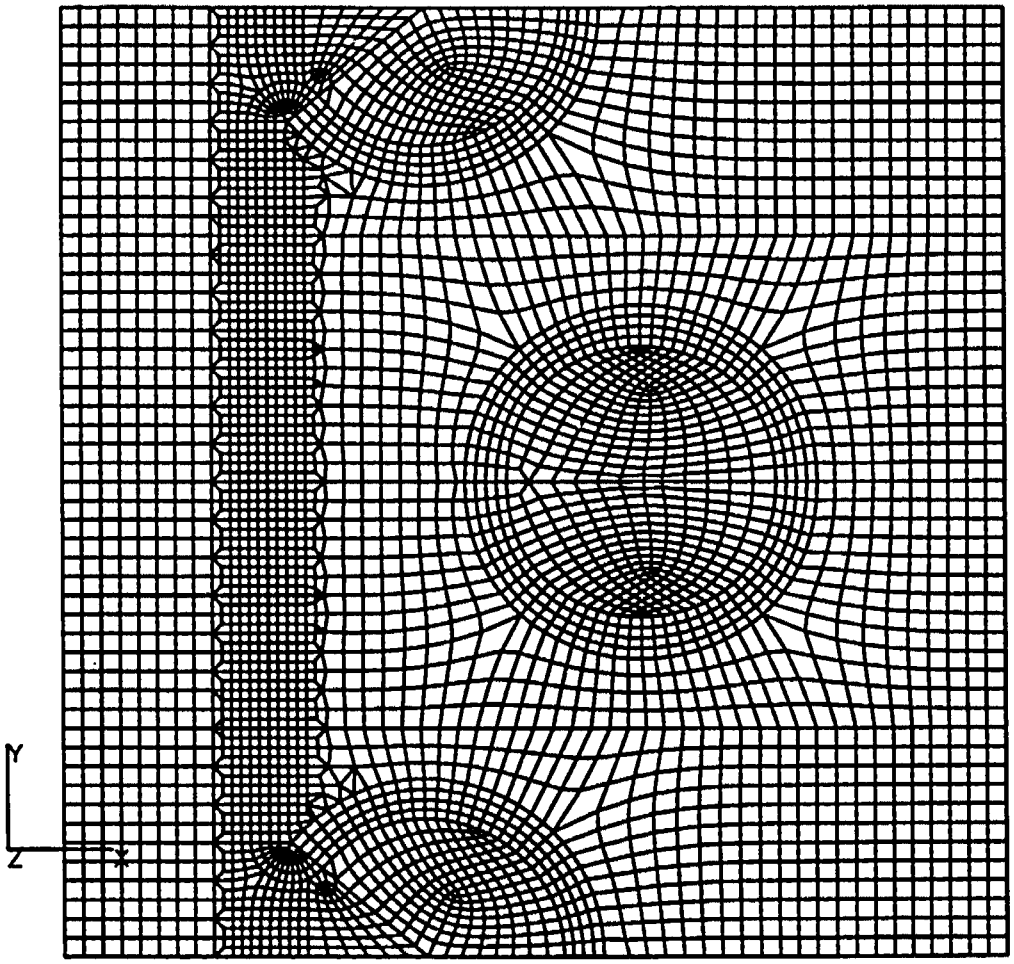

Figure 3.7 A two-dimensional unit cell model of the representative interphase of the porous coated THR consisted of a part of the implant substrate, two microspheres, and surrounding tissue.

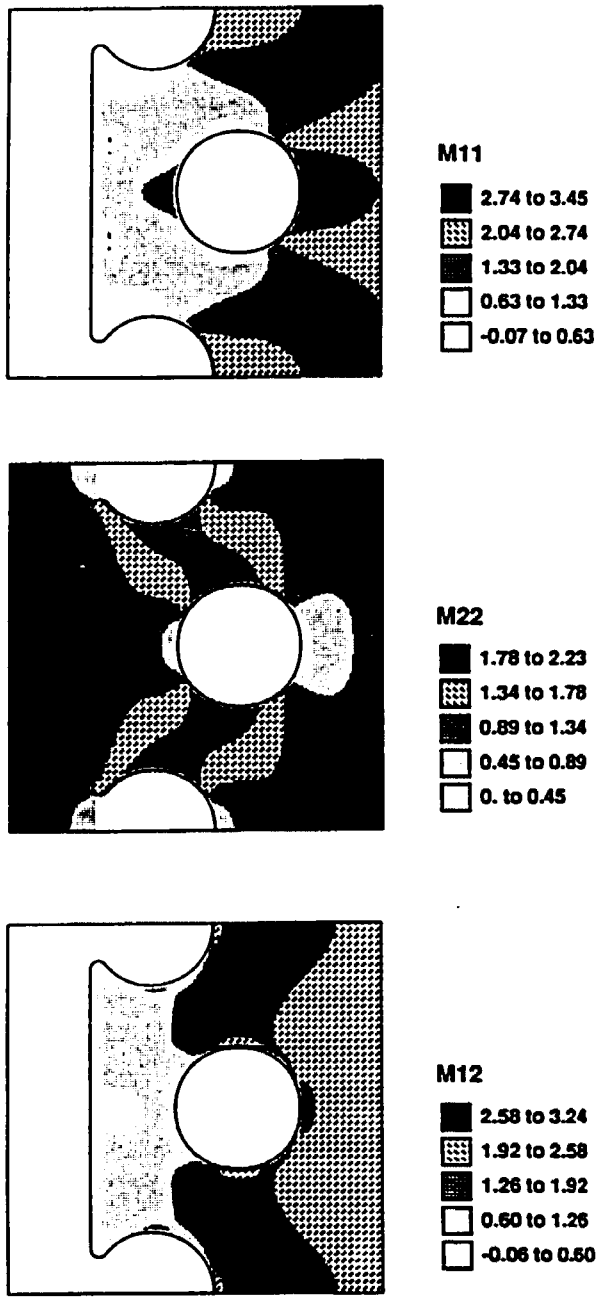

Figure 3.8 Plots of the local structure matrix for the THR unit cell model. (A) M_{11} revealed the local normal strain contour corresponding to the normal loads directed through the interface zone, (B) M_{22} corresponding to the normal loads directed along the interface, and (C) M_{12} corresponding to the shear loading.

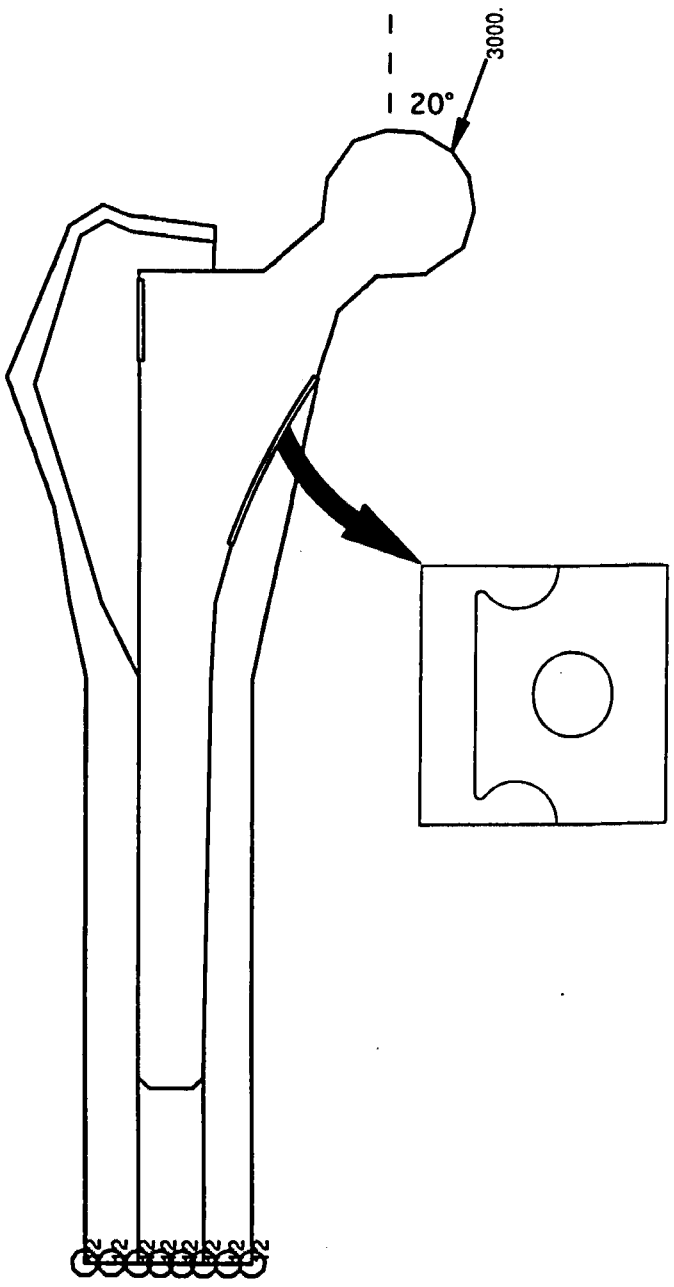

Figure 3.9 The medial-lateral section of the human femur with a total hip replacement. The global model was solved by using a standard finite element method where the interfacial zone was coupled with the homogenization unit cell model.

head at an angle of 20 degrees. The bone at the distal end was fixed in all degrees of freedom. All bulk materials were assumed to be homogeneous and isotropic. The interfacial zones near the two porous coated regions were given the effective properties calculated from the local model and all materials were assumed to be rigidly bonded. Global stresses and strains were then calculated by the standard finite element approach.

Shown in Figure 3.10 is the resultant global Mises stress contour. The equivalent stresses are concentrated on the medial and lateral surfaces of femoral neck as well as the proximal part of the prosthesis. The maximum equivalent stress, 80 MPa, is located at the medial surface of the femoral neck. The global strains from each point of the interfacial zone are used to compute the local stresses and strains through the global structure matrix obtained from the unit cell models.

3.4.5 Resultant Interfacial Stresses

On both the lateral and medial sides of the hip prosthesis, the local equivalent stresses in metal are concentrated at the sinternecks (Fig 3.11). Medially, the maximum stress, 269 MPa, is about 50 times higher than the global value at the same position. The local equivalent stresses in bone tissue are concentrated on the areas between microspheres and where the tissue contacts the outer surface of the microsphere. This is because compressive stresses dominate along the interface in this region. The maximum bone stress, 5.7 MPa, is about 5% higher than the global value. The other parts of the bone have stresses less than the stresses predicted by the global model. The global model yields average stresses and strains and it is therefore expected that the local model will yield results both above and below this average value.

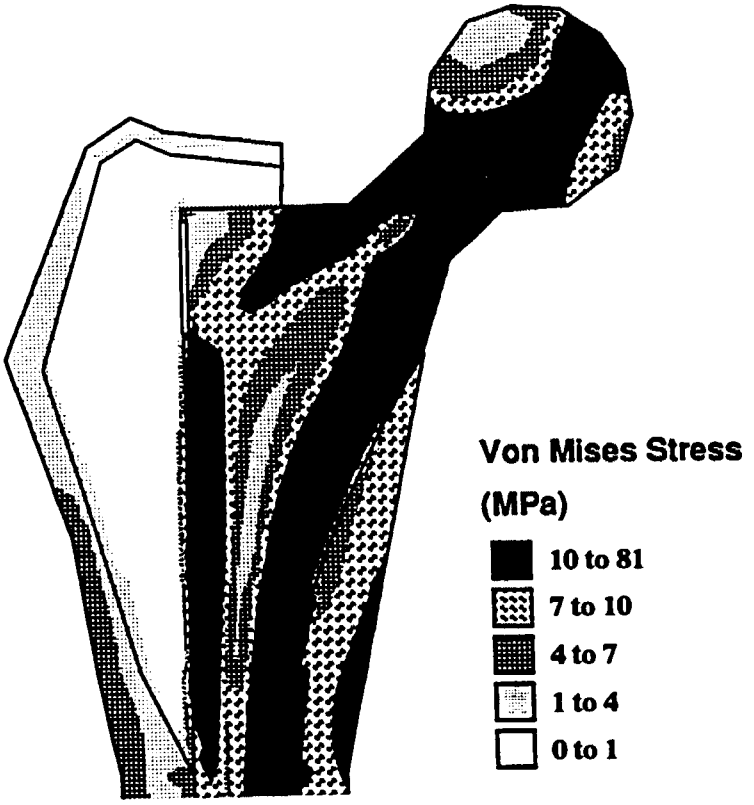

Figure 3.10 Plots of the resultant von Mises stress contour obtained from the global THR finite element model. The Mises stresses are concentrated on the medial and lateral surfaces of femoral neck as well as the proximal part of prosthesis.

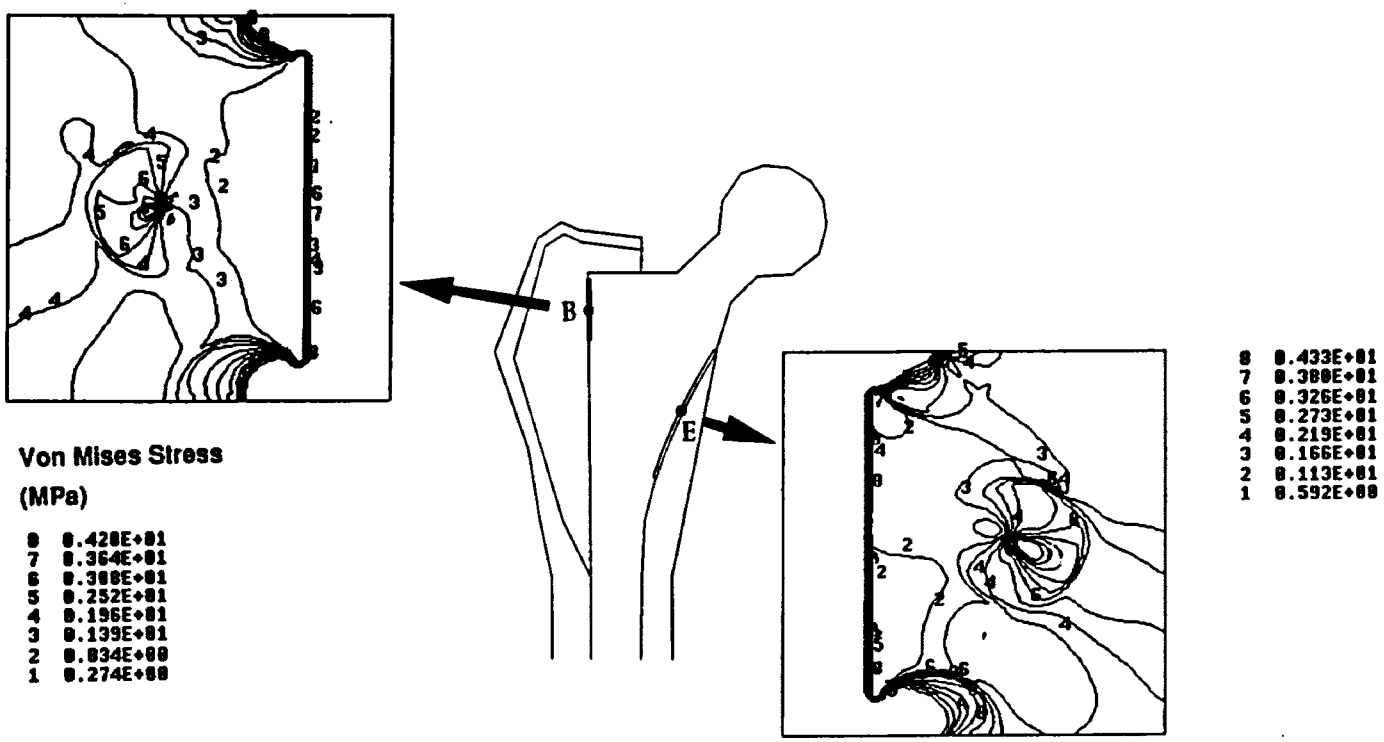

Figure 3.11 Local interfacial stresses are concentrated at the sinterneck. Medially , at the point E, the maximum stress is 50 times greater than the global value at the same position. Laterally, at the point B, the stress values are lower than those at medial side, but the stress distribution reveals a very heterogeneous feature.

3.5 Discussion

The homogenization method is advantageous because it is based on a rigorous mathematical theory reviewed in section 3.1. Two examples, a dental implant and a hip implant, have demonstrated that this method can provide solutions for interphase micromechanics. Results showed that the interphase composite was mechanically orthotropic and the stresses within the interphase were non-uniform. These results imply that load transfer from the implant to the tissue is direction oriented, and interphase failure pattern could be localized because stresses are concentrated on specific sites.

For both the dental implant and hip replacement, the local structure matrices revealed the same tendency. For normal and shear loads directed along the interfacial zone, the strains were concentrated on the outer surfaces of the threads and coating microspheres. In the case of normal loads directed through the interface, strains were concentrated in the tissue between the threads or between the microspheres. The strain concentration between two microspheres may be attributed to the rigid spring which is placed between the microspheres. The strain values may be overestimated in the idealized two-dimensional model. Overall, the results are considered reasonable since Albrektsson (1983) predicted a similar strain distributions based on the theoretical assumption for a pure shear load along the interface. The current results provide the detailed information about the distribution of local strains.

For the hip prosthesis, the stresses were concentrated on the bone near the outer surfaces of the coating particles and the sinterneck regions on the metal substrate. The importance of these results and relation to clinical findings is discussed in Chapter Seven in relation to specific hip problems.

The goal of this dissertation is to use this mechanical information to provide the solutions for the following physiological questions: i) Do tissue strains influence the modulation of the osseointegrated tissues and what is the extent to which they affect the

amount of bone ingrowth? ii) How does the amount of calcified ingrown tissue affect the failure risk of both synthetic materials and ingrown tissue? iii) Do current proximal porous coated THR designs provide a strain field which conducts larger amounts of biological fixation in the proximal region than a fully coated THR? Before I can apply the homogenization interphase model to answer the questions, I need to be aware of how accurate the predicted solutions are.

The violation of the periodicity assumption for the interphase geometry in the homogenization theory might result in an inaccuracy of the predicted stiffness and local stress. Although the ideal interphase discussed in section 2.2 is geometrically periodic in the direction along the interphase, it does not contain any repeating structures across the interphase. It is not known how well the theory can be used specifically for the interphase mechanics to predict E_{ij} and σ_{loc}.

The accuracy of the predicted E_{ij} will affect the accuracy of resultant global strains which have lately been used to compute local stresses. The accuracy of the σ_{loc} will determine the trust of the answer to the physiological questions.

However, in the results of our dental implant model the predicted stress patterns from the homogenization theory were consistent with those reported by Siegele (1989) and Rieger (1990). This sets the ground for us to believe that our analysis is on the right track.

Chapters four and five will provide validations to the E_{ij} and σ_{loc}.

3.6 Summary and Conclusions

Freeman and Tennant (1990), Huiskes and Chao (1983), Oh (1988), Skalak (1983), and Spector (1988) have suggested that the interfacial stress distributions are one of the most important factors controlling the success and failure of the hip prostheses. But there is no evidence to support such a speculation. The quantitative analysis of the

interphase mechanics accounting for the synthetic material architecture has been studied on the dental implant because it has a very small dimension, about 3 x 10 mm, for the whole implant. For large prostheses, such as tibia and hip replacements, the effect of porous coating architectures on the interfacial stresses remains unknown.

However, our THR model reveals detailed stress distribution around the synthetic microspheres, and makes significant relation to clinical findings discussed lately in Chapter Seven. Mechanical characteristics of implant/tissue interphases found from this part of the study are summarized below:

(1) Homogenization theory predicts an orthotropic interface stiffness, E_{ij}, even when the tissue and metal components are isotropic. Such an orthotropy might determine load transfer patterns and might also dictate failure patterns of interphases.

(2) Localized modeling of the interfacial zone, based on homogenization theory, has shown that stresses and strains within the zone are nonuniform. Such modeling accounts for stress and strain inhomogeneity and predicts regions of stress concentration and potential microfailure. Furthermore, the interfacial zone can now be modeled with a level of specificity that can account for histological changes in a whole implant model.

(3) The local interfacial stresses, σ_{loc}, are a strong function of the local implant and tissue architecture as well as global location and loading condition. Stress distributions on the interfacial bone tissue of the hip prosthesis are inhomogeneous and have values between 10% and 150% of the stresses predicted by the global model. The maximum local stress occurs in the metal and is several times (2 to 4) greater than the maximum global stress.

Compared to previous models listed in section 1.2, HIM not only provides more detailed stress information accounting for the interphase microstructure, but the results also reflect the effect of global shape and loading conditions on local stress distributions.

CHAPTER IV

EXPERIMENTAL VALIDATION

4.0 Introduction

The interphase between two adjacent materials exhibits its own unique response to the application of loads. This unique response mechanically distinguishes the interphase from the individual constituents. By using the homogenization theory, I have previously shown that the implant-tissue interphase composite is macroscopically orthotropic (see Chapter III). However, these results have not been experimentally validated. The experimental work proposed here is designed to validate the E_{ij} with respect to the following issues: can the homogenization theory predict the elastic constants of the interphase composite correctly and, does the change of composite constituents affect the resultant interphase stiffness?

Bimaterial composites consisting of titanium and epoxy resins were developed to mimic the composite of the porous implant/tissue interphase *(Fig 4.1)*. The metal component of the metal/resin composite included a piece of bulk metal and metal microspheres, and the architecture of this composite was the same as that on the surface of porous coated implants. Such a composite system represents the actual microstructure of a commercial THR, and makes the test results more clinically meaningful.

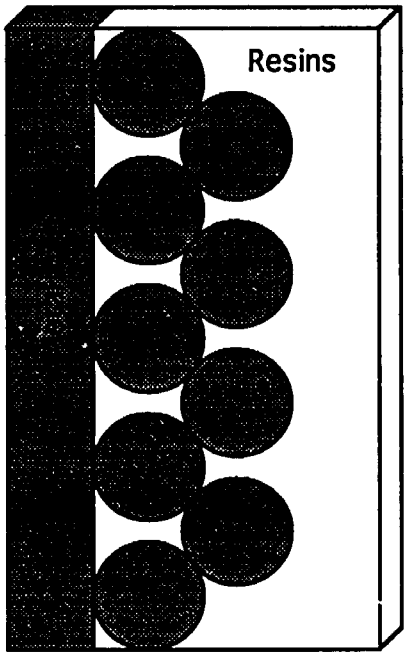

Figure 4.1 Metal-resin interphase composite

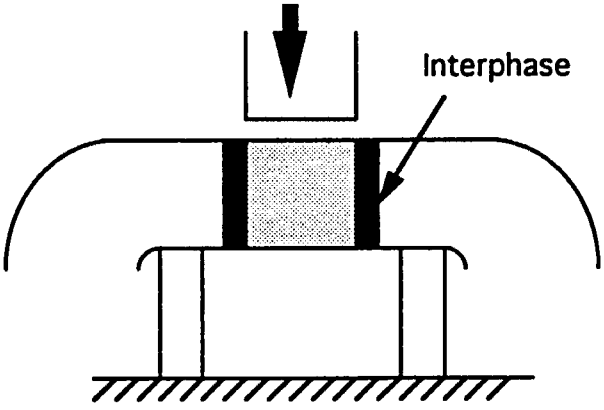

Figure 4.2 Diagram of push out test

Resins were used to eliminate variability of tissue stiffness within the testing samples. Animal studies have shown that the ingrown tissues are heterogeneous and vary in depth, distribution, and percentage of available interphase spaces during the service life of an osseointegrated implant. The large number of variable parameters involved in the implant/tissue composite obtained from an animal study could reduce the reliability of the testing results obtained from the mechanical tests. In this study, resins fully penetrated into the pore spaces of the titanium metal. This condition makes the experimental validation possible because the identical system between the testing and the analytical model can be compared. The microstructure of the metal/resin specimen represents adequately the characteristics of the microstructure of the analytical model with fully ingrown interphase developed in section 3.5. The accuracy of the analyticai model was verified through the experiments performed on the metal/resin composite.

For many years, push-out tests have been used to measure shear strength and shear stiffness of implant/tissue interphases. A schematic illustration (cross-sectional view) of the method is shown in the *Figure 4.2* A cylindrical implant core with irregular surfaces and osseointegrated tissues is pushed by an inner cylindrical post. The bottom surface of the outer cylinder of the bone tissue, opposite the post, is fixed. It is assumed that uniform shear stress exists through the entire interphase during the test. The outcome of the push-out test provides shear strength and shear stiffness of an entire implant/tissue interphase. However, not only is this test inadequate in comparison to the two-dimensional model proposed in the Chapter III, but it also fails to distinguish the material constants in the different directions.

The analytical studies in Chapter III show that the interphase composite is an anisotropic and inhomogeneous material which means that its properties vary from point to point due to their material distribution. Such an anisotropy determines load transfer patterns and may dictate failure patterns of the interphases. Testing methods should be

able to determine material constants in different directions; the push-out test is incapable of doing so. Mechanical testing protocols proposed in the following section were used to measure the orthotropic elastic constants of the composite. Such tests differ from tests used in previous studies, i.e., push-out tests (Pilliar et al. 1975, Clemow et al. 1981, Cook et al. 1988, Taylor et al. 1990).

Therefore, a mechanical testing protocol including two tensile tests and one shear test was developed and is described in this chapter. The experimental design, testing results, and the comparison of them to the results of analytical model are reported.

4.1 Experimental Design and Methods

4.1.1 Materials

The raw materials used were Ti-6Al-4V alloy plate, pure titanium powder, epoxy resins, and curing agents. The powder particles of pure titanium were spherical with a diameter of 1000 μm. The size of such particles was greater than that of commercial coating microspheres, which usually range from 400 to 600 μm. The reason of using 1000 μm microspheres is to make the pore big enough for resin infiltration. The sintering treatment for titanium and Ti-6Al-4V alloy, which was the same procedure of coating commercial alloy, produces an (α+β) lamellar microstructure *(Fig 4.3)*.

Epoxy resins are characterized by the presence of epoxide functionality. They have good adhesive properties to a very broad range of substrates and low shrinkage during curing which results in lower stress levels in the finished piece than is found in most other polymer systems with higher values of shrinkage. Another factor contributing to the epoxy is that byproducts formed during the curing reactions can be limited. Thus, there is little voids and material inhomogeneity which may affect current experiments.

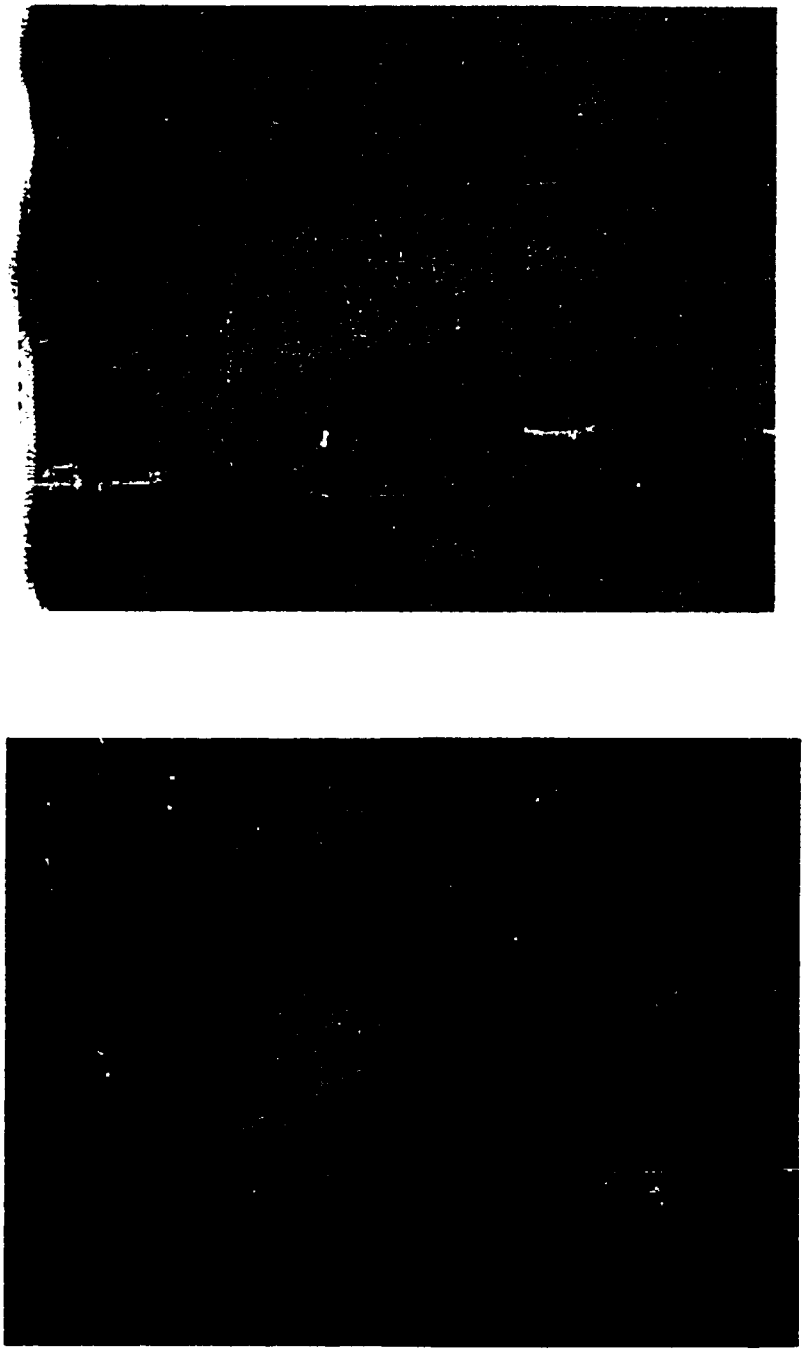

Figure 4.3 α+β lamellar microstructure of titanium alloy after heat treatment.

The homogeneous, isotropic bone tissue in the unit cell model can be easily simulated in the experiments by using epoxy.

4.1.2 Specimen Design

The representative metal/resin interphase composite is sketched in *Figure 4.4* The composite was designed to be very thin, only 1 mm, in order to meet the criteria for the plane stress analytical model. Such a composite is assumed to be orthotropic and have four independent elastic constants for two-dimensional stress-strain relations, the elastic moduli in the longitudinal and transverse directions (E_L, E_T), the shear modulus (G_{LT}), and the major Poisson ratio.

The purpose of the mechanical testing on the composite was to determine E_L, E_T, and G_{LT} through the static uniaxial tension tests. The static uniaxial tension test is probably the simplest and most widely used mechanical test.

The dumb-bell specimen, the most commonly used specimen geometry, was designed to measure the E_L and E_T using the tension test. In order to measure the G_{LT}, a specimen with rectangular shape was designed to mimic the thick-adhered tensile-lap specimen adopted from the American Standard Test Method D3983-81 (ASTM 1991). The thick-adhered tensile-lap test was used to measure shear strength and shear modulus for the adhesive material under a tensile load. The tensile load was applied along the interface.

Figure 4.5 illustrates the geometries of three types of specimens used in this study. Specimen types I, II and III represent the testing specimens for measuring E_L, E_T, and G_{LT}, respectively. Two isotropic resins were used: epoxy I, E=0.2 GPa; and epoxy II, E=3 GPa. Poisson's ratio was 0.42 for epoxy I and 0.36 for epoxy II provided by the manufacturers. The Young's moduli of these resins were within the reasonable ranges

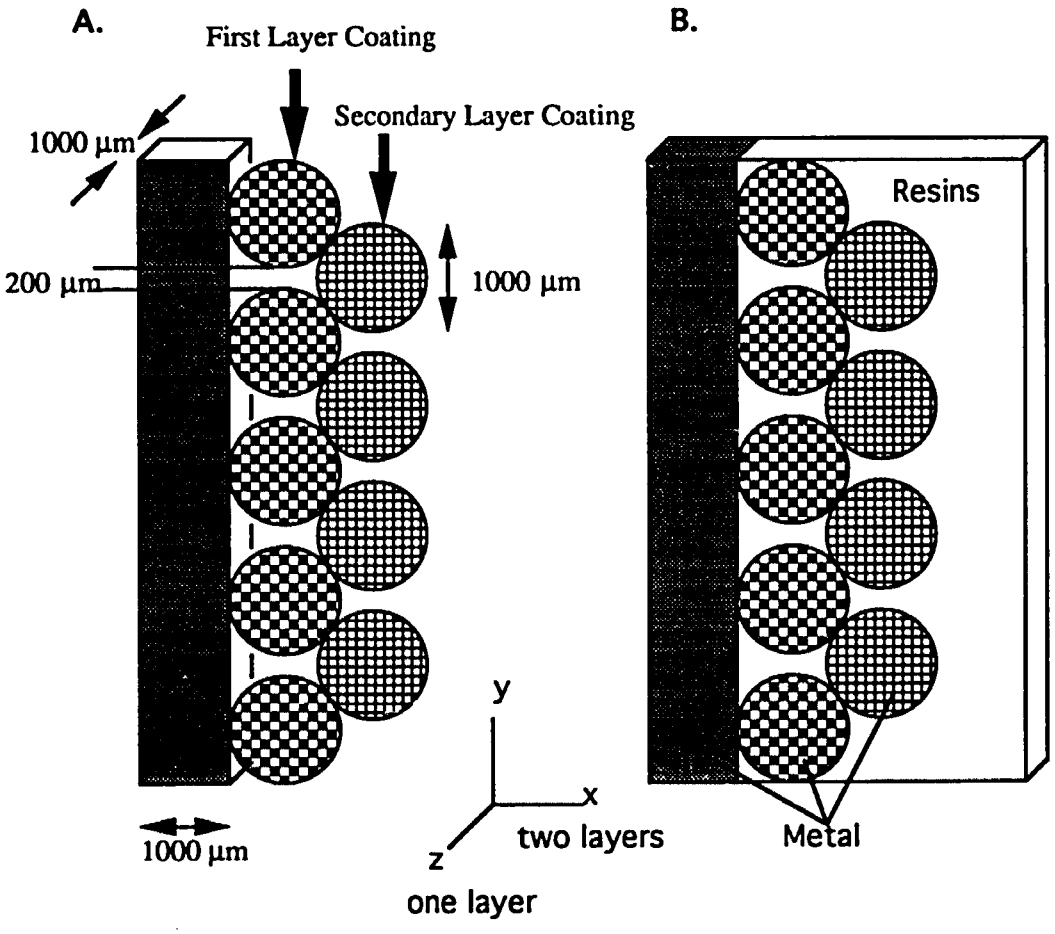

Figure 4.4 Schematic of the testing composite, (A) metal with coatings, (B) metal-resin composite

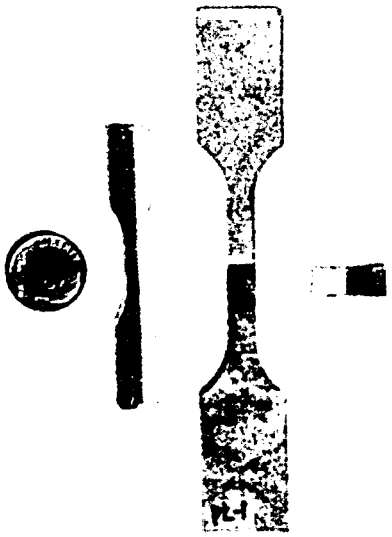

I II III

Figure 4.5 The geometries of three types of specimens used to measure orthotropic elastic constants of the bimaterial interphase composite. Specimen types I, II, and III represent the testing specimens for measuring the longitudinal, transverse, and shear modulus, respectively.

of the healing bone properties. This makes the measurements practically useful. For each resin, seven specimens were tested for each of the three specimen designs.

4.1.3 Sample Preparation

The bulk metal was machined into half of the dumb bell specimen and half of tensile-lap specimen from Ti-6Al-4V alloy plates. Powder particles were then sintered on the bulk Ti-6Al-4V alloy substrates under high temperature treatment, 1100° C. One layer of coating was sintered in the thickness; two layers were sintered across the interphase. Each microsphere in the first layer of coatings across interphases was sintered to the substrates. Each microsphere in the second layer contacted two microspheres from the first layer's coating.

In order to make the complete dog-bone and tensile-lap specimens by incorporation with epoxy resins, negative molds were fabricated using silicone rubber impression materials often used for denture impressions *(Fig 4.6)*. By pouring the epoxy resin into the mold, pores of the porous coated metal were filled with resins. The entire specimen of metal/resin composite was obtained. Finally, the specimens were polished to 600 grit to reduce any surface defects before the mechanical tests were performed.

4.1.4 Testing Methods

All three types of specimens were tested under static uniaxial tension. A uniaxial load was applied directly to the type I and type II specimens through the ends by providing a serrated-jaw-type end connection. A fixture was designed to hold the type III specimens such that shear stresses were created on the composite by applying the uniaxial tensile load (Fig 4.7). The method for measuring the shear modulus was adapted from the American Standard Test Method D3983-81 (ASTM 1991).

A

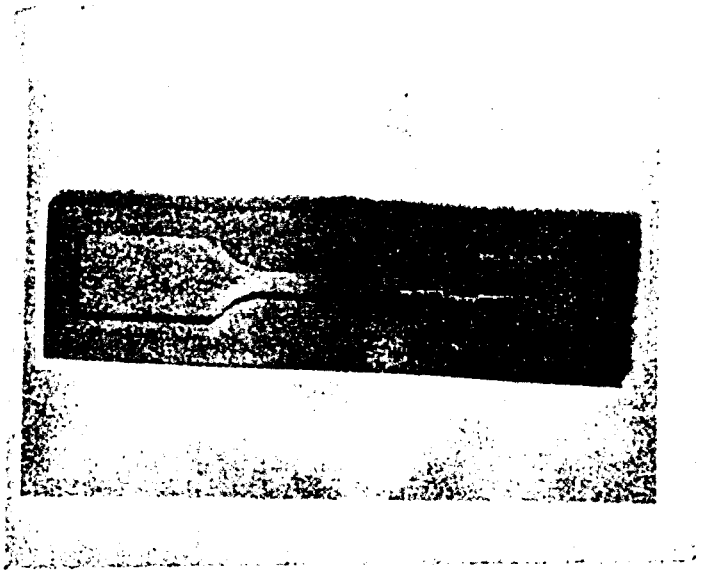

B

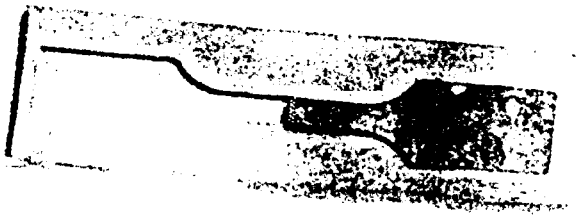

Figure 4.6 (A) The specimen negative mold made by silicone impression materials. (B) The epoxy was poured into the mold to bond with titanium metal.

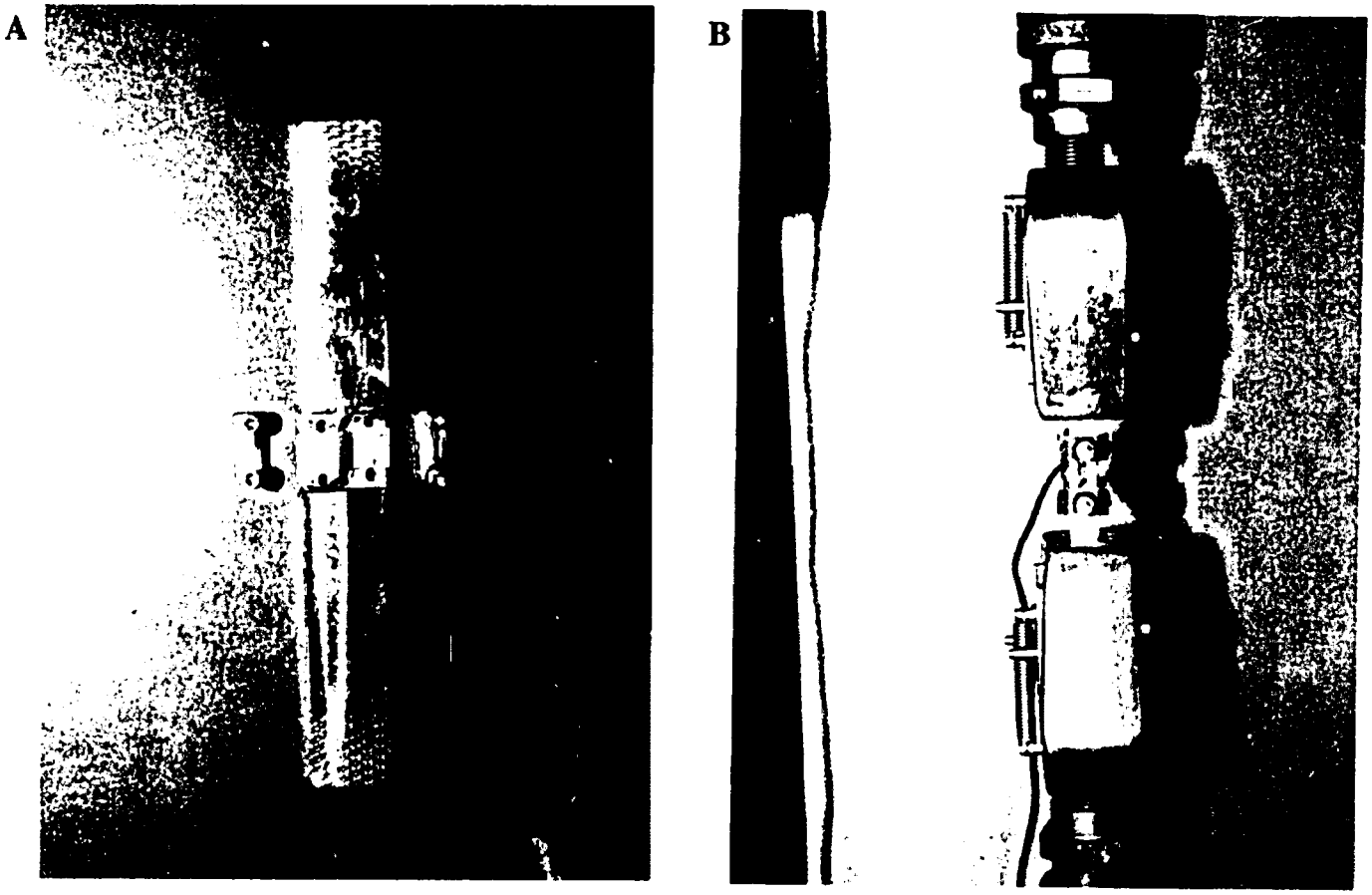

Figure 4.7 Special fixture (A) used to hold the type III specimens in such that shear stresses were created on the composite by applying the uniaxial tensile load (B)

All specimens were loaded statically on an Instron 1122 machine at a rate of 0.05mm/min until failure. The data recorded in the tension test consisted of measuring the applied load and the strain parallel to the load. The applied load was measured by means of a load cell installed with in the testing machine. The strains were measured by means of an extensometer. During the testing, a stress-strain curve was plotted for the material and the required material properties were determined. When the applied load was in the longitudinal direction, the initial slope of the stress-strain curve gave the longitudinal modulus (E_L). Similarly, the transverse (E_T) and shear (G_{LT}) modulus were determined by applying the load in transverse and shear directions, respectively. The mean value of the elastic constant for each type of specimen was compared to the value predicted from the homogenization theory using a Student's t test.

4.2 Analytical Methods

The moduli of the individual constituents used in the homogenization analysis were 110 GPa for titanium, 0.2 GPa for epoxy I, and 3 GPa for epoxy II. Details of the homogenization analysis may be found in Chapter III. The Hashin-Shtrikman (1963) and the Rule of Mixtures bounds were also calculated. Hashin and Shtrikman assumed that the overall modulus of the composite was isotropic. The upper bound of the Hashin-Shtrikman law used as the longitudinal modulus for the interphase composite is formulated as shown below:

$$E_L = \frac{9\left(K_1 + \dfrac{V_2}{\dfrac{1}{K_2-K_1} + \dfrac{3V_1}{3K_1+4G_1}}\right)\left(G_1 + \dfrac{V_2}{\dfrac{1}{G_2-G_1} + \dfrac{6(K_1+2G_1)V_1}{5G_1(3K_1+4G_1)}}\right)}{3\left(K_1 + \dfrac{V_2}{\dfrac{1}{K_2-K_1} + \dfrac{3V_1}{3K_1+4G_1}}\right) + \left(G_1 + \dfrac{V_2}{\dfrac{1}{G_2-G_1} + \dfrac{6(K_1+2G_1)V_1}{5G_1(3K_1+4G_1)}}\right)} \quad \text{.....(4.1)}$$

The lower bound of the Hashin-Shtrikman law used as the transverse modulus for the interphase composite was formulated as shown below:

$$E_T = \frac{9(K_2 + \frac{V_1}{\frac{1}{K_1 - K_2} + \frac{3V_2}{3K_2 - 4G_2}})(G_2 + \frac{V_1}{\frac{1}{G_1 - G_2} + \frac{6(K_2 + 2G_2)V_2}{5G_2(3K_2 + 4G_2)}})}{3(K_2 + \frac{V_1}{\frac{1}{K_1 - K_2} + \frac{3V_2}{3K_2 - 4G_2}}) + (G_2 + \frac{V_1}{\frac{1}{G_1 - G_2} + \frac{6(K_2 + 2G_2)V_2}{5G_2(3K_2 + 4G_2)}})} \quad \text{.....(4.2)}$$

The shear modulus of the Hashin-Shtrikman law was calculated using the following equation:

$$G_{LT} = (G_2 + \frac{V_1}{\frac{1}{G_1 - G_2} + \frac{6(K_2 + 2G_2)V_2}{5G_2(3K_2 + 4G_2)}}) \quad \text{.....(4.3)}$$

where G, K, and V represent shear modulus, bulk modulus, and material volume fraction, respectively. Here, subscripts 1 represents titanium, and 2 represents the epoxy resin.

The Rule of Mixtures used to calculate material moduli were:

$$E_L = V_1 E_1 + V_2 E_2 \quad \text{.....(4.4)}$$

$$E_T = \frac{1}{V_1/E_1 + V_2/E_2} \quad \text{.....(4.5)}$$

$$G_{LT} = \frac{1}{V_1/G_1 + V_2/G_2} \quad \text{.....(4.6)}$$

where E_i was the isotropic modulus for composite constituents, and G_i was the isotropic shear modulus for composite constituents.

4.3 Results

Tables 4.1 to 4.3 list the raw data for measured moduli for all the tested specimens. The mean value of the longitudinal modulus was 38.0 GPa for epoxy I and 45.2 for epoxy II. The change of the longitudinal modulus due to epoxy properties was less than 16%. The measured transverse moduli were 0.8 GPa for epoxy I and 13.9 for epoxy II; the shear moduli were 0.27 GPa for epoxy I and 2.9 for epoxy II. Both transverse and shear moduli for the composite containing epoxy II were ten times more than for the composite containing epoxy I. This implies that the effect of the tissue properties of implant/bone interphases on the load transfer is mainly in the transverse and shear directions.

The null hypothesis that there is no significant difference between the material moduli predicted by the homogenization theory and those obtained from experiments was tested by comparing the elastic constants E_L, E_T, and G_{LT} derived from the homogenization theory and the mean values measured from this experiment. Table 4.4. lists the moduli predicted from various composite theories and the measured moduli. No significant differences of the moduli were found between the computer predictions of homogenization theory as well as the Hashin-Shtrikman law and experimental measurements (Table 4.5). Thus the null hypothesis could not be rejected.

The other null hypothesis employed in this study is that there is no significant difference between the material moduli of epoxy I specimens and those of epoxy II specimens. However, comparison of the measured moduli for the group of epoxy I specimens with those for the group of epoxy II specimens shows that the differences are significant as shown in the Figure 4.8 ($p<0.02$). Thus the null hypothesis is rejected. Homogenization theory predicted similar results to the Hashin-Shtrikman estimates, but different from the Rule of Mixtures.

Table 4.1 Raw data of the measured logitudinal modulus (GPa) of the bimaterial interphase composite

Specimen#	Epoxy I 34*		Epoxy II 38.5*	
	EI	D	EI	D
1	36.4	2.4	46.8	8.3
2	37.9	3.9	45.8	7.3
3	42.8	8.8	50.6	12.1
4	35.1	1.1	38.2	-0.3
5	37.9	3.9	41.7	3.2
6	36.2	2.2	47.6	9.1
7	39.7	5.7	45.6	7.1
mean	38.0	4.0	45.2	6.7
SD	2.6	2.6	4.1	4.1

SD : Standard Deviation
D : Difference between measurements and those predicted by computation
* : Modulus predicted by the homogenization theory

Table 4.2 Raw data of the measured transverse modulus (GPa) of the bimaterial interphase composite

Specimen#	Epoxy I 0.83*		Epoxy II 10.6*	
	Et	D	Et	D
1	0.84	0.60	10.34	-0.30
2	0.76	-0.02	12.24	1.64
3	1.01	0.23	15.40	4.80
4	0.90	0.11	18.90	8.30
5	0.76	-0.02	14.90	4.30
6	0.61	-0.18	9.60	-1.00
7	0.73	-0.05	15.80	5.20
mean	0.80	0.10	13.90	3.28
SD	0.13	0.13	3.30	3.30

SD : Standard Deviation
D : Difference between measurements and those predicted by computation
* : Modulus predicted by the homogenization theory

Table 4.3 Raw data of the measured shear modulus (GPa) of the bimaterial interphase composite

Specimen#	Epoxy I 0.29*		Epoxy II 3.7*	
	Glt	D	Glt	D
1	0.40	0.11	2.87	-0.83
2	0.19	-0.11	4.18	0.48
3	0.20	-0.01	2.12	-1.58
4	0.30	0.01	2.80	-0.90
5	0.33	0.04	1.25	-2.45
6	0.21	-0.08	1.90	-1.80
7	0.25	-0.05	4.98	1.28
mean	0.27	-0.01	2.87	-0.83
SD	0.08	0.08	1.30	1.30

SD : Standard Deviation
D : Difference between measurements and those predicted by computation
* : Modulus predicted by the homogenization theory

Table 4.4 Experimentally Measured vs Predicted Elastic Constants for Bimaterial Composite

Composite System	Method	E_L	E_T	G_{LT}
Ti/Epoxy I	Experiment	38.0 (2.6)	0.80 (0.11)	0.27 (0.08)
	Homogenization Theory	34.0	0.83	0.29
	Hashin-Shtrikman	44.0	0.79	0.28
	Rule of Mixtures	62.8	0.46	0.16
Ti/Epoxy II	Experiment	45.2 (4.1)	13.9 (3.3)	2.9 (1.3)
	Homogenization Theory	38.5	10.6	3.7
	Hashin-Shtrikman	46.5	10.3	3.9
	Rule of Mixtures	64	7.6	2.5

( ) : STANDARD DEVIATION
Ho: Eij(homo) = Eij(exp)
$0.2 < P < 0.5$; n=7
Not Reject Ho

Table 4.5 P values in a comparison of experimentally measured vs predicted elastic constants for bimaterial composite

Composite Theory	Modulus	Ti/Epoxy I	p	Ti/Epoxy II	p
Homogenization Theory	E_L	34.0	0.2>p>0.1	38.5	0.2>p>0.1
	E_T	0.83	> 0.2	10.6	> 0.2
	G_{LT}	0.29	> 0.2	3.7	> 0.2
Hashin-Shtrikman	E_L	44.0	0.2>p>0.1	46.5	> 0.2
	E_T	0.79	> 0.2	10.3	> 0.2
	G_{LT}	0.28	> 0.2	3.9	> 0.2
Rule of Mixtures	E_L	62.8	<0.002	64	<0.002
	E_T	0.46	<0.002	7.6	<0.1
	G_{LT}	0.16	0.2>p>0.1	2.5	> 0.2

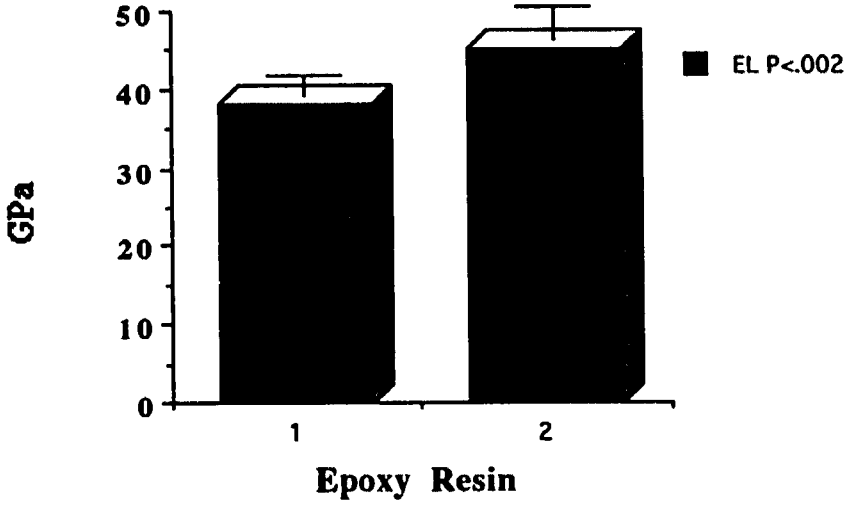

Figure 4.8a A comparison between the longitudinal modulus of the interphase composite with epoxy I and Epoxy II

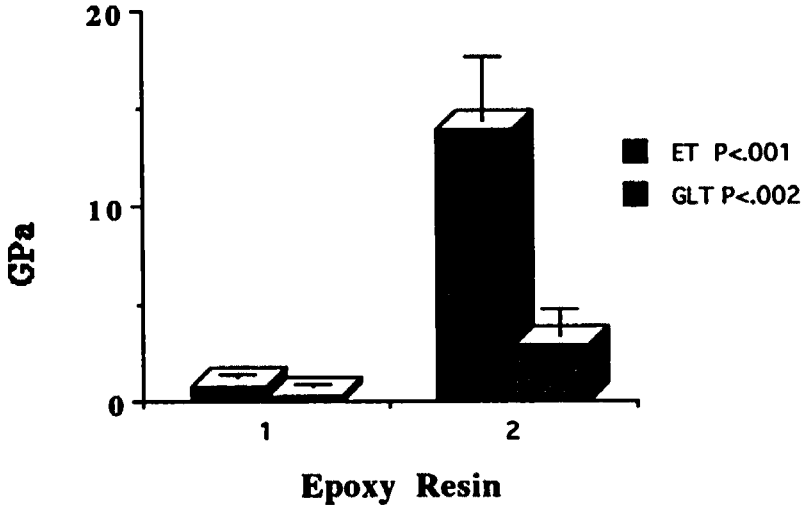

Figure 4.8b A comparison between the transverse and shear moduli of the interphase composite with epoxy I and epoxy II

4.4 Discussion

In this study, a reproducible measurement characterizing the material properties of an interphase composite was designed. The orthotropic constants of the composite materials measured by current methods differed from previous push-out measurements for interphase mechanical properties. The results demonstrate that load transfer from the prosthesis to the surrounding resin is not equivalent in all directions. The load transfer is dominant in the direction parallel to the implant surface because the longitudinal moduli of the interphase are always greater than the transverse moduli. The longitudinal modulus is 40 times greater than transverse modulus for epoxy I/metal composite, and 3.5 times for epoxy II/metal composite. The longitudinal modulus is eventually determined by the titanium which has higher stiffness than the resins, while the transverse modulus is determined by the softer component- resin. Although the measurements are performed on a resin/metal composite, this information should also be true of the actual tissue/metal composite measurements, because material properties of epoxy resins used in this study lie in the property ranges of the actual tissue. However, modifications of specimens will be required if current methods are applied to measure an actual tissue/metal interphase. In order to contain multiple layers of coating particles in the specimen, the specimens need to be thicker than 1 mm used in current experiments.

Through the experiments using metal/resin composite, the analytical models predicting composite moduli were validated. Homogenization theory predicts effective elastic properties equivalent to those predicted by Hashin-Shtrikman law. Although the upper and lower bounds of the Hashin-Shtrikman law correspond well to E_L and E_T respectively, it is important to keep in mind that Hashin-Shtrikman law predicts isotropic properties. The homogenization method, however, predicts the correct orthotropic properties. In addition, the present study assumed constituent materials to be isotropic. For the actual cases of orthotropic bone, homogenization theory might be more accurate

because it can calculate effective moduli for anisotropic constituents. Furthermore, the Hashin-Shtrikman law can only predict global properties. It cannot estimate local stresses, unlike the homogenization method which can predict local interfacial stresses.

Homogenization theory closely predicts the material moduli measured experimentally. The differences between the moduli predicted by the homogenization theory and those from measurements range from 4% to 20%. These differences are possibly attributed to the 15% errors of the micromechanical stress fields estimated in the previous study (Kohn et al., 1993). The overall elastic constants obtained from the homogenization model were slightly lower than the experimental measurements from experiments. The possible reasons for differences between the analytical and experimental results may be attributed to the periodic assumption used in the analytical model. In homgenization model, resin materials are physically dispersed into the bulk metal due to the periodic condition; thus the composite becomes softened.

With this validation, it is now possible to confirm the accuracy of the application of the homogenization theory in the interphase mechanics. The application of such technique can be better explored.

4.5 Conclusions

Homogenization theory predicts the same effective elastic constants for a bimaterial interphase composite as those measured in the experiments ($0.2<p<0.5$). The use of these material constants in the interphase of a global model is therefore reliable.

The computational prediction also reflects the influence of each interphase component on the resultant mechanical properties of the interphase composite. Thus the use of the homogenization theory to estimate local properties of an implant/tissue interphase becomes feasible even though the tissue is heterogeneous.

CHAPTER V

LOCAL STRESS VALIDATION

5.0 Introduction

This chapter focuses on examining the accuracy of the interfacial stresses obtained from the homogenization interphase model (HIM) described in Chapter III. Under the initiative, the newly devised model accounting for the structural heterogeneity of implant/tissue interphases predicted a detailed stress field which characteristically runs along lines of differences in surface configurations between the screw and microsphere, in location between the proximal and distal regions of the prostheses, and between the medial and lateral side of femur. Such characteristics of stress distributions can be very significant in studying physiological events such as material failure mechanisms and bone remodeling of the interphase. However, before these physiological events can be addressed, I must know the degree of accuracy of the stress values and how to avoid faulty data due to inaccuracies of the model.

The examination of accuracy comprises three specific aspects: (i) examination of the influence of the cell shape to the accuracy - sensitivity analysis, (ii) examination of all interfacial stresses in an entire implant model, and (iii) the study of the global boundary effect on the modeling accuracy. The influence of the cell shape on the modeling

accuracy has to do with the periodic assumption made by the homogenization theory. Earlier in section 3.5, I mentioned that the interphase composite is unidirectionally periodic. However, the periodic boundary constraints for both the horizontal and vertical directions are imposed on all the edges of the local UCMs. Thus a carefully selected shape of UCMs determining the borders may be instrumental in minimizing the errors.

Examination of all interfacial stresses in an entire implant gives us some insight into how well the HIM can be used in practical cases. In this part of study a practical dental implant is used to verify the analysis of HIM on the whole implant level. However, only the dental implant can be examined on the entire implant level because it is possible to model an implant with small dimensions, in this case 11 mm long and 3.8 mm in diameter, with standard finite element methods using a sufficiently refined mesh.

In order to extend the validation to the porous coated THR, it is necessary to research the global boundary effect on the modeling accuracy. This issue will concentrate on determining the accuracy of HIM for various boundary conditions on a rectangular block of interphase composite. From this, I will be able to determine the feasibility of the homogenization theory for the analysis of porous coated THR's.

The study of each of the aforementioned aspects involves two analytical techniques. The first technique is the direct analysis from a complete finite element model which is solved by using the traditional finite element formulation. It is assumed that the resulting Von Mises stresses (VMS^D) converge to an exact solution since the models are constructed by using highly refined meshes (Hughes, 1987). The VMS^D thus serve as a basic quantity for comparison with Von Mises stresses predicted by the homogenization analysis.

The second technique is the homogenization analysis. Detailed descriptions of the homogenization technique may be found in Chapter III.

Within the interfacial zone, the mesh densities of the direct model are equal to those of the homogenization model. The local VMS^H calculated for each nodal point of

the homogenization model is compared to the VMS^D obtained from the direct analysis for the same nodal point. The differences between the VMS^H and VMS^D on the corresponding node are referred to the percent errors of HIM formulated below:

$$100 \times \frac{|VMS^H - VMS^D|}{VMS^D}\% \qquad (5.1)$$

The accuracy is then defined as

$$(1 - error) \times 100\%$$

The average accuracy over the interfacial zone is computed to justify the effectiveness of models.

5.1 Sensitivity Analysis

To determine the sensitivity of the model to the local unit cell geometry, I constructed five unit cells, with different metal to tissue volume ratios *(Fig 5.1)*. Metal to volume ratios were altered by adding either metal or bone in the horizontal direction to expand the volume of the cell. Cell types I - V have, respectively, bone/metal volume ratios of 1.0, 1.0, 2.0, 3.0, and 4.0.

Each cell was used to construct a multiple thread model (global model) which included eight identical unit cells repeated vertically to simulate an interphase composite (Fig 5.2). A vertically imposed displacement of 0.01 mm was applied on the top surface of the model and the nodes at the bottom surface were constrained in both horizontal and vertical directions. The multiple thread models were analyzed by using both the direct finite element method and the homogenization method.

The percent errors of the interfacial stress of HIM were calculated using equation (5.1) for all five cell types. Figure 5.3 and 5.4 show the errors of HIM for the different cell types. Two important results emerged from the analysis. First, the errors are

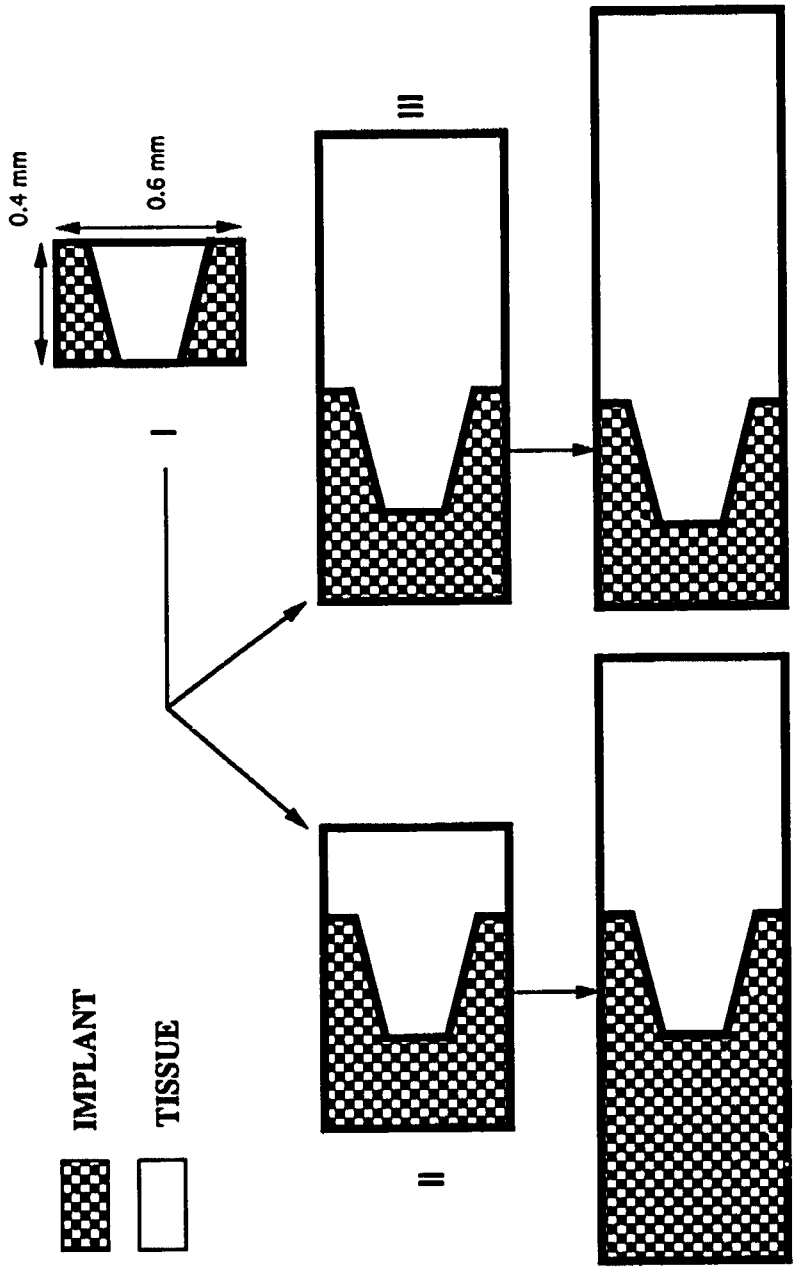

Figure 5.1 Schematical drawing of five unit cell geometries used in sensitivity analysis

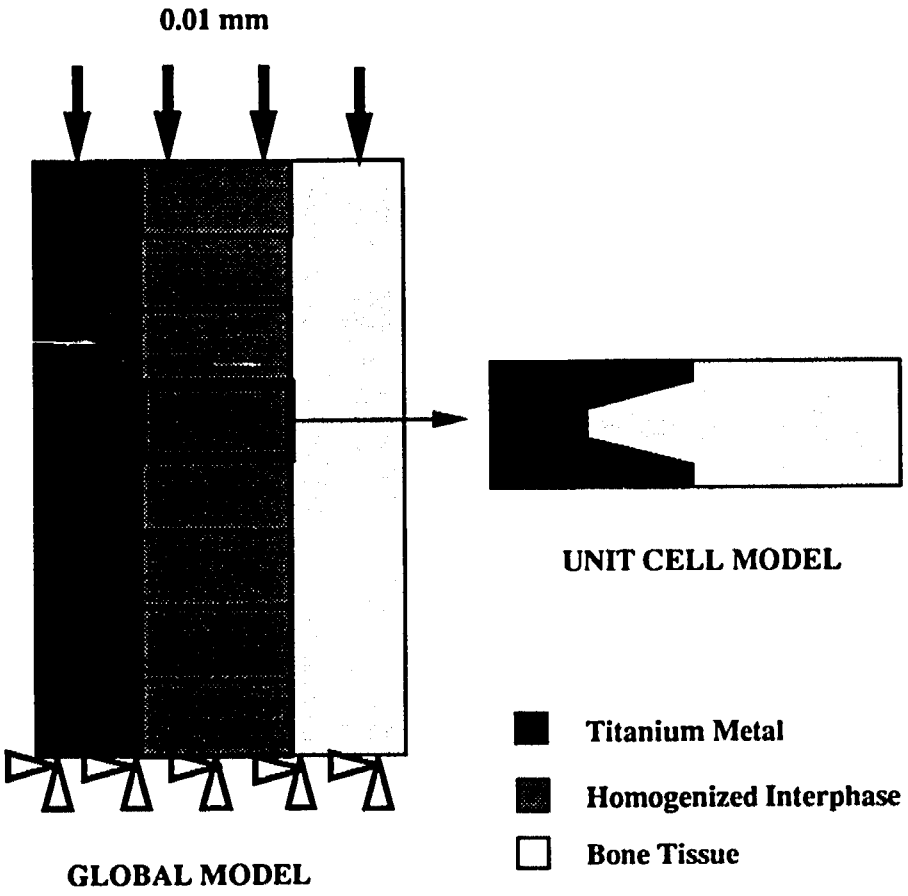

Figure 5.2 Homogenization model for sensitivity test including eight repeating unit cells

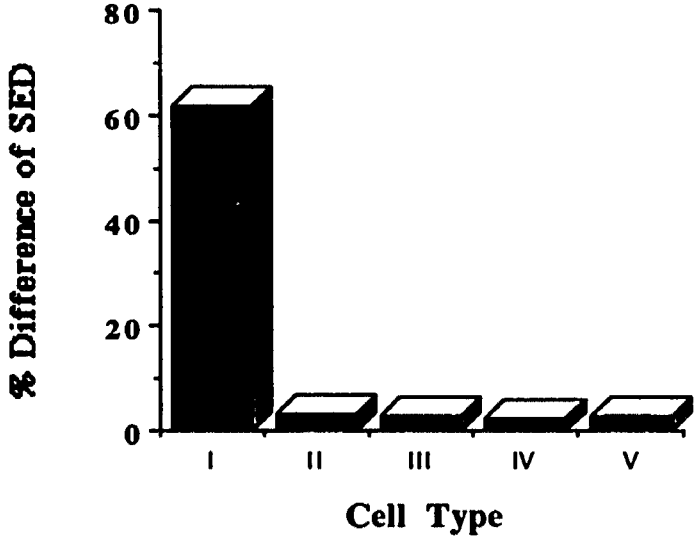

Figure 5.3 Percent difference in SED between standard and homogenization models for the different cell types subjected to a vertical load

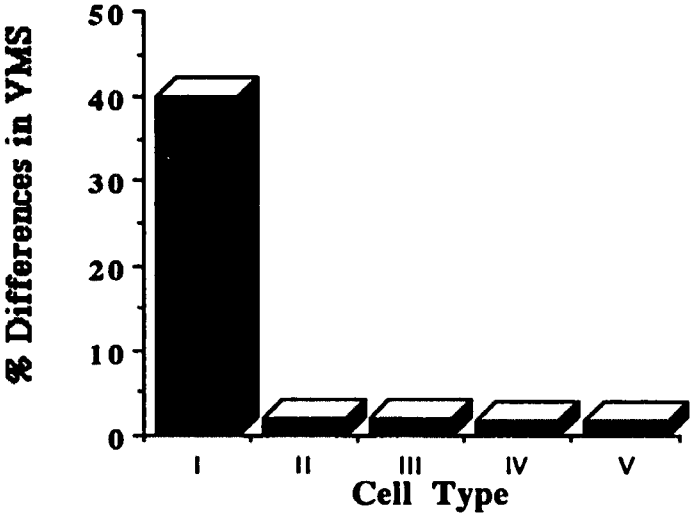

Figure 5.4 Percent difference in VMS between standard and homogenization models for the different cell types subjected to a vertical load

approximately 3% for cell types II, III, IV, and V. Therefore, the homogenization model constructed from cell types II, III, IV, and V provide accurate analyses. Second, accuracy is best achieved if unit cell type IV is used. Compared to standard techniques, a bone/metal ratio of 3:1 provides the best results. This unit cell type was used for the subsequent dental implant analyses.

The errors of HIM prediction are reduced by expanding the cell border in horizontal direction because the effect of the periodic bounary conditions imposed on the UCM can be pushed away from the interphase region. The UCM containing parts of bulk material of both metal and bone, i.e. cell type II, III, IV, and V, can push the errors away from the central region of the interphase, and provides an accurate prediction for local interfacial stresses.

5.2 Error Estimate for a Whole Implant

5.2.1 Methods

A global model of a cylindrical titanium implant was designed using a direct FE method. The model contained a total of 15,000 elements, which is within the capability of a minicomputer analysis. The model features a direct bone/implant contact *(Fig 5.5)*. A rigidly bonded interfacial condition was developed to model a well-fixed functioning implant. In the interfacial zone, the element size was 20 x 40 μm, as this is the scaling of the tissues under investigation. The bone core was 5 mm in radius from the implant surface. A plane stress model was built by means of quadrilateral elements. Titanium and bone were assigned Young's moduli of 110 GPa and 5 GPa, respectively, with Poisson's ratios of 0.30 and 0.35, (Ashman and Van Buskirk, 1987). All materials were treated as being homogeneous, isotropic, and linearly elastic. Distributed vertical loads 1 N/mm (1 Pa-mm) were applied to the top surface of the implants. The bone below the apex was taken to be fixed in all degrees of freedom.

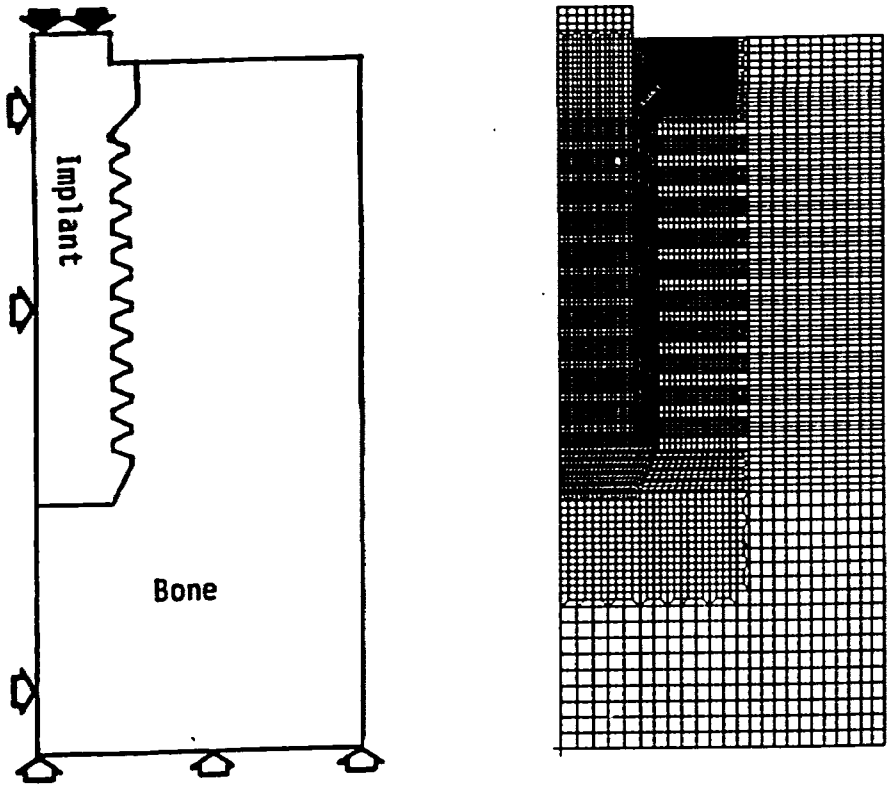

Figure 5.5 Cross-section of the global dental implant model. (A) material distributions in the model, and (B) finite element meshes for the direct FE analysis.

For the homogenization analysis, the same size dental implant was used. The global model contained a layer of interfacial zone where the material properties were calculated from the UCM. For detailed information of the model the reader is referred to section 3.3.

5.2.2 Results

The equivalent stress in the bone for the threaded implant analyzed by the direct FE model is concentrated on the alveolar crest and apical regions *(Fig. 5.6A)*. The middle region of the bone between the first and last thread reveals a low stress value- less than 0.06 MPa. Equivalent stresses are sustained by the implant body with values from 1.41 to 0.16 MPa, and decrease gradually from the coronal portion to the apex. Similar to the Mises stresses, the compressive stresses are concentrated on the coronal portion of the implant *(Fig. 5.6B)*. Tensile stresses *(Fig. 5.6C)* are concentrated on all threads and the implant apex, ranging from 0.1 MPa to 0.3 MPa.

The predictions of stress distribution throughout the entire interfacial zone are consistent with the findings of the homogenization interphase model discussed in section 3.3.5 (Fig 5.7). A comparison of the direct FEM with the HIM for the entire dental implant reveals promising results; the maximum difference of interfacial Mises stress is 15%. The errors in the HIM are less than 15%, and the HIM is valid at the whole implant level. Therefore, it is now possible to quantify stress patterns within the interfacial zone and account for the local micromechanical behavior around individual surface structures for whole implants.

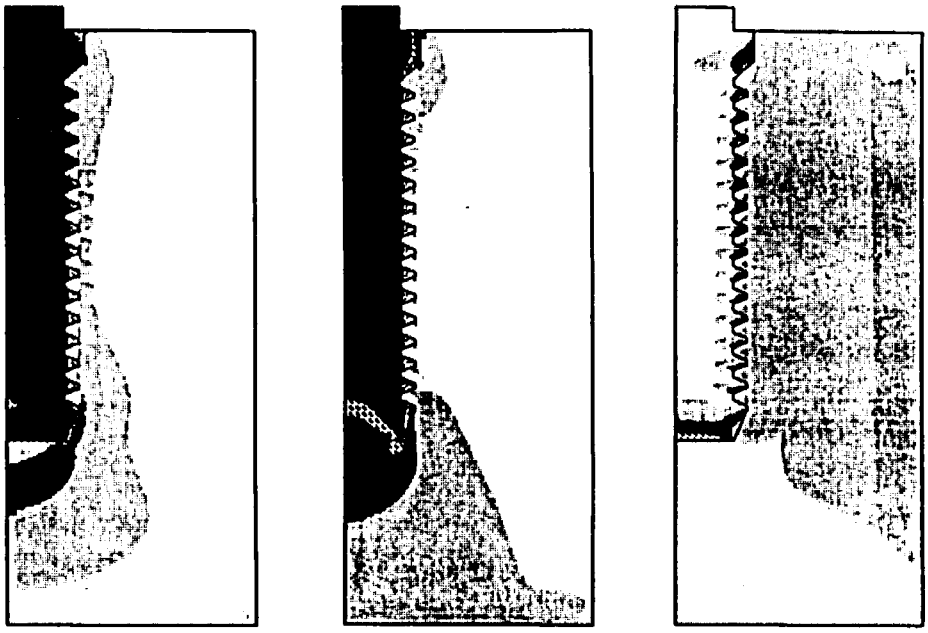

Figure 5.6 Stress contour of the standard whole implant model solved by a direct finite element analysis. (A) Von Mises equivalent, (B) Minimum principal (mainly compression), and (C) Maximum principal (mainly tension) stresses.

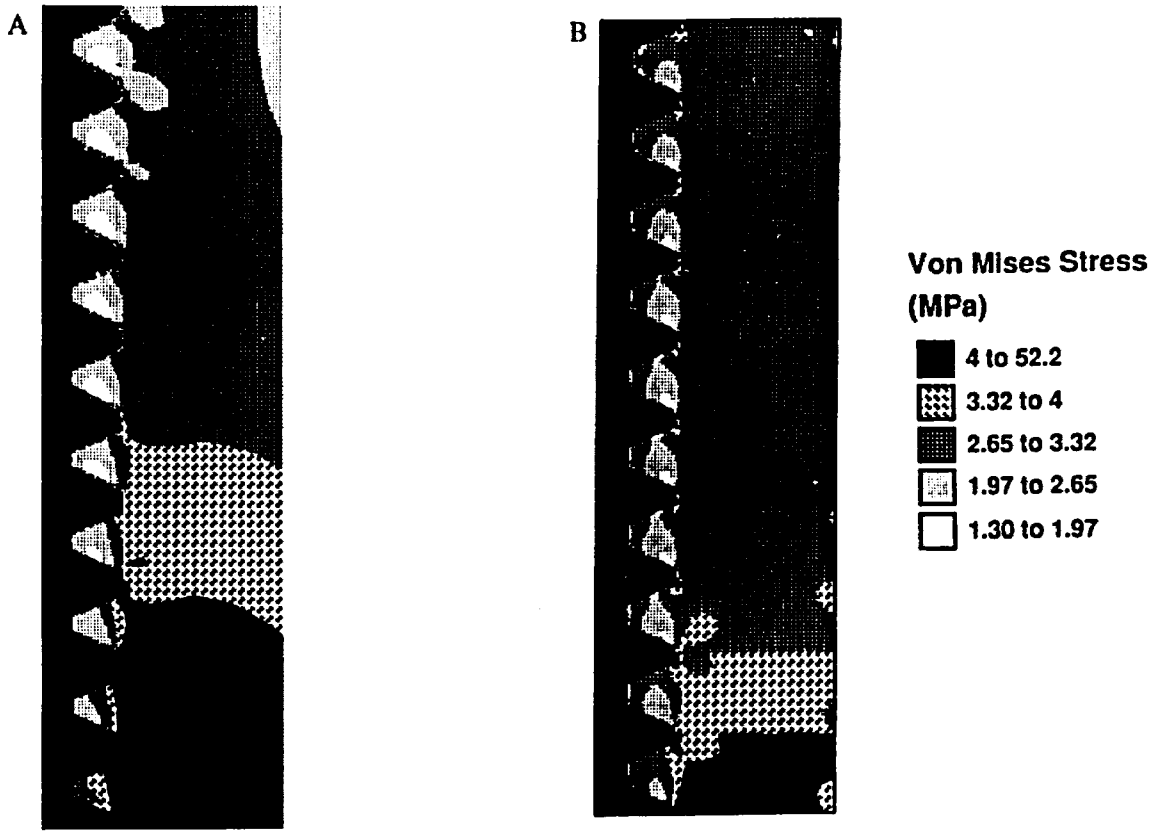

Figure 5.7 Interphase Von Mises stress contour of the direct whole implant model (A), and homogenization model (B).

5.3 Error Estimate for Different Loading Conditions

5.3.1 Methods

The objectives of the study reported in the current section are to develop error bounds on the homogenization technique for various boundary conditions and to determine the feasibility of the homogenization theory for the analysis of a porous coated THR. The unit cell used to calculate the effective elastic constants of the porous implant/tissue interphase included part of the implant substrate, two microspheres and bone. The microspheres contacted one another at two points (Fig 5.8). Each of these materials was assumed to have homogeneous, isotropic material properties (E_{bone} = 1 GPa, $E_{titanium}$ = 110 GPa) and to be rigidly bonded. The diameter of each microsphere was 300 μm. The full dimension of the unit cell was 900x450 μm and contained 550 quadrilateral elements. Periodic constraints were imposed along the edges of the cell.

The global model was a two-dimensional model (2.9x3.6 mm) of a porous coated implant and surrounding tissue, having 8 unit cells and 5500 quadrilateral elements (Fig 5.9). This model was used so that equivalent meshes could be generated in order to compare the homogenization and the direct FE models and quantify the error bounds. All bulk materials were assumed to be homogeneous and isotropic. The interfacial zones near the two porous coated regions were given the effective properties calculated from the local model and all materials were assumed to be rigidly bonded. Global stresses and strains were then calculated by the standard finite element approach. A complete global model containing the architecture of the interfacial zone was also modeled using a commercial finite element code (ABAQUS). The errors of the homogenization model were defined as the percent difference in von Mises stress (VMS) between homogenization and standard models having similar mesh densities.

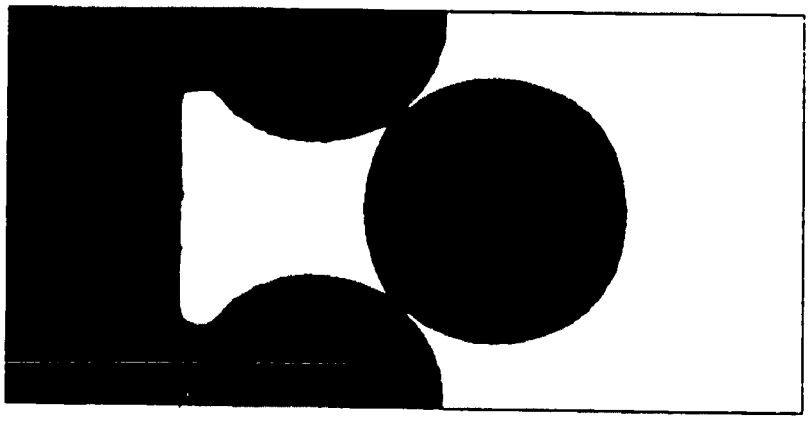

A

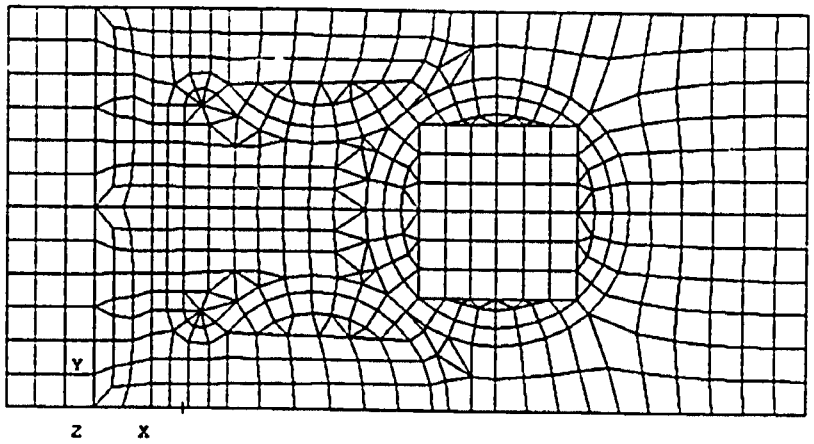

B

Figure 5.8 A. material distribution- black for metal and white for bone of unit cell model used for error estimate with respect to different boundary conditions , and B. finite element meshes of such unit cell model.

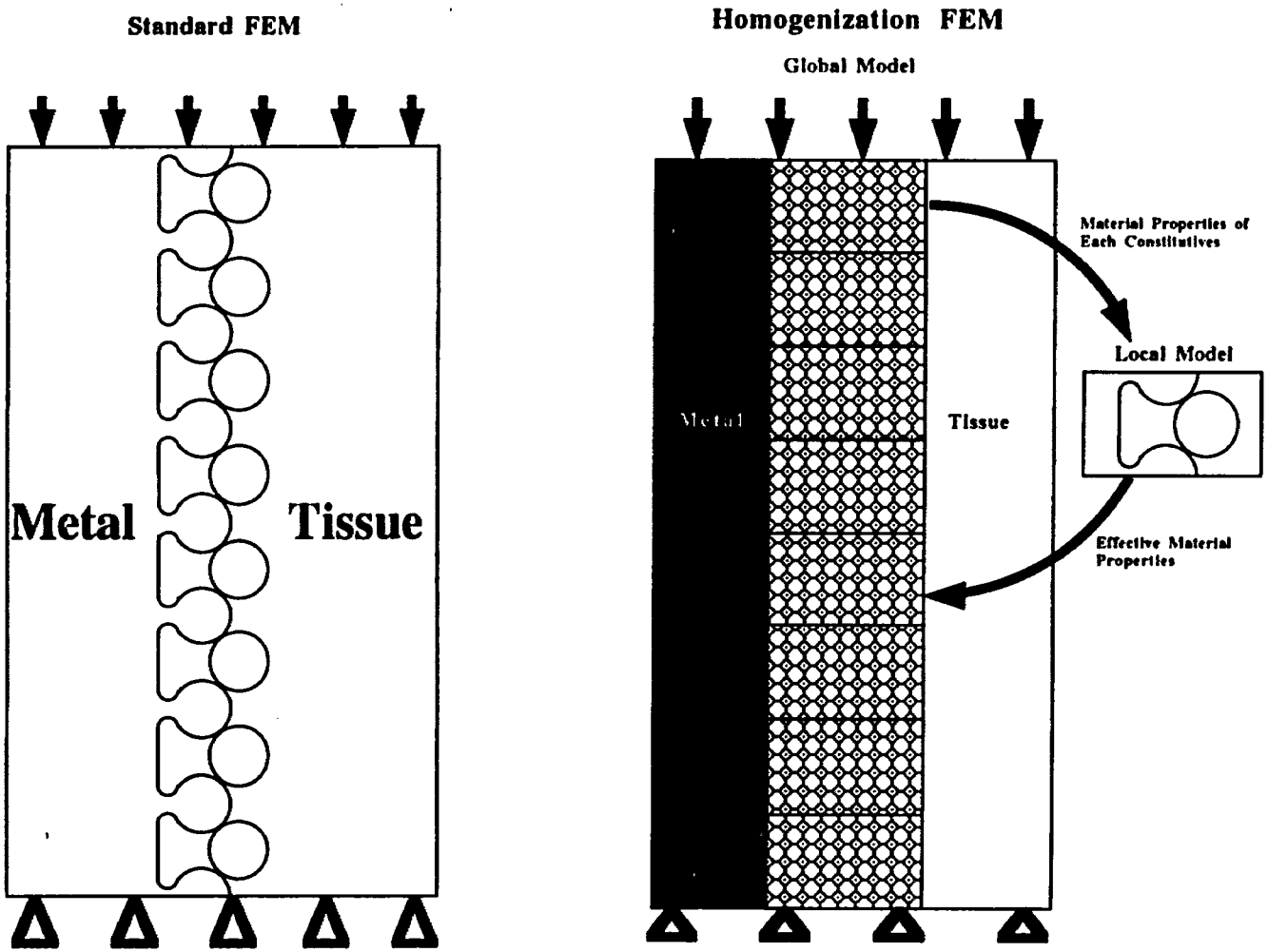

Figure 5.9 Eight cell models for error estimate: (A) direct finite element model, (B) homogenization finite element models

Table 5.1 Average difference in VMS between homogenization and direct FEM

	Case 1	Case 2	Case 3	15°	30°	60°
Metal	0.9%	36.2%	15.5%	4.1%	9.0%	24.7%
Bone	1.6%	122.0%	4.0%	16.5%	44.7%	105.5%

Three different (unit) displacement boundary conditions were analyzed: (1) normal displacements parallel to the interfacial zone, (2) shear displacements, and (3) normal displacements perpendicular to the interfacial zone (Fig 5.10). Load cases (1) and (3) represent a simplified loading on a total hip replacement and total knee replacement, respectively. In addition, several other loading angles, intermediate to load cases (1) (0 degrees) and (2) (90 degrees), were analyzed: 15, 30, and 60 degrees.

5.3.2 Results and Discussion

The average percent differences in VMS in both the metal and bone for the different cases are listed in *Table 5.1*. The full range of errors can be determined (Fig 5.11). Case 1 (normal displacements parallel to the interfacial zone) and case 3 (normal displacements perpendicular to the interfacial zone) yielded results which agreed with the results of the direct finite element models. Case 2 had greater error. A key mathematical assumption in homogenization theory is that the microstructure of interest is periodic. The 8-cell model is periodic in only one direction. As a consequence of this unidirectional periodicity, normal loading (either perpendicular or parallel to the direction

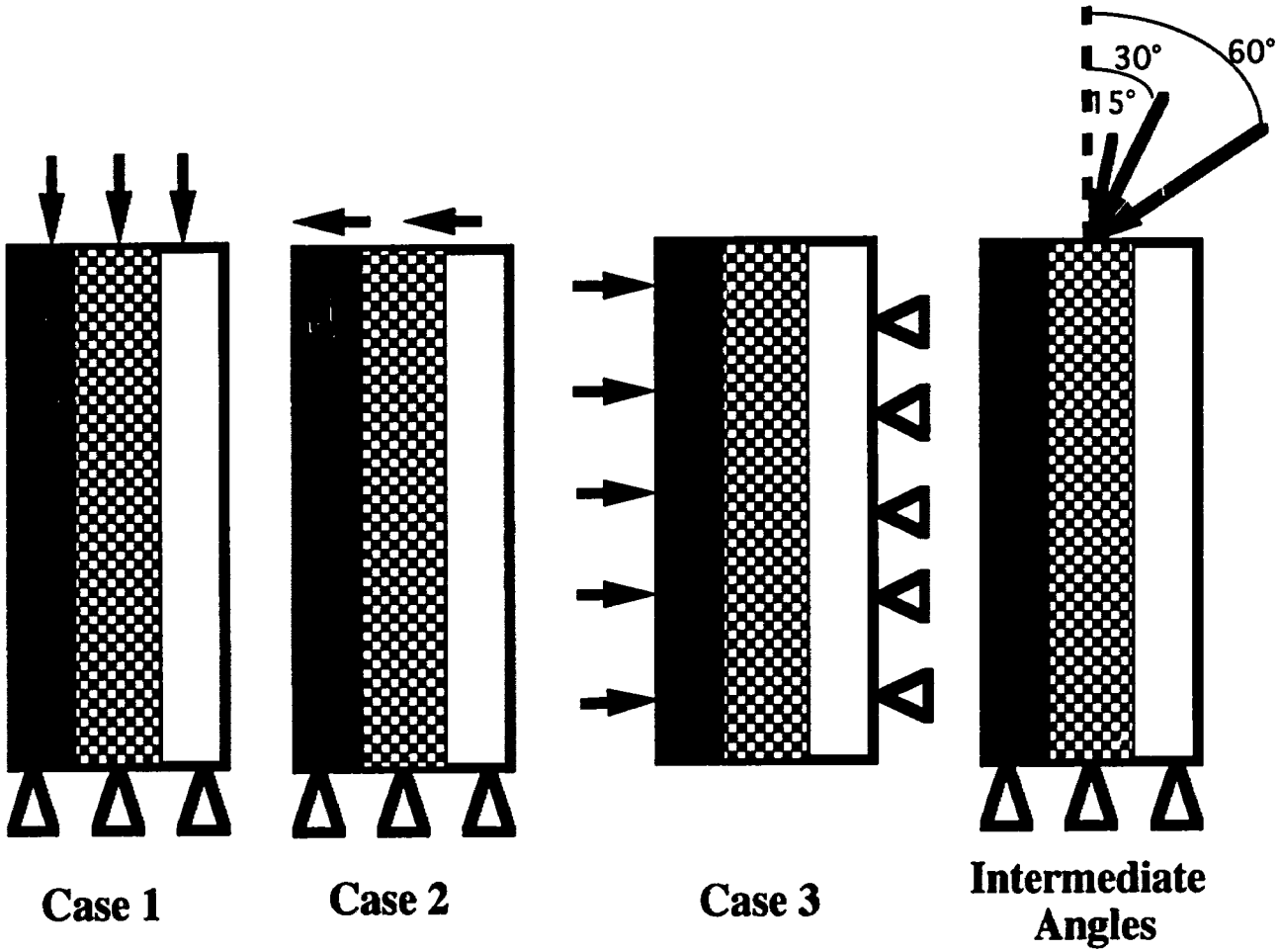

Figure 5.10 Different displacement boundary conditions for error estimation: (1) normal displacements parallel to the interfacial zone; (2) shear displacements; (3) normal displacements perpendicular to the interfacial zone; and (4) 15, 30, and 60 degrees loading cases.

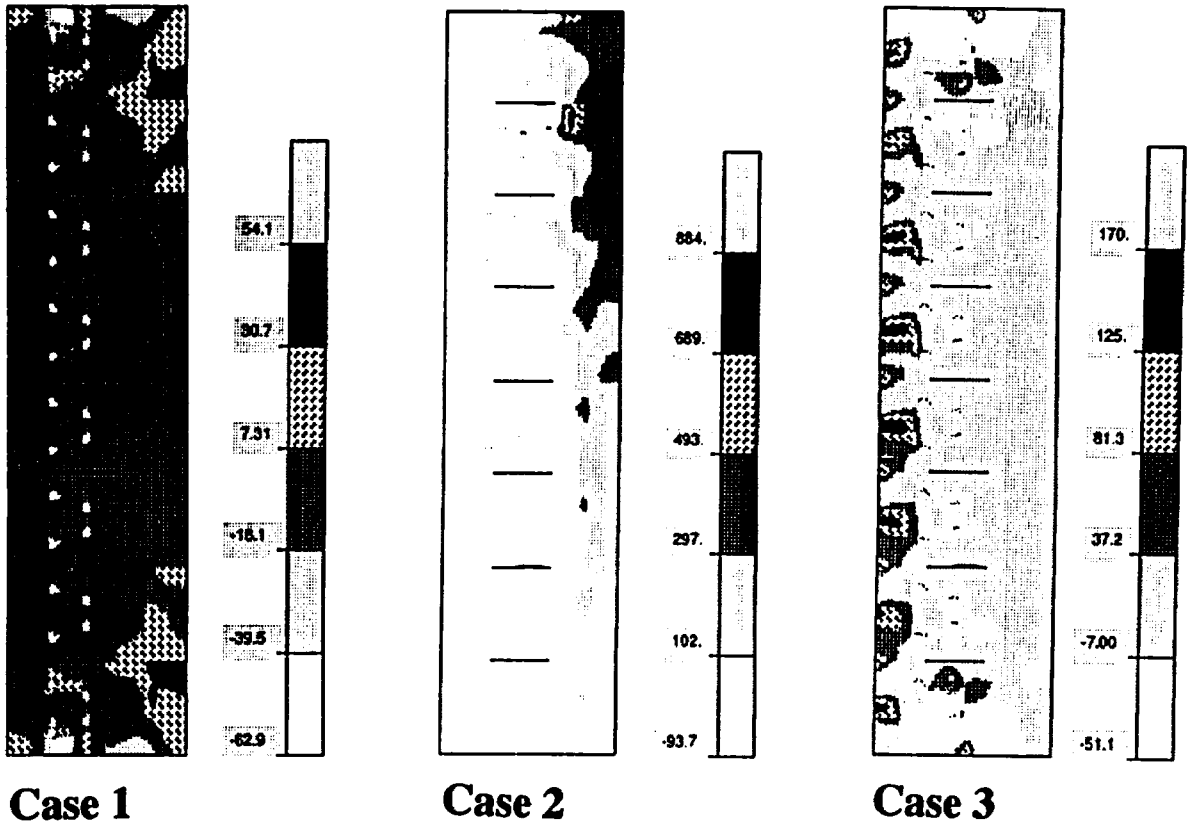

Figure 5.11 Error Distributions-Plot of Differences in Mises Stress Between Homogenization and Standard FEM for Different Boundary Conditions with Case 1, 2, and 3.

of periodicity) yielded low errors, and homogenization theory may therefore be used with confidence to model localized regions of complex microstructures for these loading conditions.

The case of shear loading differs significantly from the results obtained through standard modeling. It should, however be noted that such a load case is least physically relevant to the situation of total joint reconstruction. Cases 1 and 3, while very simplistic, can be used as a first approximation to simulate hip and knee replacement and perform parametric analyses. Loading at 15 degrees, which best simulates the loading on a hip, yielded differences of about 4% in the metal and 16.5% in the bone.

For all three cases, the average errors were generally small. The range of error values increased from case 1 to 3 to 2. However, the maximum errors all occurred at the outer surface of the substrate, since boundary effects strongly influence homogenization theory. In general, homogenization theory tends to overpredict the interfacial stresses about 2% to 15 % greater than the direct models. As a result of previous experiments shown in Chapter IV, homogenization theory seems to underpredict the values of elastic constants. These underestimated moduli may result in high global strains, and locally lead to higher interfacial stresses than those computed by direct models. As predicted by the direct models (Ko et al. 1992b), the regions of highest stress occurred at the sinternecks and at the point where the tissue contacts the outer surface of the porous coating. In these regions the errors were relatively low (< 15%). Furthermore, homogenization theory tends to underpredict the stresses in the high-stress regions; it gives a conservative estimate of interphase failure.

The results may still hold for a three-dimensional homogenization model because the geometries of the interphase composite violate the periodic assumption only in the direction across the interfacial zone.

5.4 Conclusions

In Chapter three, I discussed the development of a new analytical model HIM to quantify the interfacial stresses accounting for the material microstructure. In the current chapter I demonstrated the effectiveness of this model. Applying the HIM to the dental and hip prostheses, the local interfacial stresses can be predicted to accuracy of about 80%. By using these predicted mechanical characteristics, the mechanisms of bone ingrowth and bead debonding of the porous coated THR can be further studied.

The important conclusions drawn from the current chapter are as follows:

(1) The errors of HIM prediction are reduced by expanding the cell border in horizontal direction. The UCMs containing parts of bulk material of both metal and bone provide accurate predictions for local interfacial stresses.

(2) Evaluation of the interfacial stresses on the whole implant level points to overall errors of less than 15%. On average, the model yields more accurate results for the distribution of stresses. The stress based prediction of the location where materials might be damaged or tissues might be adapted can be precisely performed.

(3) Loading conditions normal to the interphase such as cases 1 and 3, while very simplistic, can be used as a first approximation to simulate hip and knee replacement and perform very accurate results- more than 95% accuracy. Loading at 15 degrees, which best simulates the loading on a hip, yielded errors of about 4% in the metal and 16.5% in the bone.

CHAPTER VI

INGROWTH RULE

6.0 Introduction

This chapter proposes an ingrowth rule for the investigation of mechanical adaptation of osseointegrated bone. The ingrowth rule correlates locally the strain magnitudes on the ingrown tissues with the amount of the final bone mass retained within the porous coating layer of the implant. The amount of the final bone mass retained within the porous coatings is referred to as the amount of *bone ingrowth*, the term used in other studies (Bobyn et al., 1982, 1988; Cook et al., 1988, 1989; Goldstein et al., 1991; Hollister et al., 1993; Borodkin et al., 1994; Spector et al., 1979). Instead of referring to bone maintenance, the term bone ingrowth is used in the remaining part of this dissertation.

The theoretical framework of the ingrowth rule is revealed in Figure 6.1 where the initial healing bone is assumed to be homogeneous and to fill the entire available spaces of the pores. The load on the bone-implant unit, and the geometric and material properties of both the bone and the synthetic implant consequently determine the interfacial bone strains. The ingrowth rule hypothesizes that the local bone strains initiate either a local bone formation activity (osteoblast activity) or a resorption activity (osteoclast activity).

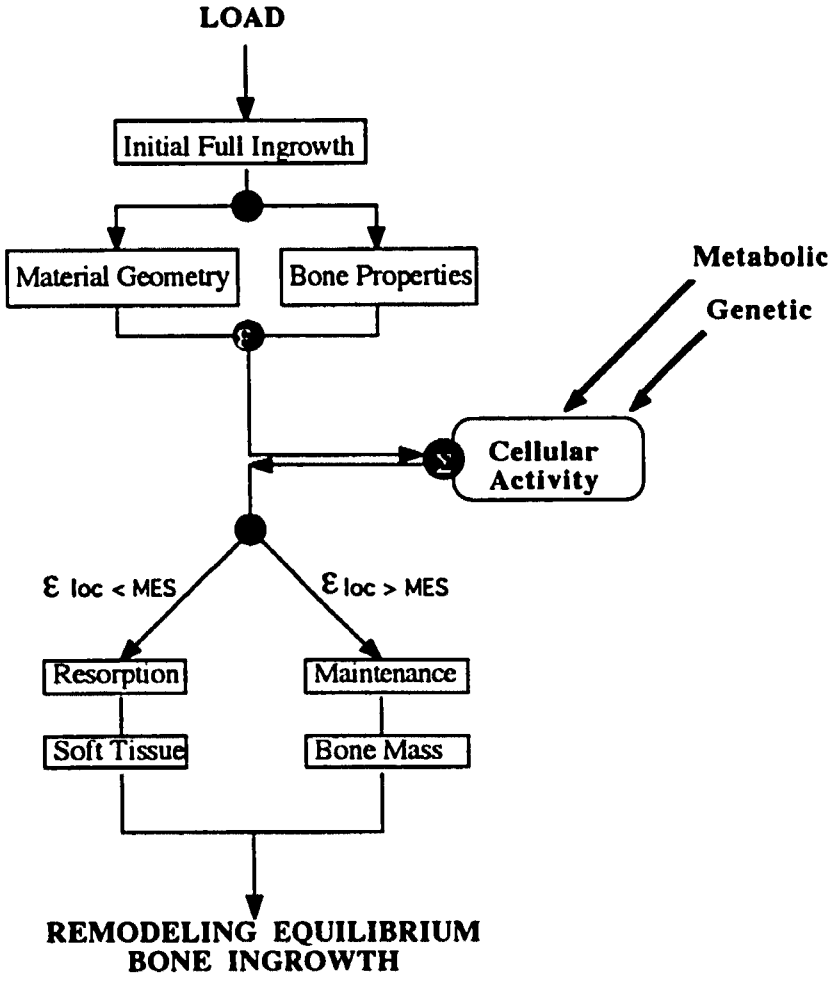

Figure 6.1 Ingrowth rule describing how the osseointegrated tissue remodels with the local tissue strains

If the bone is subject to strains greater than some threshold value, it will undergo a maintenance process in which tissue activity reaches an equilibrium state. Otherwise, the bone is resorbed and replaced with soft tissue. This rule transforms mechanical characteristics of the interphase strains to quantitative indicators of measuring the degrees of biological fixation onto an implant. Such indicators are later used in chapter VII for the evaluation of orthopaedic implants to predict the long-term bone remodeling effects around a particular implant design.

6.1 Background

Two issues need to be established to support the ingrowth rule. The first issue is to determine whether the tissue strains influence the formation and resorption of the osseointegrated tissue. If it is determined that it does, then another important issue is to determine what magnitudes of tissue strains affect the amount of bone ingrowth inside the coating layer of a porous coated implant.

The first issue is related to existing bone remodeling theories. Wolff (1892) proposed that the internal structures of a normal bone are allocated appropriately to carry the applied stresses; this is known as Wolff's law. While Wolff's law is true for bone adaptations, its validity for the bone-implant interphase tissue is not known.

Furthermore, Wolff did not provide any detailed information about the magnitude of strains or stresses related to bone adaptation. More precisely, quantified correlations between the mechanical entities and the osseointegration are needed for the engineering design of implants. During the past several years, Frost (1988, 1989, 1990a, 1990b), Carter (1987), and Brown (1990) have gathered quantitative evidence from studies of animal models and human retrieval that bone remodeling responds to certain bone strain magnitudes. Frost (1988, 1990a, 1990b) proposed the minimum effective strain (MES), a classic benchmark of quantitative bone remodeling theory. He suggested that there exists

a MES value which determines whether the bone will respond with a resorption or formation (Fig 6.2A). Under his theory, bone strains greater than the MES value trigger an inhibition to remodeling activity and result in a net increased bone mass due to the formation and maintenance. In contrast, bone strains less than the MES value lead to a net bone loss because of the continuous remodeling rhythm of the normal skeletal organ. Since normal bone tissue has been found to maintain its mass within a certain strain range, from 1000 με to 2500 με, this study assumes that the osseointegrated bone tissues are subject to MES as well. In addition, I propose a simplified relationship between the change of bone remodeling and the strain stimuli (Fig. 6.2B). This relationship is based on Frost's theory. Only net bone maintenance and resorption are associated with tissue strains. The MES is moved along the strain axis to determine the minimal strain threshold for osseointegration.

Theoretically at the initial implantation, the porous spaces are filled with mineralized tissue due to the wound healing of skeletal systems (Brunski 1988; Spector 1988). In reality, however, bone retained in the pore region of currently used orthopaedic implants has been shown to be sporadic and varying in location anywhere from 0% to 50% of the total available pores (Hofmann et al. 1993; Galante 1988). Animal studies have shown that bone loss occurs within porous regions during the remodeling period; this limits the final amount of bone mass in porous coated implants, which might decrease the life time of biomaterials (Bobyn et al., 1982, 1988; Cook et al., 1988, 1989; Spector et al., 1979). After reaching the remodeling equilibrium, part of the osseointegrated bone tissue may resorb due to the local stress shielding resulting from a material mismatch between the prosthesis and the surrounding bone (Brunski et al., ;Frost 1988, 1990a,b).

I have demonstrated in Chapter V that tissue stresses and strains anywhere within the porous region can be quantified within 85% accuracy. Such local strains are used to predict the amount of bone ingrowth along the interphase of a canine tibia implant based

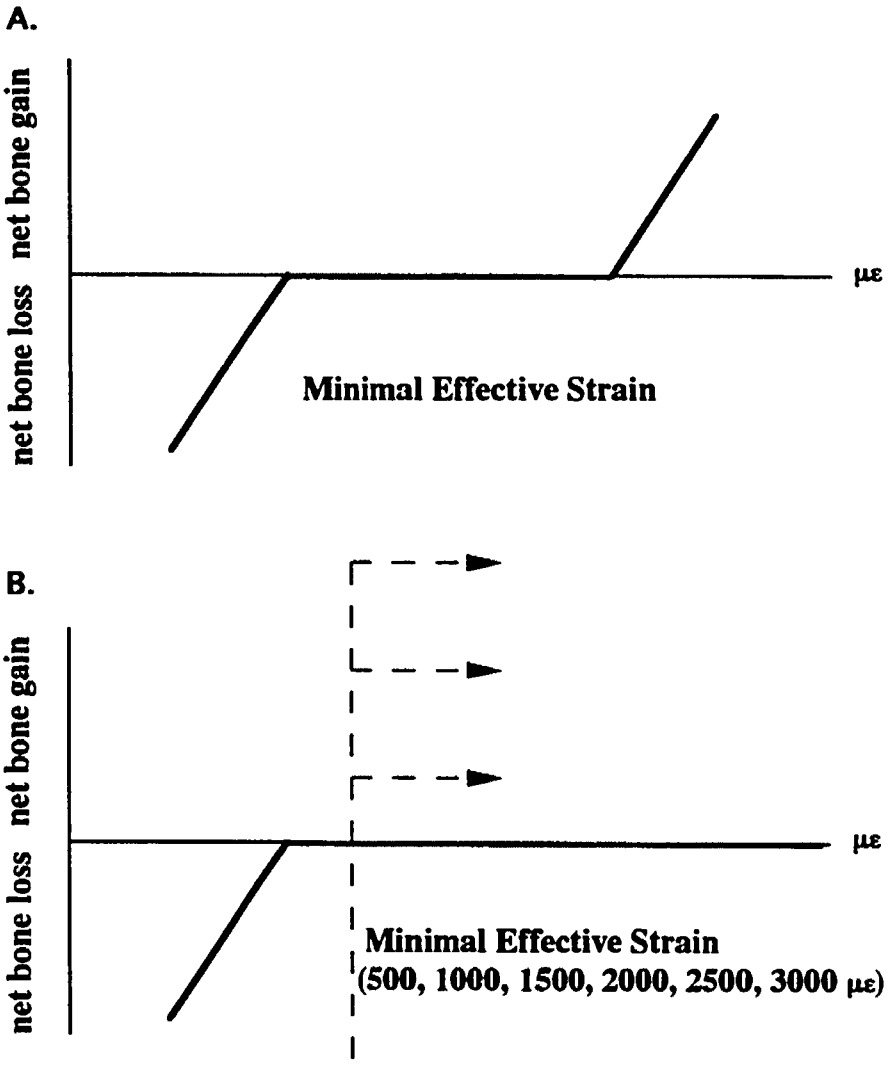

Figure 6.2 The relationship between the rate of bone mass change and the mechanical stimulus. (A) Frost's theory; (B) Presently used strain-remodeling relationship.

on the ingrowth rule. The resulting data is compared with the available experimental data to test the hypothesis of the ingrowth rule that local bone strains determine interfacial bone formation and resorption activities. The statistical correlation coefficient from the comparison provides an answer to the question of whether the tissue strains influence the modulation of the osseointegrated tissue.

6.1 Methods and Models

A histological section of a porous coated tibia implant from an experimental canine study (Goldstein et al. 1991) was used to construct two-dimensional finite element models. The interfacial zone between the implant and the tibia was analyzed by using the homogenization theory. The homogenization interphase model applied to calculate the strain fields of the interphases was based on the homogenization modeling scheme discussed in section 3.2; both global and local models were constructed.

The bone properties in the local model were varied with 1, 5, and 10 GPa to simulate the possible ranges of the healing bone property within the interphase. The two-dimensional global models contained implant substrate, four conical projections, an implant-bone interfacial zone, tibial cortical shell, and tibial trabecular bone (Fig 6.3). The implant was placed on the top surface of the proximal metaphysis of the tibia in which the trabecular bone was a major component. The shape of canine tibia was distally extended to include the tibia diaphyseal region made of cortical bone. Trabecular bone occupied most spaces of the tibial metaphysis; only the cortical bone was modeled for the tibial diaphysis.

Titanium alloy and bone were assumed to be isotropic and homogeneous. The material properties used for these materials in the global model are listed in Table 6.1. The interfacial regions between the implant and the bone were modeled as a composite material having the orthotropic material properties C_{ij} obtained from the local analysis.

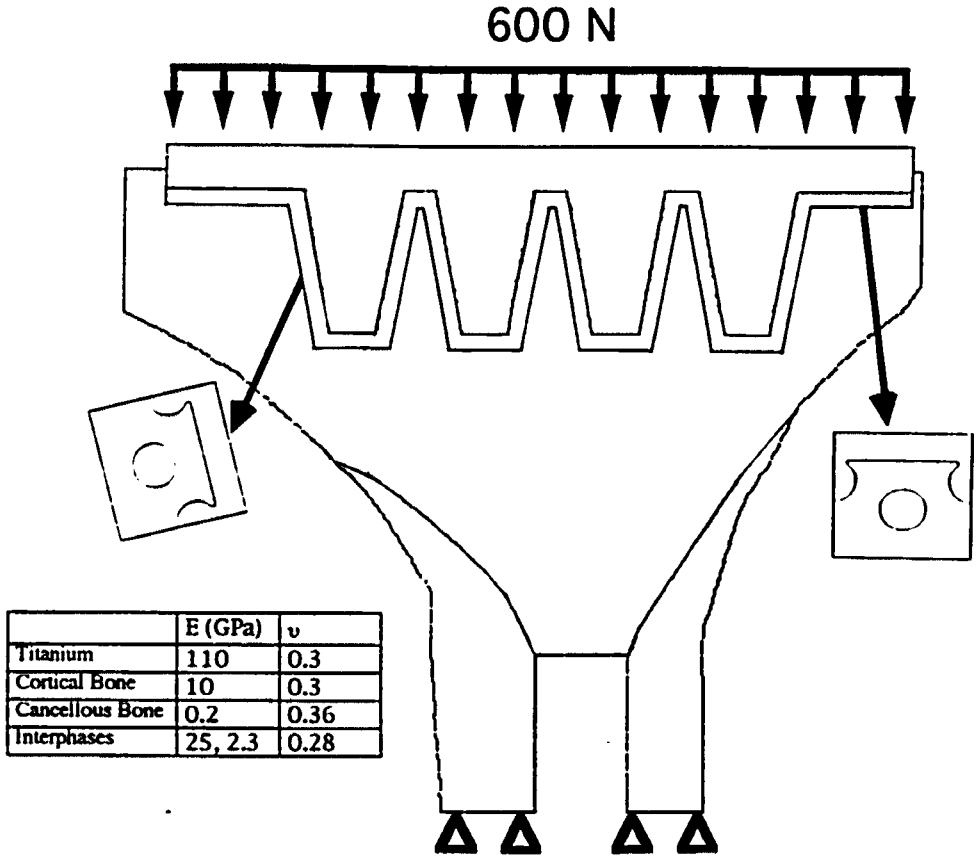

	E (GPa)	υ
Titanium	110	0.3
Cortical Bone	10	0.3
Cancellous Bone	0.2	0.36
Interphases	25, 2.3	0.28

Figure 6.3 Cross-section of the tibia-implant complex. The interfacial zone is constructed by using the homogenization unit cell models.

Table 6.1 Material properties used in the tibia implant model. (A) Isotropic materials; (B) Orthotropic material constants computed by the homogenization theory.

A. Isotropic elastic constants

Materials	E (GPa)	υ
Titanium	110	0.3
Cortical Bone	10	0.3
Cancellous Bone	0.2	0.36

B. Orthotropic interphase elastic constants

Bone Used	E_T (GPa)	E_L (GPa)	G_{LT} (GPa)	υ_{LT}	υ_{TL}
1 GPa	2.26	25.69	0.81	0.03	0.29
5 GPa	10.00	30.06	3.61	0.10	0.30
10 GPa	18.32	35.25	6.74	0.16	0.30

Since the properties of healing bone used in the local model varied from 1 to 5 to 10 GPa, three sets of the C_{ij} were used to build three global models. The only difference in these global models was the values of the interfacial elastic constant; the geometry, boundary conditions, and applied loads for all the models were the same.

The applied load of 600 N acting on the experimental canine tibia was measured by using a Fuji pressure sensitive film (Borodkin et al. 1994). The load was applied parallel to the long axis of the tibia and uniformly distributed on the top surface of the tibia implant. The nodes at the distal end of tibial diaphysis were fixed along both x and y directions.

A plane stress condition based on continuum mechanics was used to solve the strain distributions for both the local and the global FE models. The local strains of each element in the interphase were computed using the equation (3.7) $\varepsilon_{ij} = M_{ijkl}\varepsilon_{kl}$ where ε_{ij} represents the local interfacial strains, and ε_{kl} represents the global interfacial strains. When the element strain was greater than the MES, that element was labeled a bone element. On the contrary, when the element strain was less than the MES, the element was labeled as a fibrous tissue element. The areas of all bone elements were summed to calculate the total bone volume (V_b), while the areas of all fibrous tissue elements were added together to calculate the total volume of fibrous tissue (V_f). The percentage of bone ingrowth, Ip, was then quantified using the following formula

$$I_p = \frac{V_b}{V_b + V_f} \tag{6.1}$$

The estimated Ip values were compared to the actual measurements of bone ingrowth (Ia) in the experimental study reported by Goldstein (1991). The results from the comparison of Ip and Ia are categorized into two classes: fine subdivision and coarse subdivision. The classification is based on the number of regions used for calculating Ip and measuring Ia within the entire interfacial zone. For the fine subdivision, twenty five subdivisions of the tibia-implant interphases were used to quantify Ip and Ia (Fig 6.4 a).

Such category was based on the smallest areas on which the experimental data was measured. Within each subdivision, one average Ia and one average Ip were obtained through measurement and computation, respectively. Nine subdivisions were designed to perform the coarse subdivision case (Fig 6.4 b).

The statistical analysis of the comparison was accomplished by means of a linear regression:

$$I_a = A + B \times I_p \tag{6.2}$$

where A and B are population parameters. This expression is recognized as the general equation for a straight line. During the fitting of the regression function for Ia and Ip, a coefficient of determination, r^2, serving as a measure of the strength of the straight-line relationship was generated. A value of $r^2 \geq 0.5$ indicates that the single factor Ip could explain more than 50% of relationship with Ia. Therefore, Ip was considered the dominant factor to determine Ia and the correlation between Ia and Ip was significant if $r^2 \geq 0.5$.

The Ip values for three different interfacial C_{ij} (bone modulus of 1, 5, and 10 GPa) and the six different MES (threshold 500, 1000, 1500, 2000, 2500, and 3000 με) were compared to the experimental results. These strain values were chosen according to Frost's theory.

(a) Coarse Regions (9 subdivisions):

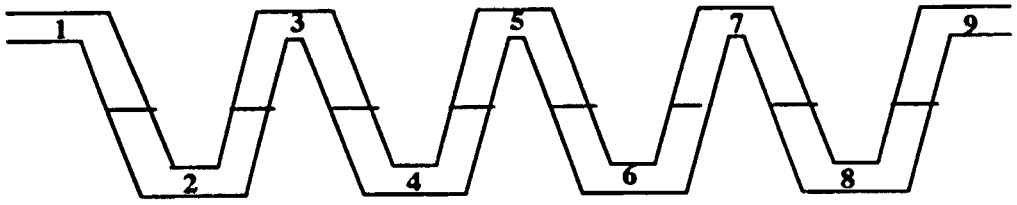

(b) Fine Regions (25 subdivisions):

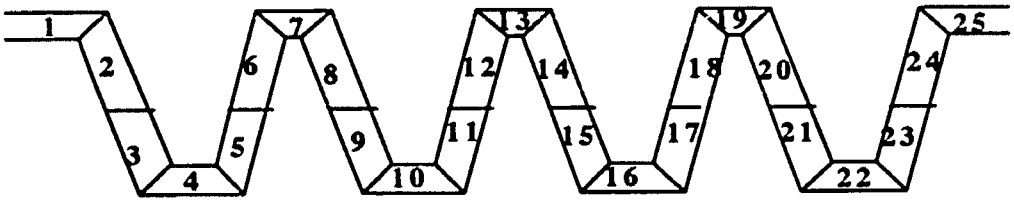

Figure 6.4 Two categories for quantifing the amount of bone ingrowth at the interphase regions: (a) 9 subdivision case where the interphase is divided into 9 areas, labeled from 1 to 9; and (b) 25 subdivision case where the interphase is divided into 25 areas, labeled from 1 to 25. Within the area of each subdivision, the amount of bone ingrowth is averaged.

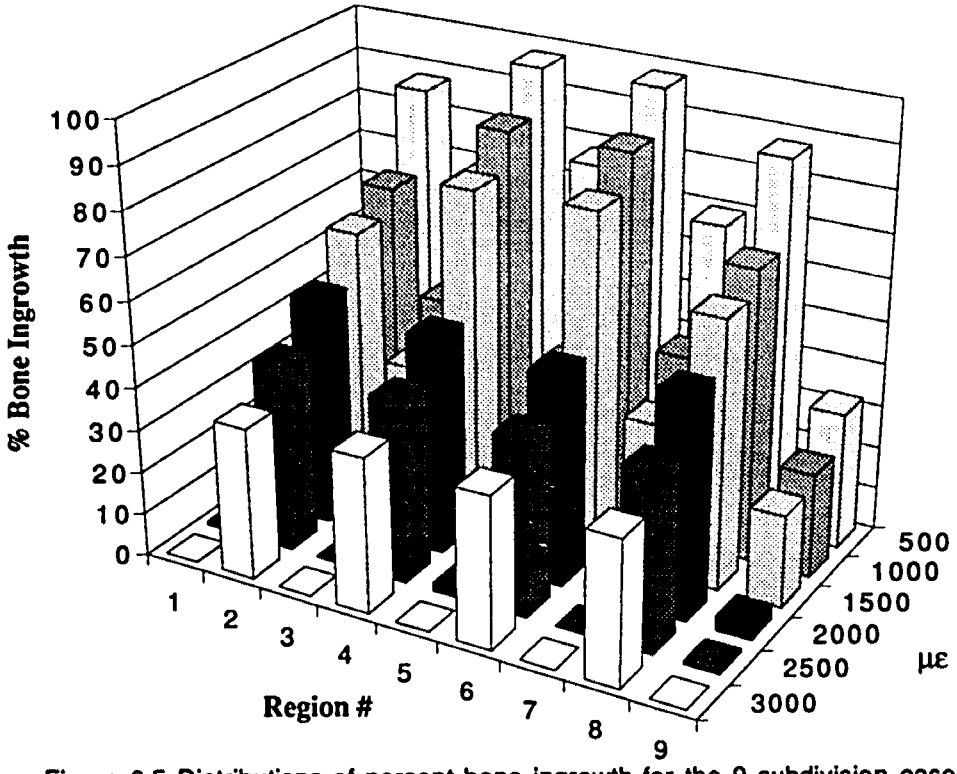

Figure 6.5 Distributions of percent bone ingrowth for the 9 subdivision case with 1 GPa bone modulus

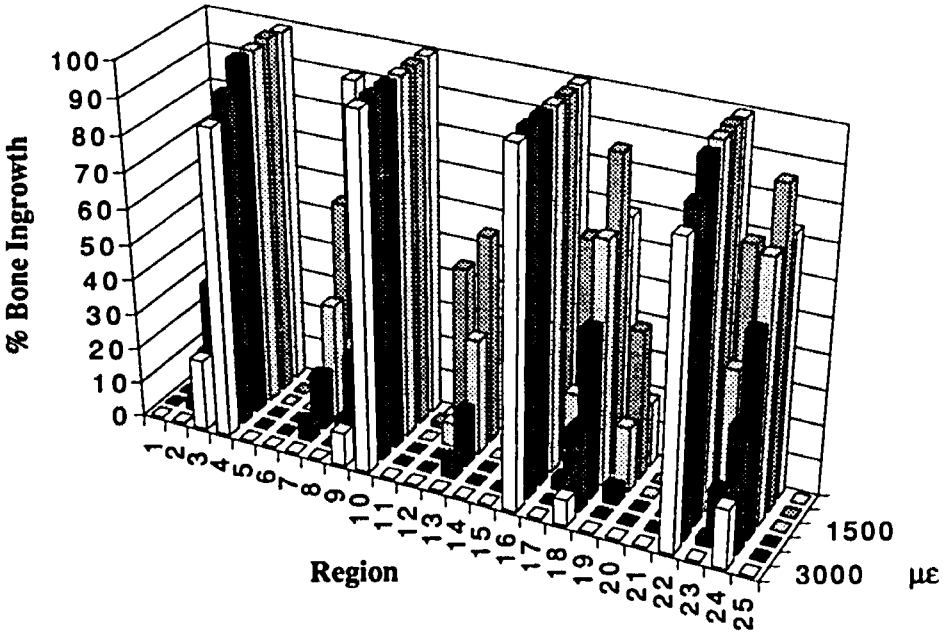

Figure 6.6 Distributions of percent bone ingrowth for 25 subdivision case with 1 GPa bone modulus

6.2 Results

The predictions for bone ingrowth, Ip, along the tibia-implant interphase based on Young's modulus of the interfacial healing bone being 1 GPa are shown in Figure 6.5 and Figure 6.6. In the case of the interfacial zone divided into nine subdivisions, the amount of bone ingrowth is higher at each cone tip than at each cone valley (Figure 6.5). The percent ingrowth decreased with the increase of the strain threshold (MES). The average percent ingrowth ranged from 72, 71, 58, 51, 42, and 35% at the cone tips to 32, 26, 15, 4, 3, and 0% at the cone bases for MES equivalent to 500, 1000, 1500, 2000, 2500, and 3000 με, respectively.

Figure 6.6 is a plot of the ingrowth (Ip) distribution along the interfacial zone for the case with 25 sundivisions. The ingrowth trend is similar to that of the 9 subdivision case; the highest amount of bone ingrowth, 95%, was located in the cone tip regions.

In general, the bone ingrowth predicted by different models with varying bone moduli, i.e., 5GPa and 10GPa, revealed similar distribution patterns for both the 9 and the 25 subdivision cases (Fig 6.7, Fig 6.8). However, when the strain threshold was greater than 2000 με, there was no ingrowth anywhere for the case with interfacial bone modulus of 10 GPa.

Overall, current results indicates that, by using 1500 με threshold with 1 GPa interfacial bone modulus, the homogenization interphase model predicts the most reasonable bone ingrowth corresponding to the actual ingrowth. The reasons are as follows:

(1) The average differences between the actual ingrowth measurements, Ia, from Goldstein's animal study and the predicted ingrowth, Ip, from analysis of models with various healing bone moduli and various strain thresholds are shown in Figure 6.9. The data indicate that the resulting bone ingrowth obtained from the case with the combination of bone modulus of 1 GPa and threshold of 1500 με exhibited the smallest

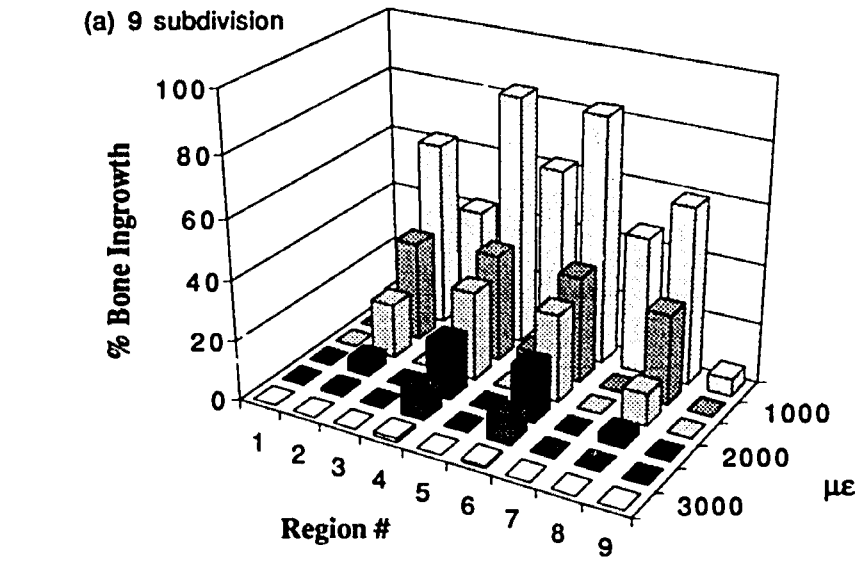

(b) 25 subdivision

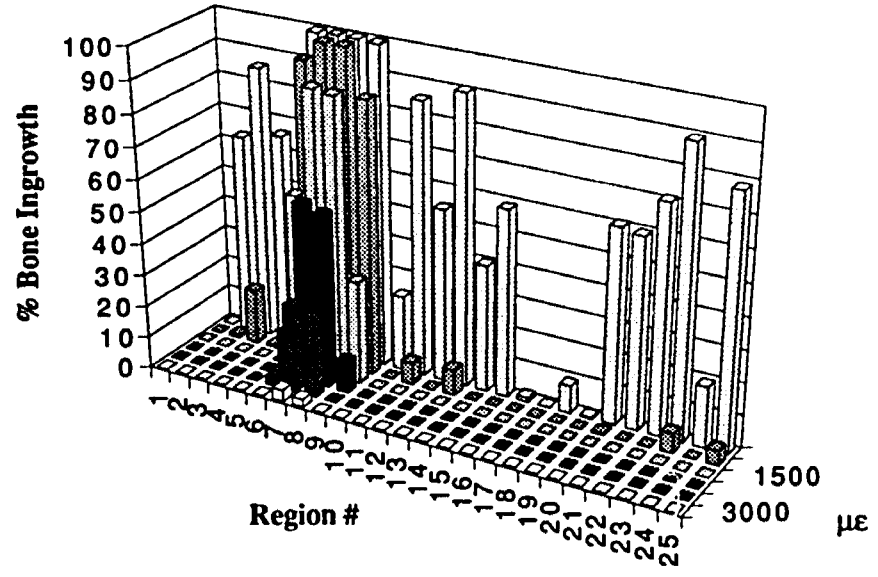

Figure 6.7 Percent bone ingrowth with the interfacial bone modulus 5GPa

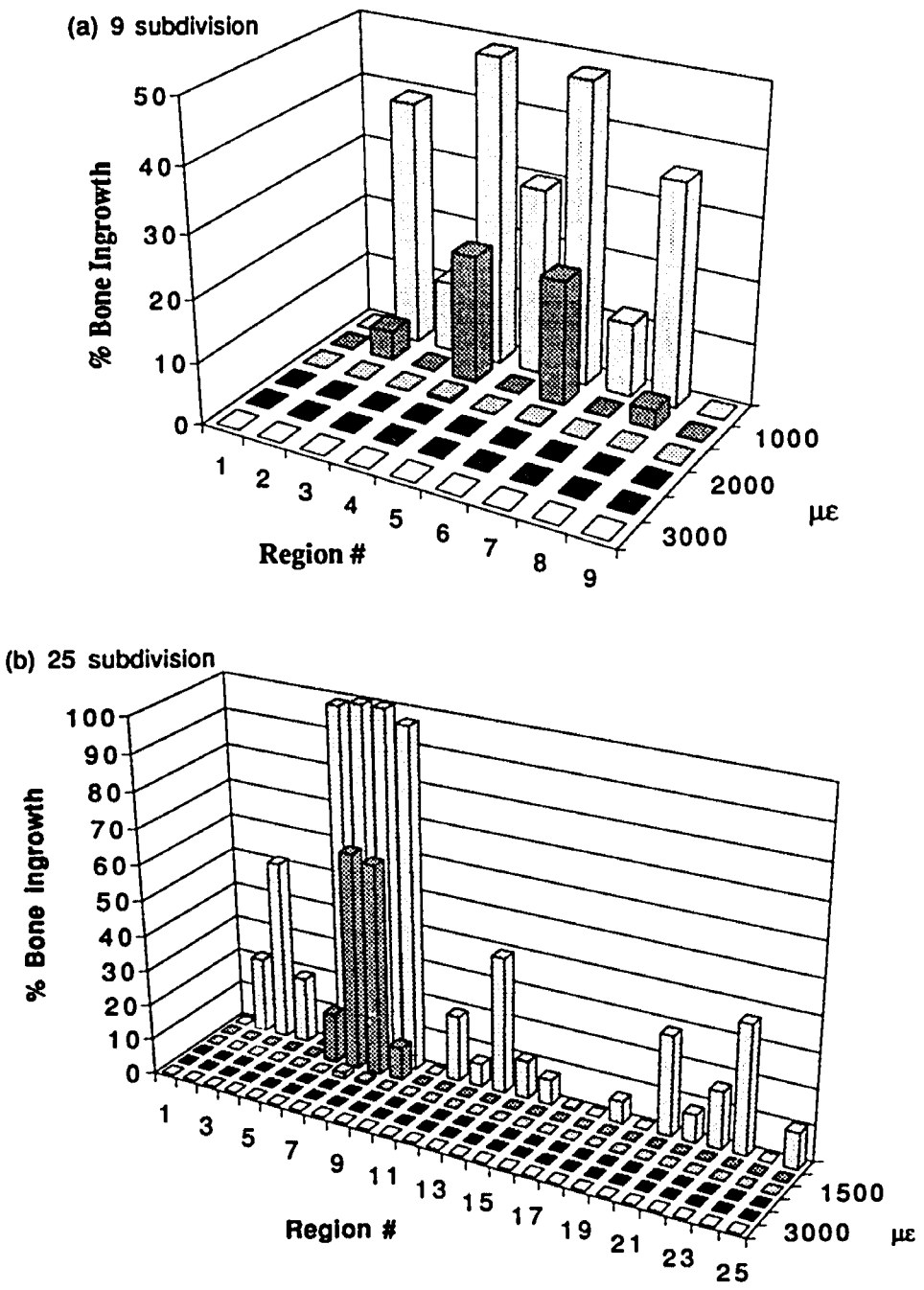

Figure 6.8 Percent bone ingrowth with the interfacial bone modulus 10 GPa

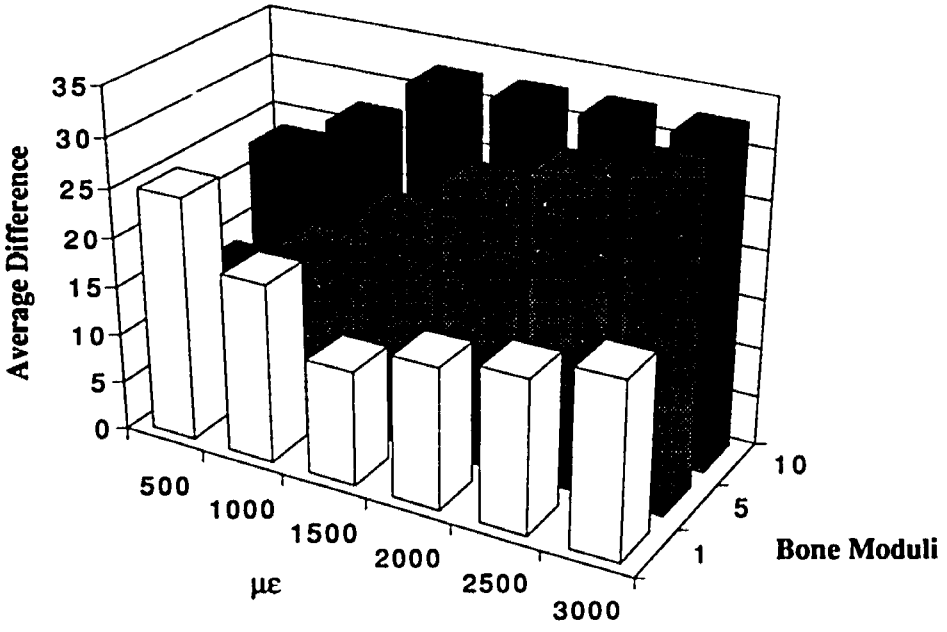

Figure 6.9 Average differences between the bone ingrowth measured from animal study and that predicted by ingrowth rule.

(a) 9 subdivision

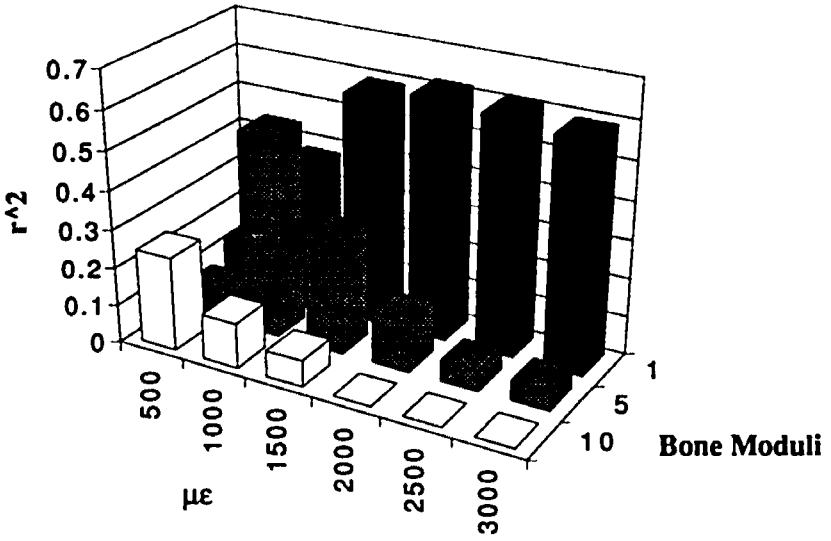

(b) 25 subdivision

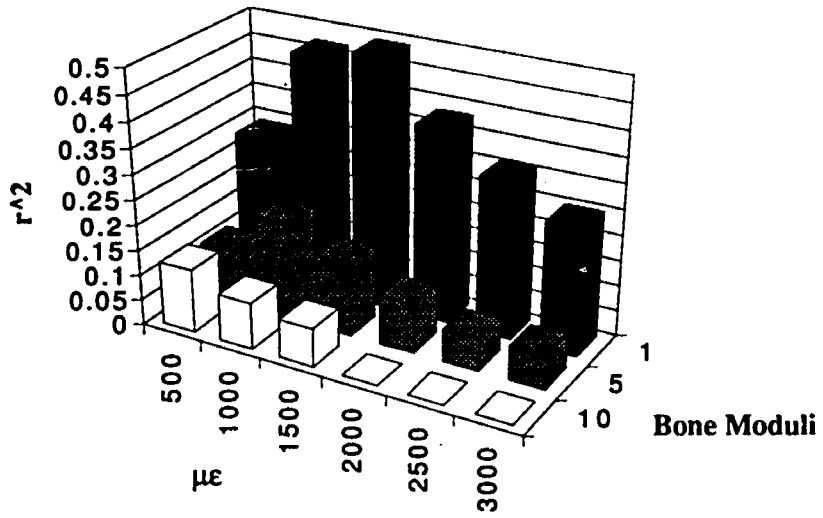

Figure 6.10 Coefficients of determination resulted from regression analysis determining relationships between the measured and predicted bone ingrowth

Table 6.2 Lists of parameters A, B, and r^2 for linear regression: Ia=A+B*Ip

9 subdivision

Bone Modulus	με	A	B	r^2
1 GPa	500	17.27	0.22	0.13
	1000	15.48	0.37	0.38
	1500	16.9	0.48	0.6
	2000	21	0.47	0.62
	2500	22.41	0.54	0.61
	3000	22.92	0.63	0.6
5 GPa	500	25.32	0.15	0.08
	1000	22.76	0.63	0.52
	1500	26.43	0.64	0.3
	2000	29.2	0.7	0.13
	2500	30.84	0.91	0.05
	3000	31.03	7.44	0.05
10 GPa	500	23.12	0.39	0.25
	1000	29.5	0.6	0.12
	1500	31	19.93	0.06
	2000	-	-	-
	2500	-	-	-
	3000	-	-	-

25 subdivision

Bone Modulus	με	A	B	r^2
1 GPa	500	4.58	0.36	0.29
	1000	15.19	0.34	0.44
	1500	19	0.37	0.5
	2000	23.52	0.33	0.38
	2500	25.86	0.32	0.31
	3000	27.44	0.29	0.25
5 GPa	500	22.73	0.18	0.11
	1000	28.1	0.25	0.2
	1500	29.34	0.29	0.15
	2000	30.2	0.4	0.1
	2500	30.84	0.7	0.06
	3000	30.92	6	0.07
10 GPa	500	26.9	0.2	0.13
	1000	30.31	0.36	0.1
	1500	30.9	16	0.08
	2000	-	-	-
	2500	-	-	-
	3000	-	-	-

- : No comparison made due to zero Ip values

deviation (11) from actual ingrowth amount.

(2) Linear regressions were used to study relationships between the measured Ia and the predicted Ip for all cases including the three different interfacial bones and six strain thresholds. Table 6.2 lists the population parameters, A and B, and the coefficients of determination, r^2, resulting from the regression analyses. The different values of r^2 for the different cases are shown in Figure 6.10. The best correlations between the predicted and the experimental results are again found in the case of 1 GPa bone modulus and 1500 με threshold, (see also Fig 6.9). In this case, r^2 is 0.5 and 0.6 for the 25 and 9 subdivision comparison, respectively. Both correlations are considered statistically significant because r^2 is $\geq$ 0.5. The slop of regression line, B, for this case is less than 1. This result implies that the ingrowth rule overpredicts the amount of bone ingrowth compared to the actual ingrowth data.

The results support the hypothesis that the tissue strains do influence the remodeling of the osseointegrated tissue, and under the fully ingrown assumption the optimum magnitude of tissue strains for prediction of bone ingrowth is 1500 με.

6.3 Discussion

The experimental data used in this study show that bone ingrowth occurs primarily around the cone tips of the tibia implant, and at the base of the cone, ingrowth is sporadic (Fig 6.11). The present results reveals a consistent distribution pattern with the experimental results (see Fig 6.5 and Fig 6.6). It has been demonstrated that the ingrowth pattern is related to the stress distributions in a multiple cone implant-tibia structure (Borodkin et al., 1994; Hollister et al., 1993). The current results demonstrate that in the global tibia model, load transfer passes mainly through the pegs where bone ingrowth amounts are high because of the higher stiffness of titanium implant compared to that of bone tissues (Fig 6.12). The valley regions between the pegs sustain very little stresses

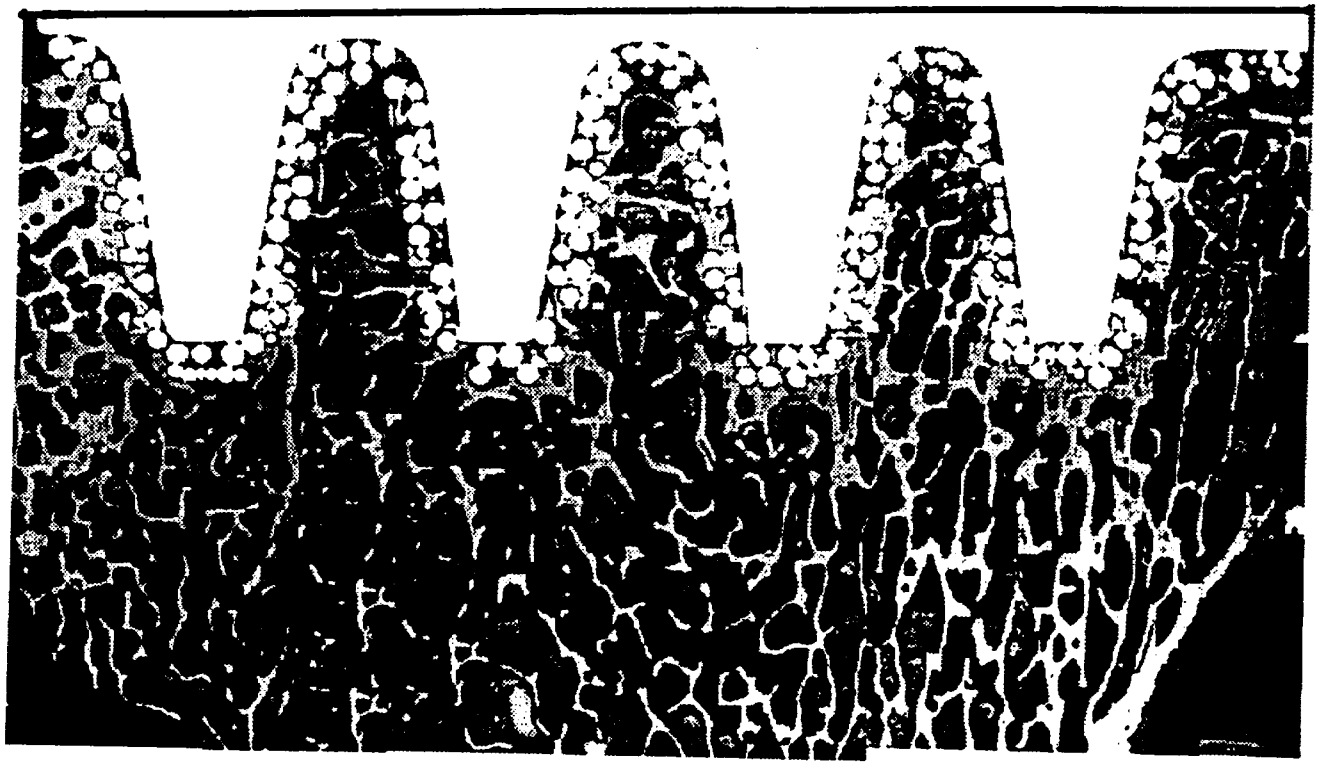

Figure 6.11 Image of bone ingrowth at canine tibia-implant interpahse. Ingrowth is primary around the cone tips, and sporadic ingrowth amount at the base of cone. The left and right hand side are anterior and posterior of proximal tibia, respectively. (data provided by Orthopaedic Research Laboratories, University of Michigan).

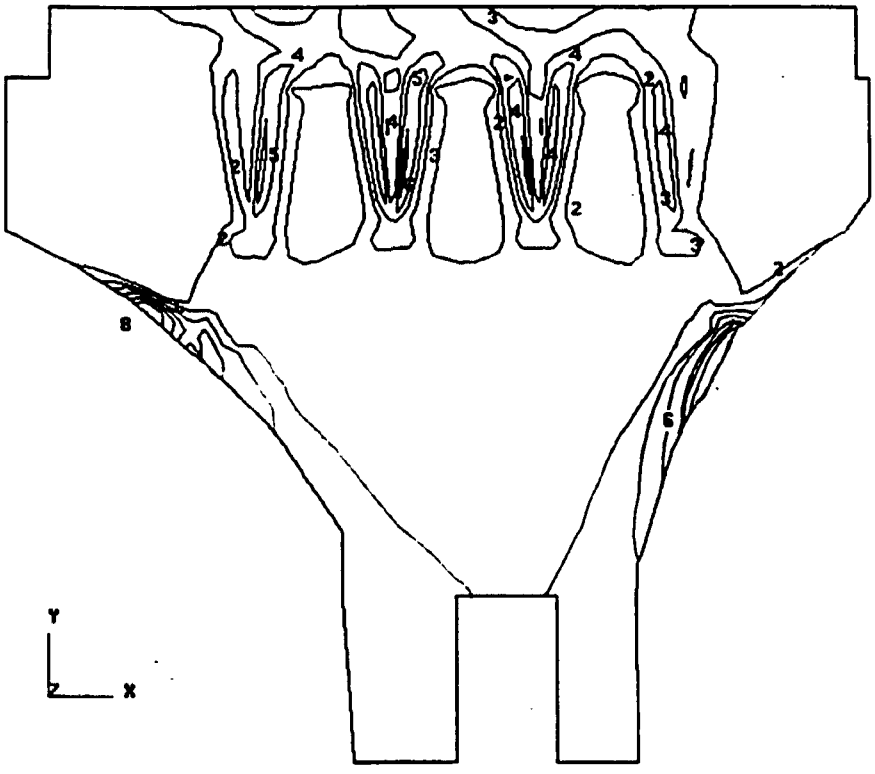

Von Mises Stresses (MPa)

8	0.251E+02
7	0.215E+02
6	0.179E+02
5	0.143E+02
4	0.108E+02
3	0.717E+01
2	0.358E+01
1	0.000E+00

Figure 6.12 Contour plot of Von Mises stress distribution on the tibia implant. Stresses mainly pass through the pegs where bone ingrowth is high.

and reveal very small amounts of bone ingrowth. The correspondence of low stresses to low ingrowth and vice versa implies that a relationship may exist between mechanical stimuli and osseointegration.

The parametric study of the ingrowth rule provides further solid evidence in support of such a relationship. The bone ingrowth predicted by using an osseointegrated bone with 1 GPa modulus and a strain threshold of 1500 με can be statistically correlated to the actual amount of bone ingrowth obtained from the animal study. This 1500 με is within the strain range proposed by Frost in his bone remodeling theory (1988). Strain above or below 1500 με cannot provide a correlation greater than 50% between Ia and Ip. Physiologically, a mechanical strain greater than 1500 με may inhibit the bone remodeling activities which cause net bone loss in the skeleton during a normal physiological rhythms. Although this dissertation is not concerned with the why or how adaptation mechanisms are performed, it does show that the result of adaptation i.e., implant osseointegration, and the tissue strain exhibit significant correlation.

The current study overpredicts bone ingrowth compared to the actual ingrowth. A major reason is that the interphase was assumed to be initially fully ingrown with mineralized tissue. Such an ideal situation could be achieved in a biocompatible implant system, for instance a titanium implant, if the host tissue is healthy and the implant is immobilized during the healing stage. Animal studies have also shown that full ingrowth is possible at the early stage after implant surgery (Bobyn et al., 1982). In reality, however, the ingrowth may not be complete due to several reasons among which are the healing capability of the host tissues, the variability of pore size, and the impossibility to fully immobilize the implant. These conditions may lead to partially ingrown interphases and may alter the values of bone ingrowth Ip predicted by the ingrowth rule. In Chapter Seven, I have shown that the change from a fully ingrown to a partially ingrown situation results in a reduction of percent bone ingrowth, about 10%. The current model based on initially fully ingrown assumption appears to overpredict the resultant bone ingrowth

possibly because the initial intrephase of the canine tibia implant is not completely ingrown with mineral tissue.

Furthermore, the model largely overpredicts bone ingrowth at the tips of each cone, 95%. This can be attributed to the errors resulted from boundary conditions. The interphases at the cone tip are primarily subjected to a normal load across the interphase equivalent to the boundary condition analyzed in case 3, Chapter V. In case 3, it was shown that the interfacial stresses are overpredicted, about 15% greater than the actual stresses. It could be that the overpredicted ingrowth at the cone tips in the current study results from a synergy between the interphase condition and the loading condition.

Recently, in the Orthopaedic Laboratories at the University of Michigan, Hollister (1993) and Borodkin (1994) have quantified the relationship between mechanics and the bone ingrowth through a global finite element model and experiments. Hollister (1993) studied bone adaptation around the same tibia implant using a topology optimization method. The topology optimization method minimizes the structure compliance and results in high bone density in the areas where the strain energy density is concentrated. Hollister's predictions showed that the bone density distribution near the proximal tibia was always concentrated at the cone tips, and there was zero bone density at the cone bases. This is explained by the fact that bone prefers to be placed at the cone tip because the tibia-implant unit intends to minimize the compliance for the entire structure. In a regression analysis (coarse subdivision) between the actual ingrowth measurements and the predicted bone densities, Hollister's results showed that the correlation was statistically significant when the areas of interphase subdivision are relatively large (Table 6.3). In this dissertation such a global comparison corresponds to our 9 subdivision case. However, Hollister showed that if the comparison (fine subdivision) is performed by using refined subdivision, corresponding to our 25 subdivision case, the relationship between the predictions and the measurements is not significant mainly

Table 6.3 Coefficient of determination, r^2, obtained in present study vs. those obtained by Hollister et al.

Study	Coarse Region (9 Subdivisions)	Fine Region (25 Subdivisions)
Micromechanical Analysis (Present Study)	0.6	0.5
Global Optimization (Hollister et al. 1993)	0.6	0.25

because the predicted bone densities at the cone bases are almost equal to zero, and predicted densities are much higher than found experimentally.

Furthermore, Borodkin (1994) correlated the distributions of strain energy density along the interphase to the actual measurements of bone ingrowth using the same ingrowth data. She averaged ingrowth data along the interphase for all cones into mean values for a universal cone, and successfully correlated these mean ingrowth data to the averaged strain energy density predicted from a global FE model. However, she could not statistically relate the ingrowth measurements to the strain energy density for each corresponding cone.

Previous studies predict bone ingrowth in general, and provide valuable information for the shape designs of prostheses. However, in order to understand the mechanisms of osseointegration and to design the coating regions on the prosthesis to obtain the most efficient biological fixation due to bone ingrowth, the studies of bone adaptation need to be extended to account for the microstructure of porous coatings. In

other words, the local correlation (25 subdivision comparison) needs to be statistically significant for the ingrowth rule to be valid.

The present study provides a global-local mechanical model which accounts for the microstructure of the interphases. The amount of bone ingrowth for both coarse (9) and fine (25) subdivision cases is estimated based on the ingrowth rule. The initial healing bone tissue with bone modulus 1 GPa provides the most effective FE model for the estimation of the amount of bone ingrowth. The average deviations of the predicted ingrowth amount from the measurements are less than 15%. When the average areas become large, such as the 9 subdivision case, the coefficient of determination, r^2, in this study approaches the value (0.6) predicted by the global optimization theory (Table 6.3). For the local bone adaptation resulting from the local microstructure influence, this study provides much better correlation (r^2=0.5) than the global optimization theory (r^2=0.25).

The results demonstrate that both global comparison and local comparison between the estimates and the actual ingrowth measurements exhibit strong correlation. The results indicate that there exists a mechanical reason for osseointegrated bone adaptation. This study supports the ingrowth rule and provides evidence that Wolff's law is valid within the interfacial zone. The most important result is that 1500 με represents the minimal effective strain- a strain threshold for osseointegration around porous coated implants.

Note that in analyzing the current tibia model, a single, vertical, load was used. The effect of the other loading components on the resultant ingrowth is not studied in this dissertation. However, a previous study has shown that the vertical load is the dominant mode of loading on the canine tibia (Borodkin et al., 1994). Other loading conditions did not exhibit a significant correlation to the actual ingrowth results (Hollister et al., 1993). It is believed that the current results should hold even though the implant is under a multiple load situation. The ingrowth rule proposed in this dissertation can now be used

to study the performance of biological fixation onto the porous coated implants.

CHAPTER VII

HIP PROSTHESIS EVALUATION

7.0 Introduction

This part of my research is an attempt to characterize the performance of currently used porous coated total hip replacements (THR) by analyzing the micromechanics of the implant-tissue interphase. Two major issues associated with the interphase micromechanics which determine the success of the cementless porous coated implants are: (1) the eventual bone-ingrowth into pores in the prostheses, and (2) the minimization of the destruction of the fixation materials, i.e. tissue damage and coating debonding. These two issues are directly dependent on the mechanical stresses and strains, and will be investigated by using the information obtained from the homogenization interphase modeling.

First, the assumption is that the more bone ingrowth that occurs, the more successful the implants are. In Chapter VI, I provided evidence that the amount of bone ingrowth is related to tissue strains within the interphases. I also defined an ingrowth rule stating that the strain threshold for osseointegration is 1500 $\mu\varepsilon$. In the current chapter the ingrowth rule is used to quantify the possible bone ingrowth along the THR-femur

interphase. The quantified values for bone ingrowth from FE models are some of the indicators used in the evaluation of the commercial THR design.

Second, a factor influencing the life time of THR is the failure of the ingrown tissue and the coating materials. Tissue damage may result in a loosening of the interface between the implant and the femur; debris denuded from implant coatings decreases the performance of THR and causes adverse tissue reactions. Both interfacial loosening and coating debonding ultimately reduce the longevity of the prostheses. This study predicts the potential for tissue microdamage and coating debonding on the basis of the von Mises yield criteria for structural materials by using the quantified interfacial stresses. Again, the estimated values of the above events are used to evaluate the design of porous coated THR.

Since proximally coated (40% coatings) and fully coated THR (80% coatings) are probably the most often used hip prostheses today, this chapter focuses on the evaluation of these two implant designs.

Clinical reports have concluded that the lack of bony-implant interdigitation at the proximal femur is most likely associated with the use of a fully coated THR. Proximal femur failure has also been found in patients implanted with fully coated THR (Gustilo 1988). It has been speculated that the bending stress on the proximal region for a fully coated THR can be shielded due to firmly distal fixation. It is also stipulated that osseointegration is regulated by mechanical stimuli; thus stress shielding may result in less depth of bone apposition onto the proximal interphase which may ultimately lead to implant failure. However, mechanical analyses have not provided detailed information to support these speculations. In chapter 6, I have shown that the Wolff's law is valid at the implant interphase. The present study addresses two questions: (1) does the current proximally porous coated THR design provide a strain field which leads to more biological fixation in the proximal region than a fully coated THR? (2) How does the amount of calcified ingrown tissue affect the risk of material failure and tissue damage?

In what follows, I will first estimate the amount of bone ingrowth (Ip) for both 40% coated and 80% coated THR based on the ingrowth rule. THR homogenization models with initially fully ingrown interphases are used to calculate the percentage of bone ingrowth. Next, the number of possible failure sites (N_m) of implant materials and the microdamage (Nb) of ingrown bone are calculated to account for the potential of implant failure. Finally, partially ingrown implant/tissue interphases with an incomplete bone ingrowth, based on the computed Ip from the initially full ingrown interphase, are taken into account in the study of the material failure risk and implant stability by evaluating the changes of the stress fields which deviate from fully ingrown interphases.

The analyses of I_p, N_m, and Nb show whether the different THR designs influence the potential for material and tissue microdamage of the implants, and how well the proximally porous coated THR can be fixed.

7.1 Methods and Data Calculations

Total hip replacements were examined by means of the two-dimensional interphase modeling technique described in Chapter II. The design of the models was based on the assumption that the material properties of titanium metal and both cortical and trabecular bone were isotropic and homogeneous (Table 7.1). The material properties of the implant/tissue interphase in the global models were the anisotropic properties obtained from the previously developed homogenization unit cell model (UCM) in which bone had a modulus 1 GPa. The global hip models were fixed in all degrees of freedom at the distal end of the femur. A concentrated force of 3000 N was applied at the femur head having a 20° inclination with the y-axis.

Both 40% coated and 80% coated THR included one model for the fully ingrown interphase and one model for the partially ingrown interphase. Figure 7.1 lists the four numerical global models which are analyzed. The UCM of the fully ingrown interphase

Table 7.1 Material properties used in THR model. (A) Isotropic materials; (B) Orthotropic material constants computed by the homogenization theory.

A. Isotropic Elastic Constants

Materials	E (GPa)	υ
Titanium	110	0.3
Cortical Bone	10	0.3
Cancellous Bone	1	0.35

B. Orthotropic Interphase Elastic Constants

Bone Used	E_L (GPa)	E_T (GPa)	G_{LT} (GPa)	υ_{LT}	υ_{TL}
1 GPa	2.26	25.69	0.81	0.03	0.29

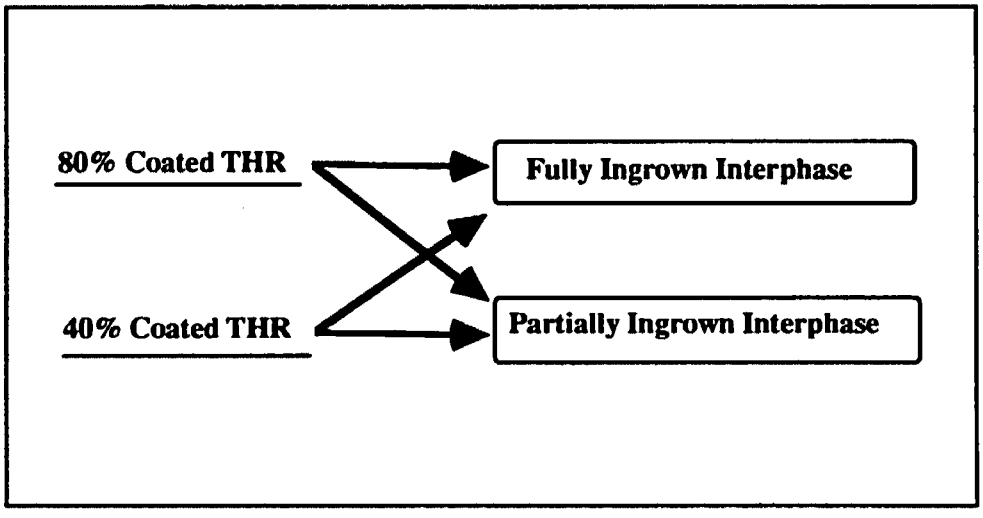

Figure 7.1 Four global THR models analyzed in this dissertation

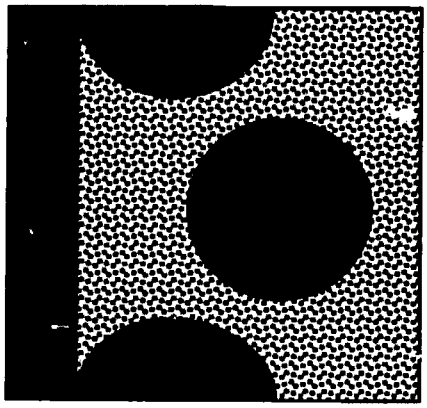

A. Fully Ingrown Interphase

Metal Bone

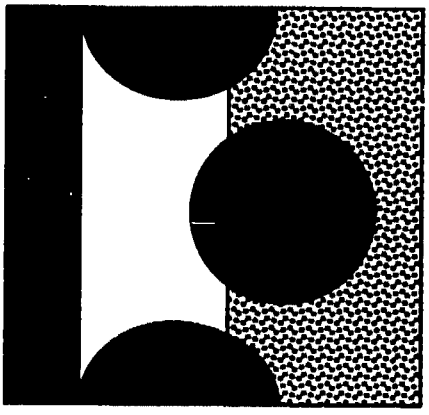

B. Partially Ingrown Interphase

Soft Tissue

Figure 7.2 Schematic of both fully ingrown interphase UCM (A), and partially ingrown interphase UCM

and the UCM of the partially ingrown interphase are shown in Figure 7.2. The difference between these two local models is the distribution of osseous contents in the tissue region. Bone mass filled all tissue region in the case of fully ingrown interphases because of the assumption that the healing process was initially complete. The percentage of bone mass in the partially ingrown interphase was obtained from the calculations of Ip in the fully ingrown interphase model; the remaining part of the tissue domain was filled with fibrous tissue.

The UCM was about 910 x 910 μm and contained two microspheres, 300 μm in diameter with pore size of 200 μm. The effective interphase stiffness (Cij) in the THR was calculated by analyzing the UCM for both full and partial ingrowth.

The two porous coated regions within the prosthesis, the medial and the lateral side, were different for 40%, and 80% coatings (Fig 7.3). The global models were computed by the standard finite element procedure. Following this, a coupled global/local modeling was performed and local interfacial stress and strain fields were obtained (see Chapter III).

The ratio of the highly strained tissue areas (strains $\varepsilon > 1500$ με) to the total available porous areas (I_p) was calculated. Local interphase stresses were used to predict the potential of coating debonding within the interphase. Metal failures were assumed to occur in the areas where the local Von Mises stress (τ) was greater than the yield strength of titanium (850 MPa). Tissue microdamages were assumed to occur in the areas where the local Von Mises stress (τ) was greater than the yield strength of cortical bone (120 MPa). The total number of failure sites of the materials within the interphase, N_m and N_b for titanium metal and ingrown bone, respectively, were determined. A comparison between the Ip, Nm, and Nb for 40% and 80% coated prostheses was performed. The resulting information can be used for the evaluation of commercial implant designs.

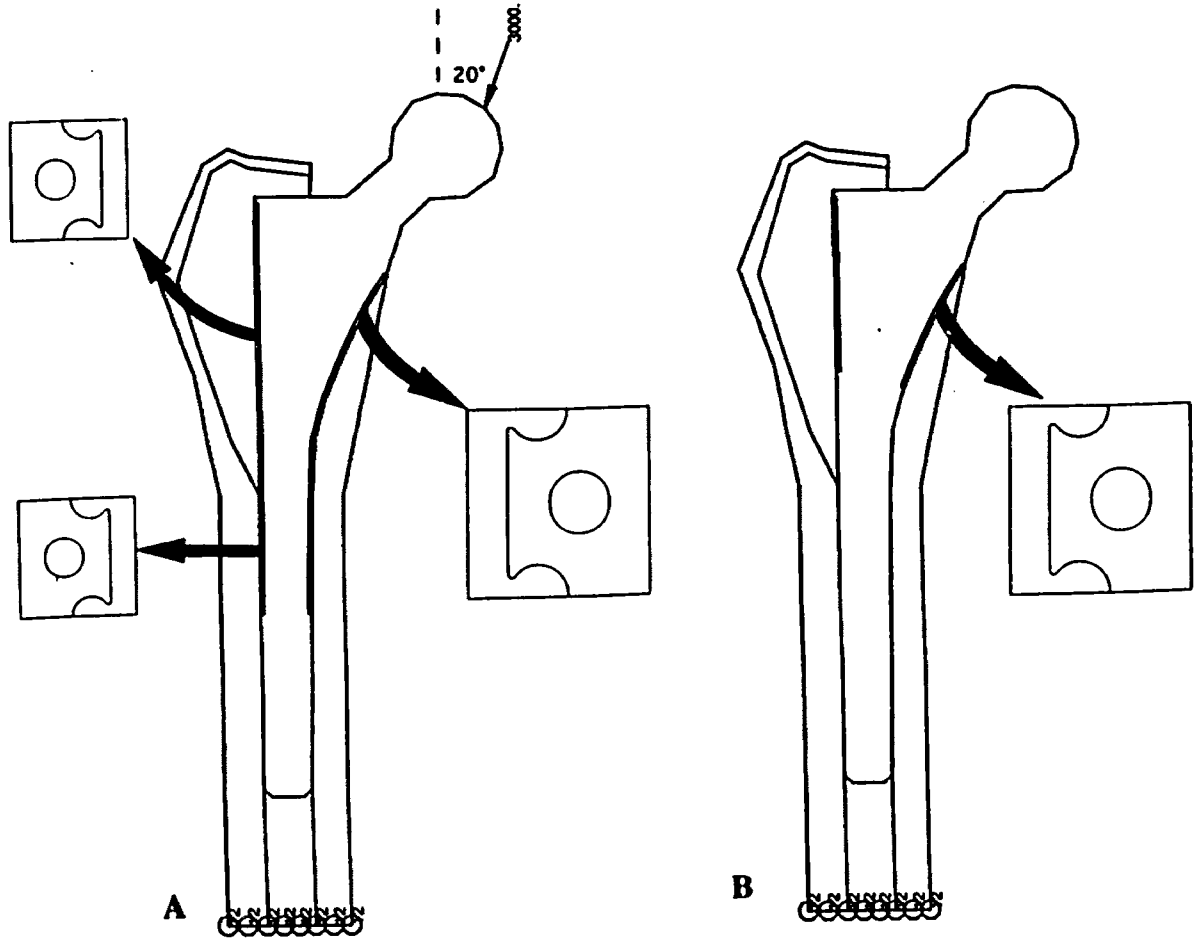

Figure 7.3 Cross-section of the 80% (A) and 40% (B) coated THR models.

7.2 Results

Shown in Fig 7.4 are the global Von Mises equivalent stress distributions of the 40% and 80% coated THR models with a fully ingrown interphase. The Von Mises stresses for both implants are similarly distributed and concentrated at the neck of femur with a maximum value of 80 MPa. The stresses passed mainly from the medial surface of the proximal stem to the lateral side of the implant's distal end. The cortical bone apical to the implant's distal end sustained high stresses- about 50 MPa. The trabecular bone region carries very little stress- less than 1 MPa.

The resultant local stresses at the trabecular bone-implant interphase, lateral side of the prosthesis, are shown in Figure 7.5. Peak Von Mises stresses, 55 MPa, were concentrated at the sinterneck areas. The maximum bone stress was up to 3.5 MPa for 80% coated THR and 6 MPa for 40% coated THR; both are located at the outer surfaces of the microspheres. On the medial side of the prosthesis, Von Mises stresses, 105 MPa, were again concentrated at the sinterneck areas (Fig 7.6). Stresses in bone were concentrated on the outer surfaces of the microspheres. No substantial difference in the maximum stress of bone between the two implant designs, 7 MPa for 40% THR and 8 MPa for 80% THR, could be found.

None of these maximum stresses exceeded the yield strength of bone. Tissue microdamage did not seem to occur for either prosthesis design. More stresses was transferred into the osseous tissue in the 40% coated THR than in the 80% coated THR. No metal failure was predicted in the cases with fully ingrown interphase; a 2% failure rate was predicted at the distal end of 80% coated THR where the maximum stress 970 MPa was located on the sinterneck region and exceeded the yield strength of titanium. The resulting material failure rates, Nm and Nb, and percent bone ingrowth Ip are listed in Table 7.2.

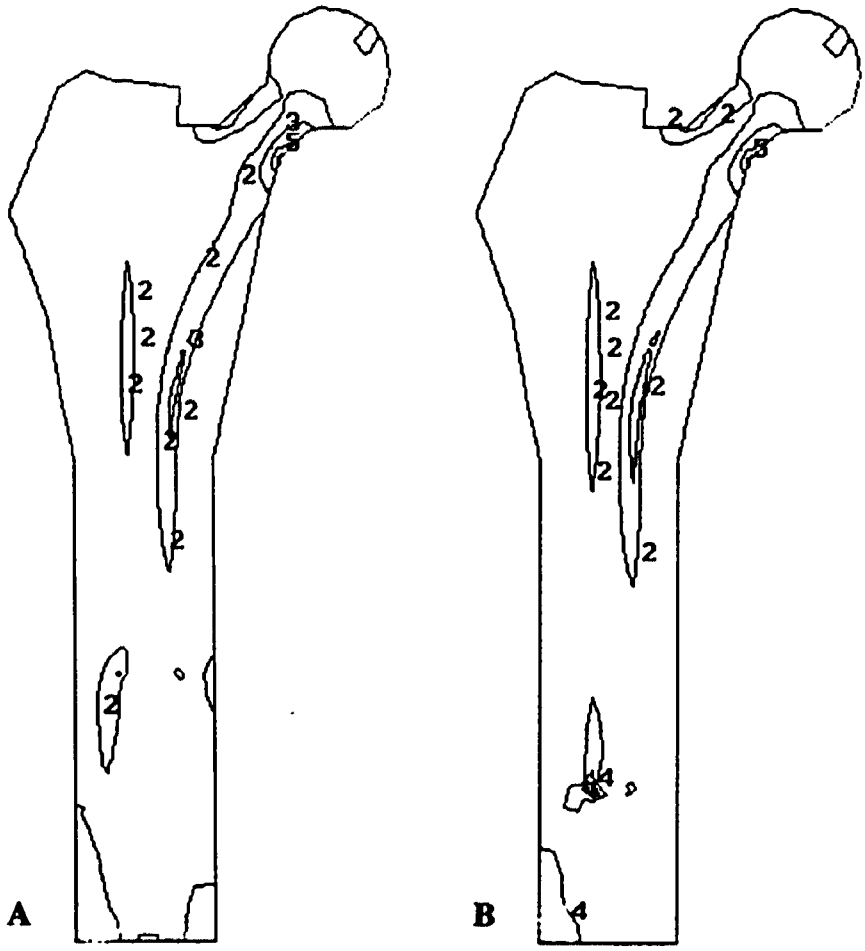

Figure 7.4 Global Mises stress distributions of 80% (A) and 40% (B) coated THR models.

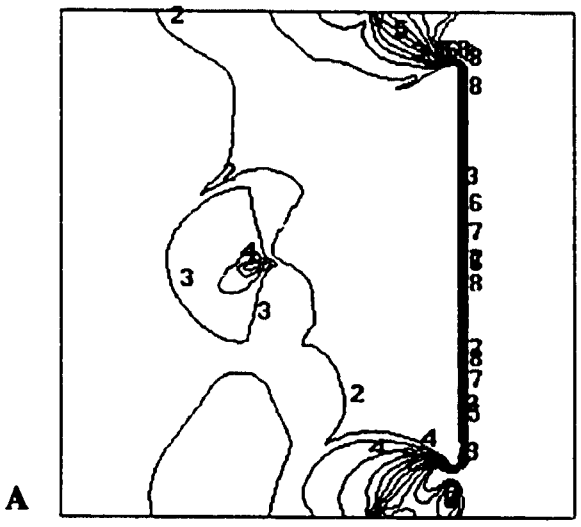

A

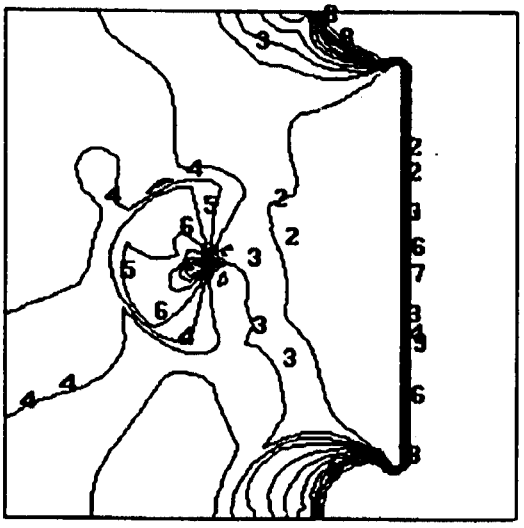

B

Von Mises Stresses (MPa)

8	0.420E+01
7	0.364E+01
6	0.308E+01
5	0.252E+01
4	0.196E+01
3	0.139E+01
2	0.834E+00
1	0.274E+00

Figure 7.5 Local stress contour on lateral interphase of both 80% (A) and 40% (B) coated THR models.

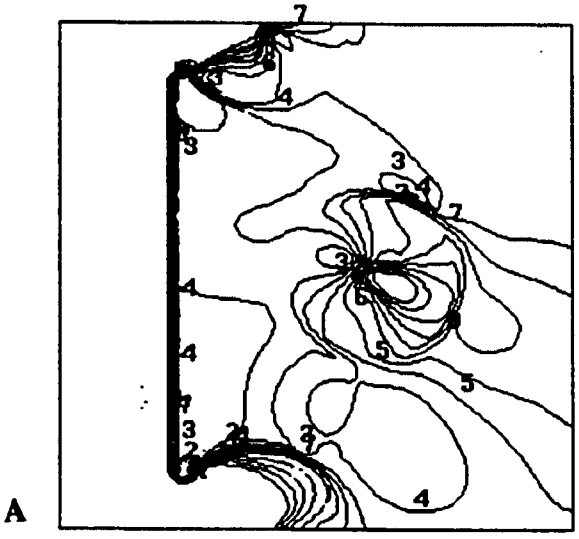

A

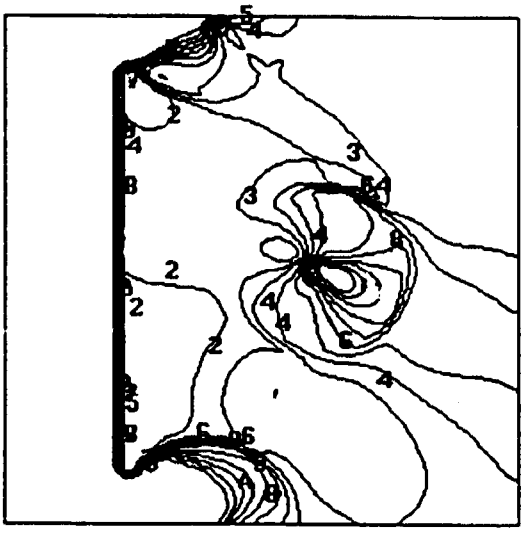

B

Von Mises Stresses (MPa)

8	0.433E+01
7	0.380E+01
6	0.326E+01
5	0.273E+01
4	0.219E+01
3	0.166E+01
2	0.113E+01
1	0.592E+00

Figure 7.6 Local stress contour on medial interphase of both 80% (A) and 40% (B) coated THR models.

Table 7.2 Lists of the predicted bone ingrowth, potent of material and bone failure with respect to different prosthesis designs

	Fully Ingrown		Partially Ingrown	
	Proximal coated	Fully coated	*Proxmal coated*	Fully coated
Ingrowth%	*49*	35	*41*	28
Metal Fail%	*0*	2	*0*	0
Bone Fail%	*0*	0.8	*0*	22

Titanium Yield Stress = 850 MPa
Bone Yield Stress = 120 MPa
Strain Threshold = 1500 με

The percentage of bone ingrowth for both 40% coated and 80% coated THR was calculated by analyzing local tissue strains. The 1500 με threshold (see ingrowth rule in Chapter VI) was used to compute the volume ratio of high strain areas ($\varepsilon > 1500$ με) to the total available pores. The proximally coated THR resulted in higher bone ingrowth (49%) than the fully coated THR (35%) in the proximal region of the stem.

The results showed that the interfacial zone contained 49% osseous bone and 51% fibrous tissue for the proximally coated THR, but 35% osseous bone and 65% fibrous tissue for the fully coated THR once the osseointegration reached the remodeling equilibrium. The volume percentages of these tissue ingredients were used to construct the local UCM of the partial ingrowth interphase for the corresponding THR. The homogenization model was once again applied to analyze the partially ingrown interphase models.

For THR models containing partially ingrown interphase, the global Von Mises equivalent stress distributions for the 40% coated and 80% coated THR showed no differences. The path of the loading transmission was identical to that of the fully ingrown THR- through the femur neck, and the medial surfaces of the proximal stem, to the lateral side of implant's distal end. The trabecular bone region carried low stresses, less than 0.8 MPa.

The computed local tissue stresses at the trabecular bone-implant interphase were extremely high compared to those in the fully ingrown interphase models. The maximum tissue stress within the partial ingrown interphase was about 130 MPa for 80% coated THR and 20 MPa for 40% coated THR. While the maximum tissue stress for 40% coated THR was below the yield strength of cortical bone, 22% of the total coatings of the 80% coated THR had the maximum tissue stress above the yield strength. All of the yield loci for 80% coated THR were concentrated on the proximal femur. Microdamages were expected to occur at these yield loci. This implies that interfacial loosening occurs more

easily on this type of prosthesis design. The proximally coated THR showed 41% bone retention, and the fully coated THR showed 35% bone retention. Results showed very little reduction of bone ingrowth from the equilibrium state in the fully ingrown situation.

7.3 Discussion

In this study, I focus on investigating the interphase characteristics of the hip implants including bone ingrowth, material failure, and tissue damage. Results show that bone ingrowth is incomplete, and ranging from 35% to 49%. Compared to the bone ingrowth data from the human retrieval- which range from 20% to 50% at the proximal femur (Bloebaum et al. 1993; Galante 1988; Sumner et al. 1992; Zettl-Schaffer et al. 1993), the present results point to higher ingrowth amounts. The two-dimensional models and the idealized coating structures used in this study may provide an explanation of the phenomenon. However, the current results provide reasonable estimates for bone ingrowth mainly because the study accounts for the effect of coating architecture on the local tissue strains.

The trend observed in this study, higher bone ingrowth for proximally coated implants than for fully coated implants, is consistent with Zettl-Schaffer's study (1993) and Engh and Bobyn's observations (1985). Engh and Bobyn observed the loss of bone density along the proximal coating regions of fully porous-surfaced implants in both animal and human studies. In contrast, partially (proximal) coated femoral implants showed more densification of osseointegrated bone than fully coated implants in the proximal femur. Oh (1988), Freeman (1990), Spector (1988), and Bobyn (1988) have suggested that the bone resorption or formation may be caused by the manner of proximal stress transfer. With a long porous-surfaced stem, proximal femur may undergo stress shielding because most of the load will pass through the well-fixed distal stem; this condition limits the percentage of bone ingrowth of porous coated implants which may

decrease the life time of biomaterials (Bobyn et al., 1982; Cook et al., 1988, 1989). However, without mechanistic evidence to support this assumption, the expanded application of the partially coated THR cannot be fully explored.

This study provides an understanding of the mechanisms which lead to differences in bone ingrowth between the different prosthetic designs. When the hip implant is loaded, the proximal healing tissue around each coating microsphere in a proximally coated THR sustains more stress than in a fully coated THR. The outcome from such stress transfer leads to more bone ingrowth for a proximally coated THR than a fully coated THR. The result gives a positive answer to the question posed in the Introduction - do current proximally porous coated THR designs provide a strain field which conducts more of biological fixation in the proximal region than a fully coated THR?

Actually, the bone ingrowth obtained from the fully ingrown interphase models represents the biological fixation on the implant after the osseointegration reaches a remodeling steady state. If that has been achieved, what is it that the ingrowth will accomplish in addition? I have posed a parallel question in the Introduction- how does the amount of calcified ingrown tissue affect material failure risk and implant stability? The partially ingrown interphase models analyzed in this study provide an answer to the question. The results demonstrate a very high risk of material failure for the fully coated stem with a partially ingrown interphase condition. Because small amount of bone ingrowth remains in the interphase after the remodeling equilibrium, resulting from the initial fully ingrowth condition, the loading transmitted through these small bone areas causes a high stress concentration effect. These tissue microdamages are concentrated on the proximal femur and can later or likely lead to implant loosening or bone fracture when the implanted prosthesis is in function.

Pedersen et al. (1990, 1991) revealed a similar trend by using an isolated local model which contains several coating particles and ingrown bone. They found that

ingrown bone was subjected to a high stress if the ingrowth did not completely penetrate the porous spaces in the coating layer. They suspected that the bone in the high stress region may be deformed and cause implant subsidence. But they couldn't, however, identify the specific areas in which the tissue undergoes yielding behaviors and the extent to which tissue damage was affected by different coating designs of THR.

The current partially coated THRs which reduce the coating areas on the stem, were designed for the following reasons: to prevent a proximal stress shielding which may lead to bone atrophy, and to reduce the possibilities for coating debonding.

In this study, I provide the mechanical basis to support the believe that the partially coated THR results in more bone ingrowth because less bone is resorbed due to stress shielding. However, the results cannot strongly support the use of partially coated THRs for the reduction of coating debonding. Fully coated THR exhibits only 2% metal failure rate under the condition that the interphase is initially filled with bone. The maximum stress of 970 MPa is not much greater than yield stress of 850 MPa for titanium, and is most probably released if the metal undergoes plastic deformation. Using partially coated THR's does not result in a benefit for the prevention of coating debonding.

Despite the minimal effects on the reduction of metal failure, the partially coated THR eliminates tissue damage which seem likely to occur for the fully coated THR. Therefore, reduction of coating areas on the implants are considered important with respect to minimizing implant failure risk. With this analysis, the reasons for using a partially coated THR design are as follows: to prevent a proximal stress shielding which leads to bone atrophy, to reduce the possibilities for coating debonding, and to reduce osseointegrated tissue damage which may cause implant loosening.

The evaluation of the performance for the currently used porous coated THR can be summarized as follows:

(1) to proximally coated THR provides a strain field conducive to more bone ingrowth and thus results in a more clinically stable situation,

(2) no failures result from the prosthesis with the proximally coated design, which can also lead to better clinical results, and

(3) a high risk of proximal femoral failures such as implant loosening and femur fracture is predicted for the use of the fully coated THR.

CHAPTER VIII

CONCLUSIONS AND FUTURE WORK

8.0 Predictions Provided

The present study has provided a new method, the homogenization method for the quantification of the interphase stresses and strains, that accounts for the architectures of the interfacial constituents. The homogenization method makes the correct predictions about the elastic properties of the bimaterial interphase composite as confirmed in the dissertation by experimental measurements. In addition, the model estimates the implant-tissue interfacial stresses with 85% accuracy in comparison to the direct finite element model.

It was demonstrated that the heterogeneity of interfacial stress patterns of a porous coated implant depends not only on the metal microstructure, but also upon the anatomical sites along the interphase region and also the ingrowth. Two loci of high stress concentration appear to be the sinterneck, between coating particles and metal substrates, and the tissue near the outer surfaces of the coating particles. The interfacial stress values on the medial surface of the hip prosthesis are 50 times greater than those on the lateral surface. The local stresses reflect the coupled effect of the global implant shape, global boundary conditions, and the material surface architecture. Analysis of

these local stresses and strains confirms an earlier hypothesis that the architecture and location of implant coatings are the major factors determining local stresses and strains of the implant interphases.

The results from the tibia implant study support the hypothesis that the interfacial strain influences the remodeling response of the osseointegrated tissue. A strain magnitude of 1500 με was found to serve as the threshold determining whether bone formation or resorption occurs at the interphase. The amount of bone ingrowth estimated through this strain criteria showed significant correlation with the ingrowth data obtained from the animal study.

The model simulation for different prosthetic designs allowed the quantification of characteristics associated with the implant design such as amount of bone ingrowth, potential of material failure, and degrees of tissue damage. This information is crucial for the interpretation of the results obtained from clinical observations, and helps to better understand the design of prostheses.

8.1 Mechanical Characteristics

Several significant mechanical characteristics of implant/tissue interphases result from the current analysis. They distinguish mechanically the interphase from the individual constituents. The characteristics are summarized below:

(1) The implant-tissue interphase composite is macroscopically orthotropic, even when the tissue and metal components are isotropic. Such an orthotropy might determine load transfer patterns and might also dictate failure patters of interphases.

(2) The local interfacial stresses, σ_{loc}, are inhomogeneous. They are strongly influenced by the local implant and tissue architecture as well as the global location and the loading condition. Stress values fluctuate above and below the stresses predicted by the global model.

(3) Osseointegration provides optimal strain threshold of 1500 με. The healing bone within the interfacial zone maintains bone mass if it's strain is greater than 1500 με; otherwise the bone undergoes a resorption process.

8.2 Clinical Implications

Other important results relate the clinical performance of different prosthesis designs to the interphase mechanical characteristics.

(1) Proximally coated THR provides more bone ingrowth than the fully coated THR because the proximally coated THR can effectively distribute load transfer through the coating regions onto the osseointegrated tissue.

(2) No failures result from the prosthesis with the proximally coated design. The proximally coated THR may lead to a better clinical performance because no implant loosening will result from the mechanical damage.

(3) A higher risk of proximal femur failures such as implant loosening and femur fracture due to tissue damage is predicted for the use of the fully coated THR; this condition may decrease implant longevity.

8.4 What to Do Next

The differences in clinical performance between the fully coated THR and partially coated THR may be related to differences in the mechanical characteristics of the interphase. However, this study only focuses on the mechanical influence of implant material architectures. Biological factors such as the healing capability of host tissues or surgical variances which effect clinical performance were not studied. The investigation was based on a bioinert material system which makes it reasonable to assume that the interfacial zone is homogeneous and completely filled with the mineral tissue. This

condition requires immobilization after the surgery. Further studies should incorporate heterogeneous interphases into the models since the complete immobilization of patients is virtually impossible. Animal studies can be designed to obtain such heterogeneities. Perhaps animals with an implantation period between two to four months can provide the information on healing processes and tissue architecture which help study biological effect on the interphase mechnaics.

A long-term implantation animal model, greater than one year, is also suggested in order to further test the hypothesis proposed in this dissertation. Both fully and partially coated THRs can be implanted into adult dogs in order to determine any differences in bone ingrowth and tissue damage between these two prosthesis designs.

Aside from the view of initial full ingrowth of the bone tissue, this study also rests on the assumption that the microspheres are periodically distributed on the implant surface. This assumption may underestimate some effects of local defect which may result in local stress concentrations and lead to failure loci. In reality, the sintered microspheres are not periodically located on the implant surface. A more detailed model including real microsphere distribution will be useful in identifying the failure site for each specific case.

In conclusion, the two-dimensional model has provided an easy access to the measurement of micromechanics of implant-tissue interphases. However, it may oversimplify the results by not considering the three-dimensional anatomy. The further development of a three-dimensional model will lead to a better understanding of the mechanisms of osseointegrated tissue remodeling and the mechanical performance of different hip prosthetic designs.

BIBLIOGRAPHY

Albrektsson T, Branemark P-I, Hansson H-A, Kasemo B, Larsson K, Lundstrom I, McQueen DH, Skalak R (1983): The interface zone of inorganic implant in vivo: titanium implants in bone. *Ann Biomed. Eng.* 11:1-27.

Albrektsson T, et al. (1988): Osseointegrated oral implants: A Swedish multicenter study of 8139 consecutively inserted Nobelpharma implants. *J. Periodontol* 59(5): 287-296.

Andriacchi TP, Galante JO, Belytschko TB, Hampton S (1976): A stress analysis of the femoral stem in total hip prostheses. J. Bone Jt Surg. 58 A: 616-624.

Arvidson K, Frykholm HA, Konow L, Lothigius E (1994): Results from prospective studies with Astra Tech dental implants. J. Dent. Res. 73:299.

Ashman RB, Van Buskirk WC (1987): The elastic properties of a human mandible. *Adv. Dent. Res.* 1(1): 64-67.

ASTM Standard D3983-81 (1991) Measuring strength and shear modulus of nonrigid adhesives by the thick-adhered tensile-lap specimen. Philadelphia: American Society for Testing and Materials.

Babuska I (1976): Homogenization approach in engineering. Proc. 2nd Int. Symposium on Comp. Mech. in App. Science and Eng. 137 153. Berlin. Heidelberg, New York: Springer

Bloebaum RD, Bachus KN, Rubman MH, Dorr LD (1993): Postmortem comparative analysis of titanium and hydroxyapatite porous-coated femoral implants retrieved from the same patient. J. Arthroplasty 8(2): 203-211.

Bobyn JD, Engh CA (1988): Bone ingrowth and remodeling in canine and human porous-coated hip replacement. In: Fitzgerald R (ed) *Non-Cemented Total Hip Arthroplasty*, Raven Press, Ltd., New York, pp.49-67.

Bobyn JD, Pilliar RM, Binnington AG, Szivek JA (1987): The effect of proximally and fully porous-coated canine hip design on bone modeling. *J. Orthop. Res.* 5: 393-408.

Bobyn JD, Pilliar RM, Cameron HU, Weatherly GC (1980a): The optimum pore size for the fixation of porous surfaced metal implants by the ingrowth of bone. *Clin. Orthop. Rel. Res.* 150: 150-263.

Bobyn JD, Pilliar RM, Cameron HU, Weatherly GC (1980b): The effect of porous surface configuration on the tensile strength of fixation of implants by bone ingrowth. *Clin. Orthop.* 150: 263-270.

Bobyn, JD; Cameron HU; Abdulla, D; Pilliar, RM; Weatherly, GC (1982): Biologic fixation and bone modeling with an unconstrained canine total knee prosthesis, Clinical Orthopaedics and Related Research 166:301-312.

Borodkin JL, Eadie JS, Choi K, Hollister SJ, Goldstein SA (1994): The effect of mechanical stimuli on bone ingrowth into porous coated implants. 40th Annual. Meeting, Trans. ORS, New Orleans, Louisiana

Brånemark P-I, Breine U, Adell R, Hansson B-O, Lindstrom J, Ohlsson A (1969): Intraosseous anchorage of dental prostheses. I. Experimental studies. Scand. J. Plast. Reconstr. Surg. 3:81-100.

Brånemark P-I, Hansson B-O, Adell R, Breine U, Lindstrom J, Hallen O, Ohman A (1977): Osseointegrated implants in the treatment of the edentulous jaw. Scand. J. Plast. Reconstr. Surg. 11: Suppl. pp.16

Brown TD, Pedersen DR, Gray ML, Brand RA, Rubin CT (1990): Toward an identification of mechanical parameters initiating periosteal remodeling: a combined experimental and analytical approach. J. Biomechanics. 23(9): 893-905.

Brown TD, Pedersen DR, Radin EL, Rose RL (1988): Global mechanical consequences of reduced cement/bone coupling rigidity in proximal femoral arthroplasty: a three-dimensional finite element analysis. J. Biomechanics. 21(2): 115-129.

Brunski JB (1988): The influence of force, motion, and related quantities on the response of bone to implants. In: Fitzgerald R (ed) *Non-Cemented Total Hip Arthroplasty*, Raven Press, Ltd., New York, pp.7-21.

Brunski J, Hipp JA, and El-Wakad M (): Dental implant design: biomechanics and interfacial tissues. J. Oral Implantology. 365-377

Brunski JB (1991) Influence of biomechanical factors at the bone-biomaterial interface. In: Davies JE (ed) *The Biomaterial Interface*, University of Toronto Press, pp.391-405.

Brunski JB, Moccia AF, Pollack SR, Korostoff E, Trachtenberg DI (1979a): The Influence of Functional Use of Endosseous Dental Implants on the Tissue-implant Interface. I. Histological Aspects. *J. Dent. Res.* 58(10):1953-1969.

Brunski JB, Moccia AF, Pollack SR, Korostoff E, Trachtenberg DI (1979b): The Influence of Functional Use of Endosseous Dental Implants on the Tissue-implant Interface. II. Clinical Aspects. *J. Dent. Res.* 58(10):1970-1980.

Cameron HU, Pilliar RM, and Macnab I (1973): The effect of movement on the bonding of porous metal to bone. J. Biomed. Mater. Res. 7:301.

Carter DR (1987): Mechanical loading history and skeletal biology. J. Biomechanics. 20: 1095-1109.

Carter DR, and Giori NJ (1991) Effect of mechanical stress on tissue differentiation in the bony implant bed. In: Davies JE (ed) *The Biomaterial Interface*, University of Toronto Press, pp.367-379.

Chandler H, Reineck FT, Wixson RL, and McCarthy JC (1981) Total hip replacement in patient younger than thirty years old. *J. Bone Joint Surg.* 63A: 1426-1434.

Chen H-H, Wang Y-J, Lee M-C (1991): Stress analysis of hip endoprosthesis with various interface conditions. J. Orth. Surg. ROC. 7: 327-335.

Cheng CL, Gross AE (1988): Loosening of the porous coating in total knee replacement. *J. Bone Joint Surg.* 70-B(3): 377-381.

Clemow AJT, Weinstein AM, Klawitter JJ, Koeneman J, and Anderson J (1981) Interface mechanics of porous titanium implants. *J. Biomed. Mater. Res.* 15:73-82.

Cook SD, Barrack RL, Salkeld SL, Prewett AB, Edmunds JO (1993) Bone ingrowth into a porous-coated total shoulder component retrieved postmortem. J Arthroplasty 8(2): 189-194.

Cook SD, Thomas KA, and Haddad RJ (1988) Histologic analysis of retrieved human porous-coated total joint component. *Clin. Orthop.* 217:293.

Cook SD, Walsh KA, and Haddad RJ (1985): Interface mechanics and bone growth into porous Co-Cr-Mo alloy implants. Clin. Orthop. Related Res. 193:271-280.

Cook SD, Weinstein AM, and Klawitter JJ (1982): A three-dimensional finite element analysis of a porous rooted Co-Cr-Mo alloy dental implant. *J. Dent Res* 61(1): 25-29.

Cook SD; Barrack, RL; Thomas, KA; and Haddad RJ (1989): Quantitative histologic analysis of tissue growth into porous total knee components, J. Arthroplasty 4(Suppl.) 33-43.

Cook SD; Thomas, KA; and Haddad RJ (1988): Histologic analysis of retrieved human porous-coated total joint components, Clin. Orthop. Rel. Res 234: 90-101.

Cox J F, Zarb GA (1987): The Longitudinal Clinical Efficacy of Osseointegrated Dental Implants: A 3-year Report. *Int. J. Oral Maxillofac. Imp.* 2(2):91-100.

Ducheyne P, Aernoudt E, DeMeester P, Martens M, Mulier C (1978): Factors governing the mechanical behavior of the implant-porous coating-trabecular bone interface. *J. Biomech.* 11(6-7):297-307.

Ducheyne P, DeMeester P, Aernoudt E, Martens M, Mulier C (1977): Influence of a functional dynamic loading on bone ingrowth into surface pores of orthopaedic implants. *J. Biomed. Mater. Res.* 11:881-838.

Engh CA, Bobyn JD (1985) Biological fixation in total hip arthroplasty., SLACK Inc. NJ.

Freeman MAR, Tennant R (1992): The scientific basis of cement versus cementless fixation. Clinc. Orthop. Rel. Res. 278:19-25.

Frost HM (1988): Vital biomechanics: proposed general concepts for skeletal adaptations to mechanical usage. Calcified Tissue International 42: 145-156.

Frost HM (1989) Mechanical usage, bone mass, fragility: A brief overview. In: Kleerekoper M and Krane SM (ed) *Clinical disorders of bone and mineral metabolism*, New York, pp.15-42.

Frost HM (1990a): Skeletal structural adaptations to mechanical usage (SATMU): 1. redefining Wolff's law: the bone modeling problem. Anatomical Record 226: 403-413.

Frost HM (1990b): Skeletal structural adaptations to mechanical usage (SATMU): 2. redefining Wolff's law: the remodeling problem. Anatomical Record 226: 414-422.

Fyhrie DP (1986): Stress analysis and design of proximal femoral prostheses. Ph.D. dissertation, Stanford University.

Galante JO (1988): Clinical results with the HGP cementless total hip prosthesis. In: Fitzgerald R (ed) *Non-Cemented Total Hip Arthroplasty*, Raven Press, Ltd., New York, pp.427-431.

Galante JO, Lemons J, Spector M, Wilson PD, Wright TM (1991): The biological effects of implant materials. J. Orthopaedic Res. 9: 760-775.

Galante JO, Rostoker W, Lueck R, Ray RD (1971), *J. Bone Joint Surg.*, 53A:101-114.

Goldstein SA, Matthews LS, Choi K, Jepsen KJ, and Shulick AM (1991): The effect of prosthesis surface geometry on implant stability and tissue ingrowth. Trans. 37th ORS p. 92.

Guedes JM, Kikuchi N (1990): Preprocessing and postprocessing for materials based on the homogenization method with adaptive finite element methods. *Comput. Methods Appl. Mech. Engrg.* 83: 143-198.

Gustilo RB (1988): Bias femoral ingrowth prosthesis with two to five years follow-up. In: Fitzgerald R (ed) *Non-Cemented Total Hip Arthroplasty*, Raven Press, Ltd., New York, pp.413-425.

Hale TM, Boretsky BB, Scheidt MJ, McQuade MJ, Strong SL, Van Dyke TE (1991): Evaluation of titanium dental implant osseointegration in posterior edentulous areas of micro swine. J Oral Implantol. 17:118-124.

Harrigan TP, Harris WH (1991): A three-dimensional non-linear finite element study of the effect of cement-prosthesis debonding in cemented femoral total hip components. *J Biomech.* 24(11): 1047-1058.

Hashin Z (1983): Analysis of composite materials- a survey. *J. Appl. Mech.* 50:481-505.

Hashin Z, Shtrikman S (1963): A variational approach to the theory of the elastic behaviour of multiphase materials. J Mech. Phys. Solids. 11: 127-140.

Hill R (1963): Elastic properties of reinforced solids: some theoretical principles. *J. Mech. Phys. Solids* 11:375-372.

Hofmann AA, Bachus KN, Bloebaum RD (1993): Comparative study of human cancellous bone remodeling to titanium and hydroxyapatite-coated implants. J. Arthroplasty 8(2): 157-166.

Hollister SJ, Fyhrie DP, Jepsen KJ, Goldstein SA (1991): Application of homogenization theory to the study of trabecular bone mechanics. *J. Biomech.* 24: 825-839.

Hollister SJ, Kikuchi N, and Goldstein SA (1993): Do bone ingrowth processes produce a globally optimized structure? J. Biomech. 26(4/5): 391-407.

Hollister SJ, Kikuchi N. (1992): A comparison of homogenization and standard mechanics analysis of periodic porous composites. *Comput. Mech.* 10:1-23.

Hughes T.J.R. (1987) The finite element method. Prentice-Hall Inc., Englewood Cliffs, New Jersey.

Huiskes R (1984): in Functional behavior of orthopaedic biomaterials, Vol. II-Applications

Huiskes R, Chao EYS (1983): A survey of finite element analysis in orthopedic biomechanics: The first decade. J. Biomechanics. 6:385-409.

Huiskes R, Snijders H, Vroemen W, Chao EYS, Morrey BF (1986): Fixation stability of a short cementless hip prosthesis. Trans. Ortho. Res. Soc. pp. 466.

Ko CC, Kohn DH, Hollister SJ (1992a): Micromechanics of Implant/Tissue Interfaces. *J. Oral Implantology* 18: 220-230.

Ko CC, Kohn DH, Hollister SJ (1992b): Stress analysis of the bone/implant interfacial zone accounting for localized architecture. Transactions of the 38th Annual Meeting, ORS, Washington, DC pp74.

Kohn DH, and Ducheyne P (1990) A parametric study of the factors affecting the fatigue strength of porous coated Ti-6Al-4V implant alloy. *J. Biomed. Mater. Res.* 24:1483.

Kohn, D.H., Ko, C.C., and Hollister, S.J., 1993, "Local Properties of Porous Coating/Tissue Interfacial Zone Based on Homogenization Theory", in *Bioengineering Conference*, N.A. Langrana, Ed., ASME BED-Vol. 24, 335-338.

Laing PG, Ferguson AB, Hodge ESJ (1960): J. Bone Jt Surg. 42A

Lemons JE (1988): Dental implant retrieval analysis. J. Dent. Education. 52(12): 748-756.

Meffert RM (1992): Treatment of failing dental implants. Int. J. Periodont. Restorative Dent. 109-114.

Messersmith PB, Cooke FW (1990) Stress enhancement and fatigue susceptibility of porous coated Ti-6Al-4V implants: an elastic analysis. *J. Biomed. Mater. Res.* 24:591-604.

Morscher E. (1984) in Morscher E, edi., The Cementless Fixation of Hip Endoprostheses, Berlin, Springer-Verlag, pp. 1-8.

Moyle DD, Klawitter JJ, Hulbert SF (1973): Mechanical properties of the bone-porous biomaterial interface: elastic behavior. *J. Biomed. Mater. Res.* 4:363-382.

National Institutes of Health Consensus Development Conference Statement on Dental Implants, June 13-15, 1988 (1988). *J Dent. Ed.* 52:824-827.

Oh I (1988): Design rationale of interference-fit total hip prostheses. In: Fitzgerald R (ed) *Non-Cemented Total Hip Arthroplasty*, Raven Press, Ltd., New York, pp.365-379.

Orr TE, Beaupre GS, Carter DR, and Schurman DJ (1990): Computer predictions of bone remodeling around porous-coated implants. J Arthroplasty 5(3): 191-200.

Pedersen DR, Brown TD, and Brand RA (1990): Bone ingrowth stress distributions within a novel prosthesis anchorage layer, 36th Annual Meeting, ORS, pp. 205.

Pedersen DR, Brown TD, and Brand RA (1991): Interstitial bone stress distributions accompanying ingrowth of a screen-like prosthesis anchorage layer, *J. Biomech.* 24: 191-200.

Pilliar RM (1983): Powder metal-made orthopedic implants with porous surface for fixation by tissue ingrowth. Clin. Orthop. Rel. Res. 176: 42-51.

Pilliar RM and Bratina WJ (1980): Micromechanical bonding at a porous surface structured implant interface-the effect on implant stressing. *J. Biomed. Engng.* 2:49-53.

Pilliar RM, Cameron HU, Macnab I (1975) Porous surface layer prosthetic device. *J. Biomed. Eng.* 10:126-131.

Rieger MR, Mayberry M, Brose MO (1990): Finite Element Analysis of Six Endosseous Implants. *J. Prosth. Dent.* 63:671-676.

Rohlmann A, Cheal EJ, Hayes WC, Bergmann G. (1988): A nonlinear finite element analysis of interface conditions in porous coated hip endoprostheses. *J. Biomech* 21(7): 605-611.

Siegele D, Soltesz U (1989): Numerical Investigations of the Influence of Implant Shape on Stress Distribution in the Jaw Bone. *Int. J. Oral Maxillofac. Imp.* 4:333-340.

Sisk AL, Steflik DE, Parr GR, Hanes PJ (1992) Alight and electron microscopic comparison of osseointegration of six implant types. J. Oral Maxillofac. Surg. 50: 709-716.

Skalak R (1983): Biomechanical Considerations for Osseointegrated Prostheses. *J. Prosthet. Dent.* 49:843-848.

Spector M (1988): Current concepts of bone ingrowth and remodeling. In: Fitzgerald RH (ed) *Non-Cemented Total Hip Arthroplasty.* Raven Press, New York, pp.69-85

Spector M, Harmon SL, and Kreutner (1979): Characteristics of tissue growth into proplast and porous polyethylene implants in bone. J. Biomed. Mater. Res. 13:677-692.

Steflik DE, Sisk AL, Parr GR, Hanes PJ, Lake FT, Brewer P, Horner J, McKinney RV (1992): Correlative transmission electron microscopic and scanning electron microscopic observations of the tissues supporting endosteal blade implants. *J. Oral Implantology* 18(2): 110-120.

Sumner DR, Turner TM, Urban RM, Galante JO (1992) Remodeling and ingrowth of bone at two years in a canine cementless total hip-arthroplasty model. J. Bone and Joint Surg., 74-A: 239-250.

Svensson NL, Valliappan S, Wood RD (1977): Stress analysis of human femur with implanted Charnley prosthesis. J. Biomechanics 10: 581-588.

Svensson NL, Valliappan S, McMahon R (1980): Finite element analysis of a simulated total hip replacement. Engng Med. 9(3): 143-146.

Taylor JL, Brunski JB, Hoshaw SJ, Cochran GVB, Higuchi KW (1990): Interfacial bond strengths of Ti-6Al-4V and hydroxyapatite-coated Ti-6Al-4V implants in cortical bone. in Tissue integration in oral, Orthopedic, and maxillofacial reconstruction, Laney WR and Tolman DE edi. Rochester, Minnesota. pp.125-132.

Vaillancourt H, Johnson WR (1990): A finite element model for porous implants. in International Conference on Development and Design with Advanced Materials. Amsterdam, Sih GC , Hoa SV ,and Pindera JT (Editors); New York; Elsevier. pp.207-235.

Weinans H, Huiskes R, and Grootenboer HJ (1990): Trends of mechanical consequences and modeling of a fibrous membrane around femoral hip prostheses. J. Biomechanics. 23(10): 991-1000.

Weinans H, Huiskes R, and Grootenboer HJ (1992): The behavior of adaptive bone-remodeling simulation models. J. Biomech. 25: 1-17.

Weinans H, Huiskes R, Rietbergen B, Sumner DR, Turner TM, Galante JO (1993): Adaptive bone remodeling around bonded noncemented total hip arthroplasty: a comparison between animal experiments and computer simulation. J. Bone Jt Surg. 11: 500-513.

Weinstein AM, Klawitter JJ, Anand Sc, and Schuessler R (1976): Stress analysis of porous rooted dental implants. *J. Dent Res* 55(5): 772-777.

Welsh RP, Pilliar RM, MacNab I (1971): J. Bone Jt Surg. 53A

Wevers HW, and Cooke TDV (1987) Bead loosening in porous metal coated orthopaedic implants: a case study. Clin. Mater. 2: 67-74.

Wolfarth D, Filiaggi M, and Ducheyne P (1990) Parametric analysis of interfacial stress concentrations in porous coated implants. *J. Appl. Biomat.* 1:3-12.

Wolff JD (1892) Das Gesetz der Transformation der Knochen. Berlin, A Hirschwald.

Yue S, Pilliar RM, and Weatherly GC (1984) The fatigue strength of porous-coated Ti-6%Al-4%V implant alloy. *J. Biomed. Mater. Res.* 18:1043-1058.

Zettl-Schaffer KF, Ghaffarpour M, McGovern TF, Engh CA (1993): Scanning electron microscopy of bone ingrowth into 40% and 80% coated AML prostheses retrieved at autopsy. Transaction of Ortopaedic Research Society. p471.